CRANFIELD UNIVERSITY

Theofanis Ampatzidis

Advanced carbon/flax/epoxy composite material for vehicle applications:

Vibration testing, finite elements modelling, mechanical and damping characterization

School of Aerospace, Transport and manufacturing
MSc by Research Course

Msc By Research
Academic Year: 2014 - 2015

Supervisors:

Dr. Hrushikesh Abhyankar
Research Fellow - Lightweight Structures, School of Aerospace, Transport and Manufacturing

Dr. Kim Blackburn
Research Fellow in Off Road Dynamics, School of Aerospace, Transport and Manufacturing

May 2015

CRANFIELD UNIVERSITY

School of Aerospace, Transport and Manufacturing
MSc by Research Course

MSc by Research
Academic Year 2014 - 2015

Theofanis Ampatzidis

Advanced carbon/flax/epoxy composite material for vehicle structures:

Vibration testing, finite elements modelling, mechanical and damping characterization

Supervisors:

Dr. Hrushikesh Abhyankar
Research Fellow - Lightweight Structures, School of Aerospace, Transport and Manufacturing

Dr. Kim Blackburn
Research Fellow in Off Road Dynamics, School of Aerospace, Transport and Manufacturing

ABSTRACT

Nowadays, research in automotive and construction industries focuses on materials that offer low density along with superior dynamic and static performance. This goal has led to increasing use of composites in general, and carbon fibre (CF) composites in particular. CF composites have been adopted widely in the space industry and motorsports. However, their high stiffness and low density leads to low damping performance, which is responsible for increased levels of noise and reduction in service life. On the other hand, natural fibres (NF) like flax fibres (FF) are capable of delivering a much better damping performance. A hybrid composite comprising of FF and CF can potentially deliver both on strength and higher damping performance.

In this study the mechanical and damping properties of CF, FF and their hybrid composites were examined. Composites' anisotropic nature affects their response to vibrations and so traditional damping experimental setups used for metals had to be ruled out. A damping set up based on Centre Impedance Method (CIM) was adopted for the purpose of this study which was based on an ISO standard originally developed for glass laminates. Standard tensile and flexural tests were conducted in order to characterise the performance of the hybrid composite. The experimental work was accompanied by finite elements analysis (FEA). The experimental data and FEA were used to optimize the hybrid structure layup with respect to damping and structural response.

Keywords: Centre Impedance Method (CIM), hybrid composites, natural fibre, loss factor, half-bandwidth method, resonant frequency, ISO 16940

ACKNOWLEDGEMENTS

Special thanks to my supervisors, Dr. Hrushikesh Abhyankar and Dr. Kim Blackburn, and to Dr. James Brighton, without their support this study would not be possible. Gratitude to Simon Stranks and to people in building 54 for their time and patience during the noisy damping experiments. Thanks to Dr. Xu and Dr. Marchante Rodriguez for their precious time. Many thanks, also, to CARBIO project and partners for their support.

Many thanks to my fellow students, Ian, Jinchun, Jonathan, Laura, Marie and Satya. Also, many thanks to the people in Composites department, and especially Jim Hurley, for their patience.

The deepest thanks go to my friends and family who had the patience and love to tolerate me and gave me great strength during this year.

TABLE OF CONTENTS

LIST OF FIGURES

LIST OF FIGURES IN APPENDICES

LIST OF TABLES

LIST OF EQUATIONS

LIST OF NOTATIONS

ζ	Damping ratio
c_c	Critical damping
h	Hysteretic damping coefficient
γ	Structural damping factor
η	Loss factor
ξ	Damping ratio
Ψ	Specific damping capacity
E	Elastic Modulus
F_{max}	Max Stress
ε_{max}	Max Strain
$E_{(s)}$	Specific Elastic Modulus
E_f	Flexural Modulus
$\sigma_{f(max)}$	Flexural strength
$E_{f(sp)}$	Specific Flexural Modulus
$\tau_{12(max)}$	Shear Strength
$\gamma_{12(max)}$	Max Shear Strain
G_{12}	Shear Modulus

LIST OF ABBREVIATIONS

ASM	American Society of Metals
ASTM	American Society for Testing of Materials
CARBIO	Carbon / bio-composite hybrid vehicle structures for reduced weight, cost and environmental impact
CFRP	Carbon Fibre Reinforced Plastic
CF	Carbon Fibre
CIM	Centre Impedance Method
CMC	Ceramic Matrix Composites
CNSL	Cashew nut shell liquid
EPSRC	Engineering and Physical Sciences Research Council
FAW	Fabric Average Weight
FE	Finite Elements
FEA	Finite Elements Analysis
FF	Flax Fibre
FFRP	Flax Fibre Reinforced Plastic
FFT	Fast Fourier Transformation
FRC	Fibre Reinforced Composites
FRP	Fibre Reinforced Plastics
GF	Glass Fibre
GFRP	Glass Fibre Reinforced Plastic
ISO	International Organization for Standardization
MMC	Meal Matrix Composites
NC	Natural Composites
NFRP	Natural Fibre Reinforced Plastics
OMC	Organic Matrix Composites
PLA	Polylactic Acid
PMC	Polymer Matrix Composites
SPC	Soy protein concentrate
SPI	Soy protein isolate
TW	Twill Weave
VBT	Vibration Beam Testing

1 INTRODUCTION

1.1 Background

One of the most important mechanical characteristics that an engineer should take into account when designing any structure is damping. Damping capacity of the material is the quantity that indicates how efficiently energy can be dissipated mainly during fatigue loadings. Efficient energy dissipation leads to reduction of the amplitude of vibrations, thus minimization of noise and failures [1], [2], [3], [4], [5]. In addition to that, damping contributes to the impact resistance of the structure: the more damped a material is, the less likely is it to fracture in impact [6].

The ideal combination of material properties is low density along with high damping capacity and good mechanical properties. When it comes to metals, these properties cannot be achieved as the microscopic mechanisms involved in internal friction (namely damping capacity) depend upon the parameters that control mechanical strength [7]. So, additional damping has to be introduced on metallic structures, normally at the expense of additional weight.

Fibre-reinforced composites (FRC) exhibit superior damping behaviour than metals, due to their various energy dissipation sources: viscoelastic nature of matrix, interphase damping mechanism, damping due to damage (matrix cracks, fibres broken etc.), viscoplastic damping and thermoplastic damping [8]. Another advantage of FRC is that they can offer far more design versatility as damping capacity, along with other specific properties, can be tailored to meet specific structural requirements [6], [9].

Natural Composites (NC), such as flax, retain and even enhance [10] the aforementioned damping characteristics of FRC and offer some additional advantages that come from their unique nature. Some of these advantages are low cost, reduced dependence on non-renewable energy/material sources and the end of life biodegradability of components [11]. On the other hand, moisture uptake, quality variations and low thermal stability are some of their negative characteristics [12], [13]. In addition to these drawbacks, the strongest NC's mechanical characteristics can be compared only with those of Glass Fibre (GF), a handicap that makes them

weak contenders for structural parts [14]. Hybrid composites can solve this issue, combining the optimum mechanical characteristics of synthetic fibres (such as Carbon Fibre (CF)) with the enhanced damping performance of NF [15].

In this thesis the mechanical and damping characteristics of hybrid CF/FF composite parts were examined and simulated in finite elements analysis (FEA) models.

1.2 CARBIO Project

This study's research was carried under the auspices of the Engineering and Physical Sciences Research Council (EPSRC) for the project: "Carbon/bio-composite hybrid vehicle structures for reduced weight, cost and environmental impact (CARBIO)", ref. EP/L505171/1 (**Figure 1-1**).

Automotive manufacturers seek to find ways to achieve optimum results in three different sectors: weight , comfort and cost. This way the strict environmental regulations and requirements are met. These sectors have impact on each other, since lightweight materials are quite expensive and cause increased noise and vibrations. A rational approach to decrease vibrations keeping the weight low is to enhance the damping performance of lightweight materials. CARBIO acknowledges that hybrid CF/FF composites could consist of a solution that will combine the advantages of FRC with the optimum damping characteristics of FF. Also, FF abundance, low cost and low density makes hybrid solution quite appealing. The project's study aim was to examine the feasibility of this solution and its performance.

Figure 1-1. CARBIO logo

2 STATE OF THE ART

2.1 Composites

2.1.1 Definition

When it comes to composites, it is difficult for a definition to cover the vast range of materials that are described by this term. A general definition is that any material consisting of two or more distinguishable components and attaining properties that are significantly different than its building blocks can be considered as a composite material. These kinds of materials have been used for centuries (straw reinforced mud bricks, Achilles' famous shield made of successive leather and metal sheets etc). Composites can, also, be found in nature, such as wood, which consists of cellulose fibres embedded in a compound called lignin [16]. Scientifically speaking, material scientists would state that a composite material consists of a chemically and/or physically distinct phase distributed within another continuous phase and its properties differ from their original ones [17]. Nowadays, composite materials mostly refer to polymer matrix which are reinforced by a wide range of fibres (carbon, glass, aramid, natural etc.) and have been used since the mid-20^{th} century. Although this is the main type of composites, there are, also, alternatives which become more and more popular.

2.1.2 Classifications

Due to their wide range of material combinations and applications, composites are classified at two distinct levels with further sub-categorization. The first level of classification is usually made with respect to the matrix constituent [5]. The major composite classes include organic-matrix composites (OMCs), metal-matrix composites (MMCs), and ceramic-matrix composites (CMCs). The first major class, “organic-matrix composite”, is generally assumed to include two types of composites: polymer-matrix composites (PMCs) and carbon-matrix composites (also known as carbon-carbon composites). PMCs are further classified in thermoplastic and thermoset composites, with the major difference being that thermoplastic can be remelted with minimal damage to the matrix, while thermosets cannot be remoulded into different shape (by heating) once they are set [17]. The second level of

classification refers to the reinforcement form: particulate reinforcements, whisker (short fibres) reinforcements, continuous fibre laminated composites, and woven composites (braided and knitted fibre architectures are included in this category). The first two classes are known as "filled materials", while the second ones are known as "reinforced materials" or "continuous composites".

2.1.3 Filled materials

Filled materials consist of a matrix that is filled with particles or whiskers so that its properties are improved. In most cases the percentage of the matrix is larger than 50%, which makes overall properties to be dominated by it. Filled materials are easier and cheaper to manufacture that continuous composites which make them quite appealing in some applications where cost is the main issue. Generally, filled materials are treated as homogenous and isotropic materials, which cancel the properties' tailoring advantage that is mentioned in the next section (**2.1.4**). In addition to this, their properties cannot compete with the high-end continuous composites [18]. In this study continuous composites were examined.

2.1.4 Continuous composites

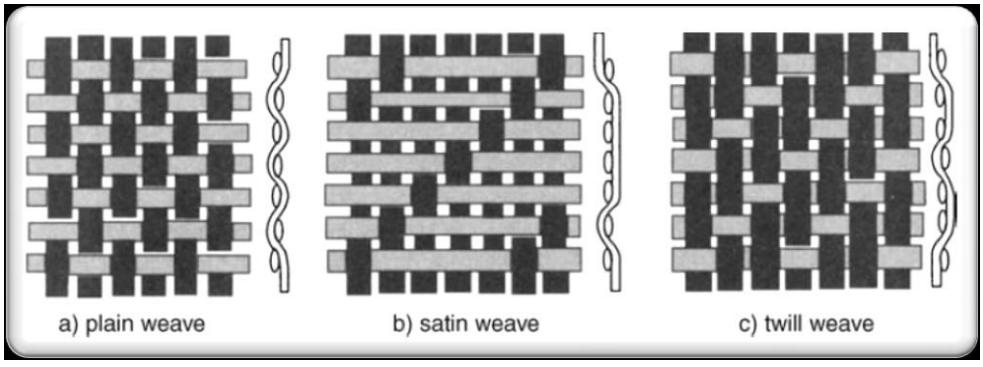

Figure 2-1. Types of fabrics [19]

Continuous fibre-reinforced composites contain reinforcements having lengths much greater than their cross-sectional dimensions. Each layer or ply of a continuous fibre composite typically has a specific fibre orientation direction. Most composite are manufactured by stacking together several layers of continuous reinforcement fabrics that form the laminate. By laying several plies with different fibre orientations, the laminate thus formed can offer properties that can be tailored based on the application and requirements. This means that local variable properties can be

achieved in a structure, reinforcing the part only in specific locations where it is needed, avoiding additional weight. The major characteristics of a fabric include its style or weave pattern, fabric count, and the construction of warp yarn and fill yarn. The combination and interaction of these characteristics determine the properties and performance of the composite. The fabric count identifies the number of warp and weft yarns per inch. Warp yarns run parallel to the machine direction, and weft yarns are perpendicular. There are basically three weave patterns: plain, twill, and satin (**Figure 2-1**). Plain weave is the simplest form, in which one warp yarn interlaces over and under one fill yarn. Twill weave has one or more warp yarns floating over at least two fill yarns. Satin weave (crowfoot) consists of one warp yarn interfacing over three and under one fill yarn to give an irregular pattern in the fabric. The eight-harness satin weave is a special case, in which one warp yarn interlaces over seven and under one fill yarn to give an irregular pattern. In fabricating a composite part, the satin weave gives the best conformity to complex contours, followed in descending order by twill and plain weaves [5]. There is, also, the unidirectional and the biaxial fabric. The first one consists of fibres with the same orientation which are held together by a standard thread, usually made of Teflon. Biaxial ones consist of fibres of two different directions which are held together the same way as in the unidirectional. It has been proven that unidirectional fabrics achieve the highest strength among the different fabric types [5].

2.1.5 . Use of composites

Due to their great strength-to-weight and stiffness-to-weight ratio, composite materials have been extensively used in high-end applications, varying from military and civil aviation to F1 race cars and sports equipment. During the recent years their application has been extended in civil engineering and every day vehicles, too (**Figure 2-2**). Nevertheless, such materials have weaknesses too; due to the highly anisotropic behaviour, small deviations in each lamina direction during layup might result in a significant reduction in strength. Similarly, their performance in “out of plane” loading (i.e. when loaded perpendicularly to the laminate) is poor [5], [20], [18] [17]. Also, although they show greater damping performance than metals, the large stiffness-to-density ratio of most of the composite materials, such as Carbon Fibre

Reinforced Plastics (CFRP), might lead to very light-weight and high-stiffness parts with low damping performance. These characteristics result in high-amplitude vibrations, noise and work life reduction [2], [21]. This is where Bio-composites come to solve the low damping issue.

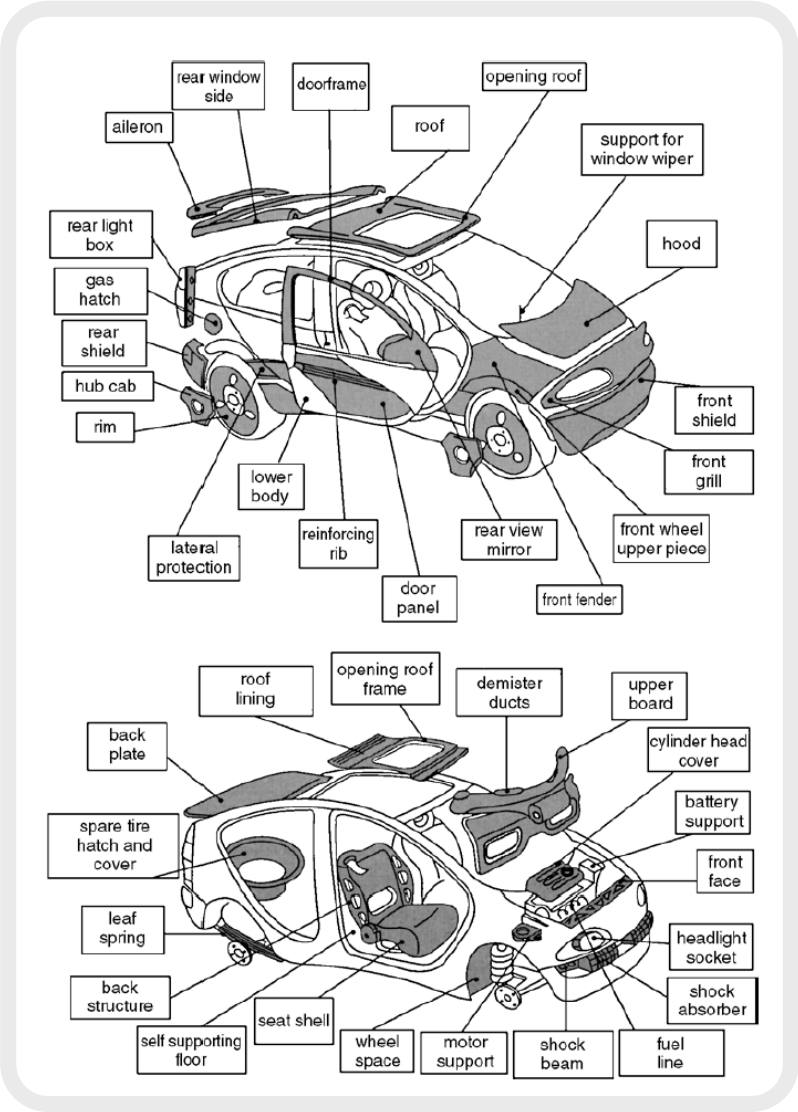

Figure 2-2: Composite parts in an Automobile [22]

2.2 Bio-composites

As mentioned before, Fibre Reinforced Plastics (FRP) consist of a widely used means of developing lightweight vehicles and machine parts, thus keeping the energy consumption at low levels. This weight saving comes with some costs in other

aspects, though. The most important of them are the high cost of production of the fibres (especially the high performance ones, such as CF, Kevlar etc.), environmental concerns and low recyclability, which led researchers and the industry to look elsewhere for better solutions.

Figure 2-3. Mercedes S class (2005) automotive components made from different Natural Fibre Reinforced Plastics (NFRP) [23]

NC have already found acceptance in many industries, especially in automotive [23], [24], [25], where there are numerous non-structural interior panels that have been manufactured using NC, along with some exterior body panels (**Figure 2-3**) [23]. Research on using NC in structural parts is, also, in process, such as ECOSHELL, whose aim was to examine whether FF can be used in a bio-composite electric vehicle's structural parts, such as the body-in-white, crash structures etc. [26], [27], [28]. NC building elements are natural fibres (NF) and matrix, which in most cases consists of simple plastic based on non-renewable petroleum resources [29]. Limited research is being conducted on bio-polymers due to its high cost [14].

2.2.1 Natural fibres (NF)

Currently the variety of materials that are being researched for use in NFRP is quite vast, with varying physical and chemical properties [14], [29],[30].

The plants, which produce NF, are classified as primary and secondary depending on their utilization. Primary plants are those grown for their fibre content while secondary plants are plants in which the fibres are produced as a by-product. Jute,

hemp, kenaf and sisal are examples of primary plants, while pineapple, oil palm and coir are examples of secondary plants [29].

There are six types of NF: bast fibres (jute, flax, hemp, ramie and kenaf), leaf fibres (abaca, sisal and pineapple), seed fibres (coir, cotton and kapok), core fibres (kenaf, hemp and jute), grass and reed fibres (wheat, corn and rice) and all other types (wood and roots) [29]. In **Figure 2-4** and **Figure 2-5** it is shown that flax fibre is among the NF that exhibit the most promising characteristics. Ramie, which has slightly better mechanical properties than flax, requires more extensive pre-treatment due to its chemical composition and regions of production, which makes it less appealing than flax [29]. This quite appealing nature of FF has led researchers to examine the possibility to use it in structural parts, with studies testing its tensile, flexural and vibration properties, as it is stated in FF chapter (**2.3**). It should be noted that NF are compared only with GF since any other comparison would be needless, mainly because of the high price, but also because of the high mechanical properties of the rest organic fibres.

Fiber type	Density (g/cm^3)	Length (mm)	Diameter (μm)	Tensile strength (MPa)	Tensile modulus (GPa)	Specific modulus (approx)	Elongation (%)
E-glass	2.5–2.59	–	<17	2000–3500	70–76	29	1.8–4.8
Abaca	1.5	–	–	400–980	6.2–20	9	1.0–10
Alfa	0.89	–	–	35	22	25	5.8
Bagasse	1.25	10–300	10–34	222–290	17–27.1	18	1.1
Bamboo	0.6–1.1	1.5–4	25–40	140–800	11–32	25	2.5–3.7
Banana	1.35	300–900	12–30	500	12	9	1.5–9
Coir	1.15–1.46	20–150	10–460	95–230	2.8–6	4	15–51.4
Cotton	1.5–1.6	10–60	10–45	287–800	5.5–12.6	6	3–10
Curaua	1.4	35	7–10	87–1150	11.8–96	39	1.3–4.9
Flax	1.4–1.5	5–900	12–600	343–2000	27.6–103	45	1.2–3.3
Hemp	1.4–1.5	5–55	25–500	270–900	23.5–90	40	1–3.5
Henequen	1.2	–	–	430–570	10.1–16.3	11	3.7–5.9
Isora	1.2–1.3	–	–	500–600	–	–	5–6
Jute	1.3–1.49	1.5–120	20–200	320–800	8–78	30	1–1.8
Kenaf	1.4	–	–	223–930	14.5–53	24	1.5–2.7
Nettle	–	–	–	650	38	–	1.7
Oil palm	0.7–1.55	–	150–500	80–248	0.5–3.2	2	17–25
Piassava	1.4	–	–	134–143	1.07–4.59	2	7.8–21.9
PALF	0.8–1.6	900–1500	20–80	180–1627	1.44–82.5	35	1.6–14.5
Ramie	1.0–1.55	900–1200	20–80	400–1000	24.5–128	60	1.2–4.0
Sisal	1.33–1.5	900	8–200	363–700	9.0–38	17	2.0–7.0

Figure 2-4. Compiled properties of NF [14]

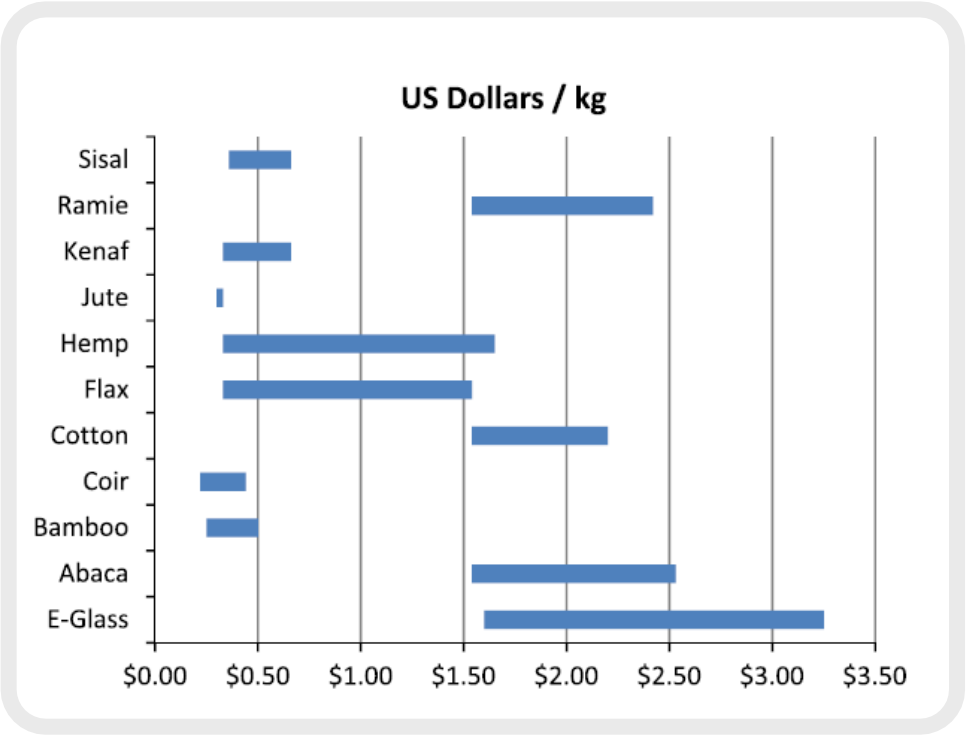

Figure 2-5. Cost per weight comparison between GF and NF [14]

2.2.2 Bio-matrix

The composites' shape, surface appearance, environmental tolerance and overall durability are dominated by the matrix while the fibrous reinforcement carries most of the structural loads, thus providing macroscopic stiffness and strength. This means that matrix properties are of extreme importance for the durability and performance of composites. Polymers market is dominated by commodity plastics with 80% consuming materials based on non-renewable petroleum resources [29]. This is mainly because of the relatively high cost of the development of biopolymers using renewable, fully biodegradable materials. Biopolymers have historically cost anywhere from about twice to ten times as much as comparable petroleum-based resins, with soy-based, cashew nut shell liquid (CNSL) resins and polylactic acid (PLA) generally being some of the most affordable and extensively studied [14], [31], [32].

PLA already has high market exposure compared to other types of bio-resins which can be explained by its good aesthetics, mechanical strength, thermal plasticity, biocompatibility and easy processability. It is a biodegradable, hydrophobic polymer produced from renewable resources such as corn, starch and sugar beet,

which are fermented to lactic acid followed by ring-opening or gradual polycondensation polymerization into PLA with expected molecular weights [33]. It has a broad range of applications due to its ability to be stress crystallized, thermally crystallized, impact modified, filled, copolymerized and processed in a variety of polymer processing equipment. PLA is fully biodegradable by hydrolysis to lactic acid, and eventually to water and carbon monoxide [14]. Its hydrophobic nature makes the NF pre-treatment necessary, due to their hydrophilic nature [33]. Although the increased production is expected to decrease the cost of their production, PLA biopolymers are expected to remain more expensive than comparable synthetic polymers [14].

CNSL constitutes nearly one third of the total nut weight; thus, most of it is obtained as a by product from the mechanical processes used to extract the edible cashew kernel [31]. *Anarcadium occidentale* is the cashew tree from which the cashew nuts are obtained and it is grown widely in coastal areas of tropical and subtropical countries. Current research on CNSL focuses mainly on the full replacement of the synthetic resins [32], with the solution of mixing it with synthetic epoxy resin already being used.

Soy-based resins are, also, another focus point of a large portion of biopolymer research. Soy protein concentrates (SPCs) and soy protein isolates (SPIs) are two common variations of soy products made by purification of defatted soy flour. Their main characteristics are their relatively low strength and high moisture absorptions, which make the hybridization with other natural or biodegradable polymers inevitable [14].

2.3 Flax

Flax (*linum usitatissimum*) is probably the oldest textile fibre known to mankind. It belongs to the bast fibres and has been used since ancient times for the production of linen cloth, mostly in the higher value-added textile market [29], [34]. Fine and regular long flax fibres are usually spun into yarns for linen textiles. Linen fabric maintains a strong traditional niche among high quality household textiles, such as bed linen, furnishing fabrics and interior decoration accessories. Shorter flax fibres produce heavier yarns suitable for kitchen towels, sails, tents and canvas. Lower fibre grades

as reinforcement and filler in composites are used in automotive interior substrates and furniture [35].

2.3.1 Origin of flax

FF is produced in the stems of flax bast plant. Like cotton, FF is a cellulose polymer, but its structure is more crystalline, making it stronger, crisper and stiffer to handle and easy to wrinkle. Flax plant grows up to 90 cm in length and average 12-16 mm in diameter and possesses strong fibres all along its stem. At the macroscopic level, a flax stem is composed of (from the outer to the inner part): bark, phloem, xylem and a central void (**Figure 2-6**). At the meso-scopic level, the cross-section of a bundle contains between 10 and 40 fibres which are linked together mainly by pectin [35]. The coarse bast fibre bundles are isolated from the stem by breaking and scutching and further refined towards technical fibres by hackling. The interphase holding the technical fibres (**Figure 2-7**) together is absent at some spots and weak in some other spots. Consequently, the technical fibres in the plant are not well defined and easily separated from the root till the tip, but are more like an arbitrary bundle of elementary fibres, separated at some points and glued together at other positions. During hackling the fibre bundles are separated by the hackling combs into the technical fibres. The elementary fibres have lengths between 2 and 5 cm, and diameters between 5 and 35 μm. The technical fibre consists of about 10-40 elementary fibres in cross section. The elementary fibres overlap over a considerable length and are glued together by an interphase mainly consisting of pectin and hemicellulose, which is a mixture of different lower molecular weight branched polysaccharides. They are not circular but a polyhedron with usually 5, 6 or 7 angles to improve the packing in the technical fibre. The elementary fibres consist of a primary cell wall (S1), a secondary cell wall (S2) and a lumen (S3), which is an open channel in the centre of the fibre (**Figure 2-6**). They contain 65-75% cellulose, approximately 15% hemicellulose (mostly xylan) and 10-15% pectin [34].

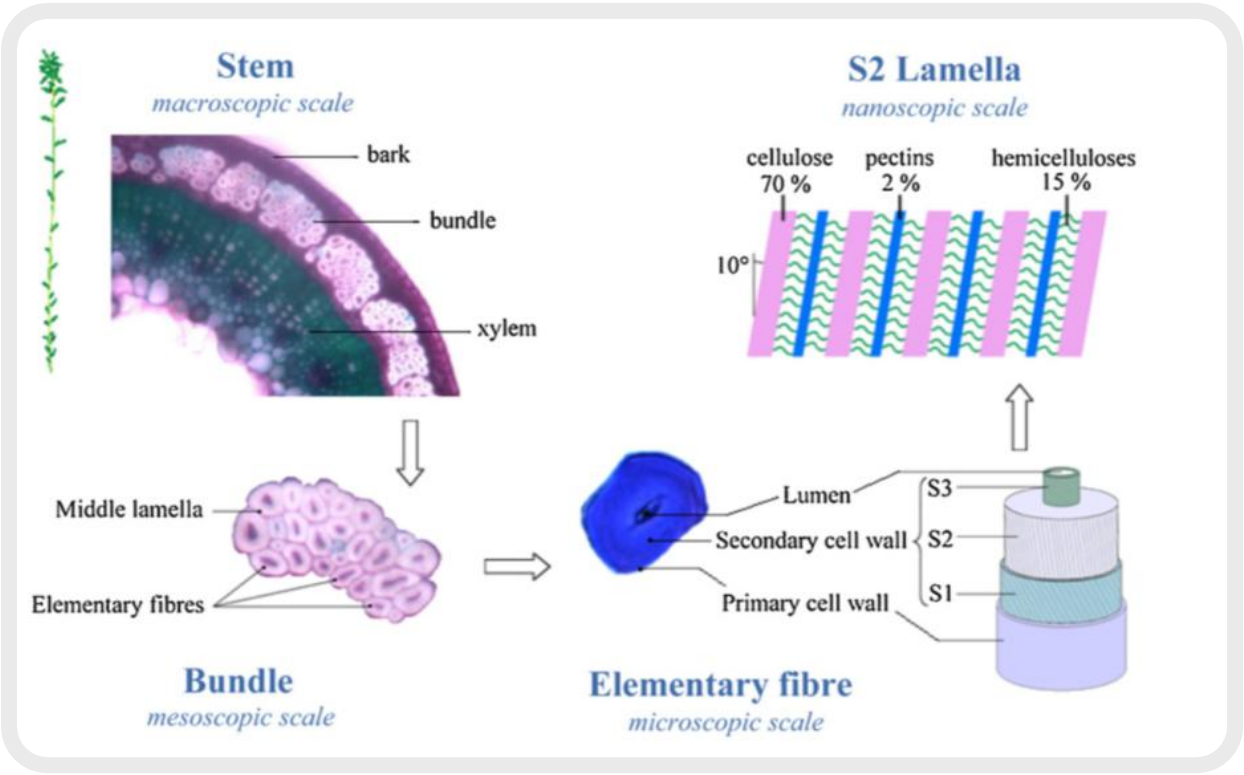

Figure 2-6. Cross-sections and schematic representations of flax at different scales, from the stem to the cellulose fibrils [36]

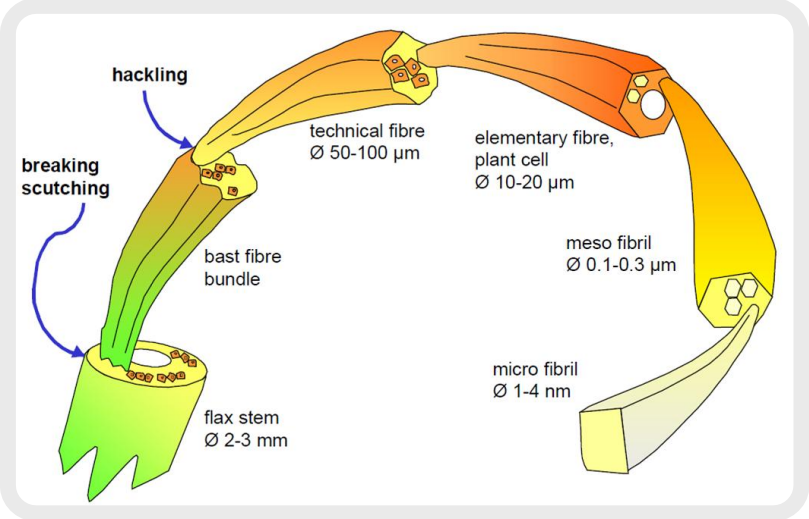

Figure 2-7. Schematic representation of a FF form stem to microfibril [34]

2.3.2 Properties

FF is the NF that has gained popularity during the recent years, mainly because it is cost-effective and offers specific mechanical properties comparable to those of GF [35], as stated in **2.2**. FF superiority in mechanical properties among NF is thought to

be due to the fact that flax has the longest elementary fibres and the smallest microfibril orientation [34]. Due to an increase in its popularity, research on FF and its properties has been extensive. Baley [37] examined the tensile behaviour of the FF and by using micro-mechanical equations estimated the Young's modulus of a FF, with his results agreeing with the experimental ones. Chalret et al. [38] investigated the non-linearity of the tensile stress-strain curve of the FF which was explained by the visco-elastoplastic behaviour of the fibre. Assarar et al. [39] examined the influence of water ageing on both Flax Fibre Reinforced Plastics (FFRP) and Glass Fibre Reinforced Plastics (GFRP) and observed that the effects were similar on both types of fibres. Zhu et al. [11] and Yan et al. [35] compiled studies on recent developments of FF and compared the material with other NF, concluding that it is the most promising NF with regards to the cost of production and its mechanical properties. The authors stated, though, that the major problem of FF is its incompatibility with some polymeric systems due to its high hydrophilicity and the degradation of its properties caused by some environmental conditions. Zhu et al. [27], also, investigated the possibility to improve the mechanical properties of FF and tannin composites using different chemical treatments, such as alkali, acetylation etc. showing that there is significant improvement in both tensile and flexural properties. Duc et al. [10], [40] investigated the damping behaviour of FFRP and compared it with CFRP's one, with FFRP exhibiting better damping than CFRP. FFRP's damping has, also, been compared with GFRP [41] by Prabhakaran et al. and it was proven that FFRP has better damping performance.

2.4 Hybrid CF/FF composites

Despite the significantly increased interest in FF and the vast knowledge of CF capabilities, there have been few studies on hybrid composites made of CF and FF. The most significant amongst them is Vanwalleghem's [15], where the damping properties of FF, CF and hybrid CF/FF composites were examined and a bicycle frame made from the hybrid material was simulated and manufactured. This study led to the production of Museeuw MF1 and MF5 bicycles (**Figure 2-8**), which were released in 2008. Others, such as Dhakal et al. [42], Fiore et al. [43] and Bagheri at al. [44], [45], [46] examined the properties of FF/CF and compared them with pure CF

or FF parts. Dhakal et al. [42] manufactured hybrid CF/FF composites and investigated the effects of carbon fibre hybridisation on the water absorption behaviour, thermal and mechanical properties of both UD and CP flax specimens. It was concluded that the hybrid solution was possible and quite appealing, since hybrids showed quite stable performance and significantly higher than pure FF. Fiore et al. [43] examined hybrid layups of two different FF fabric with the same unidirectional nonwoven CF fabric and proved that hybrid layups exhibited significantly better tensile and flexural behaviour than the pure FF ones. Bagheri at al. [44], [45], [46] performed fatigue, tensile and flexural tests on hybrid CF/FF specimens, along with some biomechanical tests (cytotoxicity and osteogenesis examination, viability tests etc.). Their studies are part of a still ongoing program to develop a new CF/FF/Epoxy bone fracture plate to be used in orthopaedic trauma applications. It has already been concluded that this solution is of a potential alternative to metallic bone implants and the research now focuses on biocompatibility issues.

Figure 2-8. Museeuw MF1 and MF5 bicycles [15], produced in 2008

2.5 Damping

When vibrations occur in a mechanical system, the forces that are generated may compromise its integrity. These forces are caused by the accelerations, velocities and displacements of the system's bodies, whose magnitude can be calculated when multiplied by mass, damping and stiffness, respectively. These three are considered to be the building blocks of mechanical systems, in much the same way that inductance, capacitance and resistance (L, C and R) are the building blocks of

electronic circuits. Of the three building blocks that make up the systems in structural dynamics, mass and stiffness are conservative, meaning that they can only store, or conserve, energy. Systems containing only mass and stiffness are therefore known as conservative systems. Damping, on the other hand, is a phenomenon during which energy is dissipated [2].

The damping capacity of a material is fundamental property for designing and manufacturing structural components in dynamic applications. Materials with high damping properties are very desirable due to their ability to suppress mechanical vibration and transmission of waves, thus decreasing noise and maintaining the stability of structural systems. Experimental and analytical characterization of damping is not easy, even with conventional structural materials, and the anisotropic nature of composite materials makes it even more difficult. Despite this fact, though, several test methods have been developed (**2.5.2.4** and **2.5.3**) to measure the damping performance in fibre-reinforced composites (FRC), since this type of material is of great interest to the industry and researchers. This interest comes from their properties, most important of which are the high strength to weight and stiffness to weight ratio. At the same time, the excellent material damping performance of FRC due to the viscoelastic characteristics of the polymer matrix, improve the dynamic performance of the structure [1]. It should be noted, though, that damping performance is compromised when the final FRC part is very light and stiff. This led researchers to examine the possibility of using FRC that offer enhanced damping performance, such as NF.

The following section delves in to details of the theory of damping and its measurement test methods.

2.5.1 Theory

2.5.1.1 Different damping modes

There are several types of damping, with viscous damping being the most common form. Viscous damping (**2.5.1.1.1**) is responsible for the energy that is lost during the fluid flow caused by the movement of the system. A typical example of viscous damping application is the damping used in vehicle's shock absorbers. Another type

of damping is the frictional one (**2.5.1.1.2**), which occurs when two objects rub against each other. The type of damping that dominates in composites is called hysteretic damping (**2.5.1.1.3**), which is caused by the deformation of structural parts.

2.5.1.1.1 Viscous damping

When mechanical systems vibrate in a fluid medium such as air, gas, water, oil etc. the resistance offered by the fluid to the moving body causes energy to be dissipated. The amount of energy dissipated depends on many factors such as the size and shape of the vibrating body, the viscosity of the fluid, the frequency of vibration, and the velocity of the vibrating body. In viscous damping, the damping force is proportional to the velocity of the vibrating body.

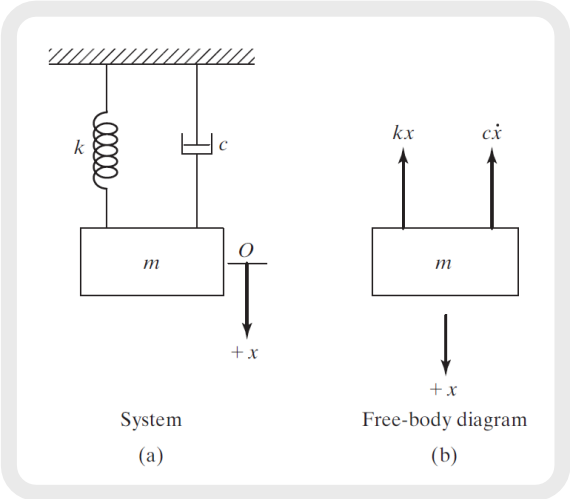

Figure 2-9: Single-degree-of-freedom system with viscous damper [4]

Viscous damping force can be expressed by **eq. (2-1)**:

$$\boldsymbol{F = -c\dot{x}} \qquad \textbf{(2-1)}$$

where c is a constant of proportionality and $\dot{x}$ is the velocity of the mass shown in **Figure 2-9**.

When the single spring mass system undergoes free vibration, the equation of motion becomes

$$\boldsymbol{m\ddot{x} + c\dot{x} + kx = 0} \qquad \textbf{(2-2)}$$

where m is the oscillating mass, x, $\dot{x}$ and $\ddot{x}$ are the displacement, velocity and acceleration of the mass, respectively, and c and k are the constants of the damper and the spring, respectively.

This is a linear, second-order, homogenous (because all terms are of the same kind), differential equation and it can be solved by trial [2]. Assuming a solution of the form $x = e^{st}$, we have the eigen or the characteristic equation of the system as

$$\boldsymbol{ms^2 + cs + k = 0} \quad \textbf{(2-3)}$$

The solution of **eq. (2-3)** is:

$$\boldsymbol{x = e^{-\frac{c}{2m}t}\left(Ae^{\sqrt{\left(\frac{c}{2m}\right)^2-\frac{k}{m}}t} + Be^{-\sqrt{\left(\frac{c}{2m}\right)^2-\frac{k}{m}}t}\right)} \quad \textbf{(2-4)}$$

where A and B are arbitrary constants depending on how the motion is started.

It is observed that the behaviour of the damped system depends on the numerical value of the radical in the exponential of **eq. (2-4)**. As a reference quality, a critical damping c_c is defined which reduces this radical to zero

$$\boldsymbol{\left(\frac{c_c}{2m}\right)^2 - \frac{k}{m} = 0} \quad \text{or} \quad \boldsymbol{c_c = 2\sqrt{km} = 2m\omega_n} \quad \textbf{(2-5)}$$

where $\boldsymbol{\omega_n}$ is the natural circular frequency of the system $\boldsymbol{\omega_n = \sqrt{k/m}}$

An important parameter to describe the damping behaviour is damping ratio ζ, a non-dimensional ratio defined as

$$\boldsymbol{\zeta = \frac{c}{c_c} = \frac{c}{2m\omega_n}} \quad \textbf{(2-6)}$$

Based on the value of damping ratio, the motion of the mass in **Figure 2-9** can be divided into the following three cases: (1) Oscillatory motion when $\zeta < 1.0$; (2) Nonoscillatory motion when $\zeta > 1.0$ and (3) Critical damped motion when $\zeta = 1.0$. In last case, the general solution of the system is $x = (A + Bt)e^{-\omega_n t}$.

Viscous damping can be used whatever the form of the excitation. The most common form of viscous damping is the Rayleigh-type damping given by

$$\boldsymbol{c = \alpha M + \beta K} \quad \textbf{(2-7)}$$

where α is the mass proportional Rayleigh damping coefficient, β is the stiffness proportional Rayleigh damping coefficient, M is the system structural mass matrix and K is the system structural stiffness matrix.

2.5.1.1.2 Coulomb or Frictional Damping

When there is sliding between two or more dry surfaces, Coulomb or frictional damping is used to quantify the energy that is dissipated. The damping force is equal to the product of the normal force, N, and the coefficient of friction μ and is assumed to be independent of the velocity, once the motion is initiated.

It should be noted that the equation changes (±, $A_{1,3}, B_{2,4}$) every half-cycle interval because of the fact that the damping force is always opposite to that of the velocity:

$$\boldsymbol{m\ddot{x} + kx = \pm\mu N} \tag{2-8}$$

This is a second order non-homogeneous differential equation. The solution can be expressed as

$$\boldsymbol{x(t) = A_{1,3} cos\sqrt{\frac{k}{m}}t + B_{2,4} sin\sqrt{\frac{k}{m}}t \pm \frac{\mu N}{k}} \tag{2-9}$$

where t is time.

2.5.1.1.3 Hysteretic or Structural Damping

In general, damping materials are polymers (synthetic rubbers) that are suitably formulated to yield high damping capacities in the frequency and temperature ranges of interest. This wide use of polymers is due to their relatively high deformations during service, which cause energy to be absorbed and dissipated by the material itself. The effect is based on the friction between the internal planes, which slip or slide as the deformations take place. When a structure made of damping materials is subjected to vibration, the stress-strain diagram shows a hysteresis loop. Therefore, the structural damping is also called hysteretic damping. The area of this loop denotes the energy lost per unit volume of the body per cycle due to the damping.

To explain the hysteretic damping, first the relationship between the response x and excitation force for viscous damping must be reviewed. For a harmonic motion, $x = Xsin\omega t$, the relationship between them is

$$\begin{aligned} \boldsymbol{F(t)} &= \boldsymbol{kXsin\omega t + cX\omega cos\omega t} \\ &= \boldsymbol{kx \pm c\omega\sqrt{X^2 - (Xsin\omega t)^2}} \\ &= \boldsymbol{kx \pm c\omega\sqrt{X^2 - x^2}} \end{aligned} \tag{2-10}$$

It can be shown that ΔW in **eq. (2-11)** gives the energy dissipated in one vibration cycle which is the area of the loop in **Figure 2-10** [2].

$$\boldsymbol{\Delta W = \oint F\dot{x}dt = \int_0^{2\pi/\omega} (cX\omega\, cos\omega t + kX\, sin\omega t)(X\omega\, cos\, \omega t)dt = \pi\omega cX^2} \qquad \textbf{(2-11)}$$

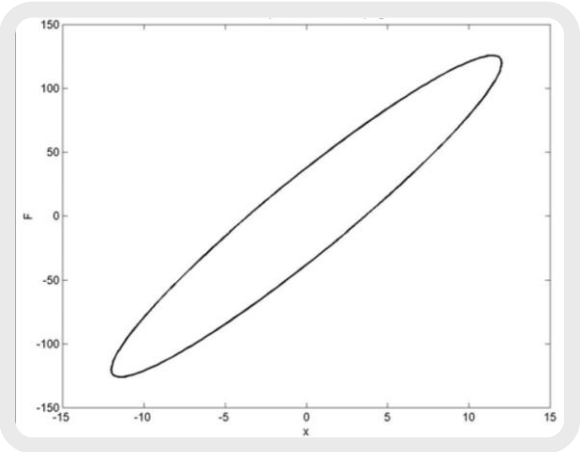

Figure 2-10: Loop for viscous damping (x axis: displacement *x*, y axis: force *F)* [47]

For the hysteretic damping, similarly, there is a hysteresis loop to be formed in the stress-strain or force-displacement curve in one loading and unloading cycle. It has been found experimentally that the energy loss per cycle due to internal friction is independent of frequency, but approximately proportional to the square of the amplitude. In order to achieve the observed behaviour from the equation above, the equivalent damping coefficient c_{eq} is assumed to be inversely proportional to the frequency as

$$\boldsymbol{c_{eq} = \frac{h}{\omega}} \qquad \textbf{(2-12)}$$

where h is a hysteretic damping coefficient.

Substitution of **eq. (2-12)** in **eq. (2-11)** results in the energy dissipated by the hysteretic damping in a cycle of motion.

$$\boldsymbol{\Delta W = \pi h X^2} \qquad \textbf{(2-13)}$$

2.5.1.2 Model of Damping Properties

2.5.1.2.1 Structural damping factor γ

Beside the viscous damping coefficient c, hysteretic damping coefficient h and the damping ratio ζ, there is another very important parameter, structural damping factor, to describe the property of the damping.

The forced motion equation of a single spring mass system with a hysteretic damper is

$$\boldsymbol{m\ddot{x} + c_{eq}\dot{x} + kx = f(t)} \quad \textbf{(2-14)}$$

For a harmonic problem ($x = Xe^{i\omega t}$), it becomes

$$\boldsymbol{m\ddot{x} + k\left(1 + i2\frac{\omega}{\omega_n}\zeta_{eq}\right)x = f(t)} \quad \textbf{(2-15)}$$

where $\zeta_{eq} = \frac{c_{eq}}{c} = \frac{h}{2m\omega_n\omega}$

For modal damping, $\omega = \omega_n$, therefore, we have

$$\boldsymbol{m\ddot{x} + k(1 + i\gamma)x = f(t)} \quad \textbf{(2-16)}$$

where $\gamma = 2\zeta_{eq} = {}^{h}/_{k}$ is called the structural damping factor or modal damping ratio.

For viscous damping, similarly, the viscous damping factor is $\gamma = 2\zeta$

2.5.1.2.2 Complex stiffness

The effect of polymer material on the damping of the whole structure is influenced by the material stiffness as well as by its damping. These two properties are quantified by the complex Young's modulus $E(1 + i\eta_E)$ or the complex shear modulus $G(1 + i\eta_G)$. η_G and $\eta_E$are usually assumed to be equal for a given material.

When the material is subjected to cyclic stress and strain with amplitude σ_0 and ε_0, the maximum energy stored and dissipated per cycle in a unit volume are:

Maximum energy stored per cycle = $\frac{E\varepsilon_0^2}{2}$

Energy dissipated per cycle = $\pi E\eta\varepsilon_0^2$

Compared to **eq. (2-16)** the complex stiffness $k(1+ih/k)$ is similar to the complex modulus $E(1+i\eta)$ or $G(1+i\eta)$. Defining the loss factor $\eta = h/k$, the complex stiffness can be expressed as $k(1+i\eta)$. η may vary from 2×10^{-5} for pure aluminum to 1.0 for hard rubber. The structural damping factor γ is equivalent to loss factor η. Loss factor is a term used to quantify damping performance.

A physical interpretation of the loss factor can be obtained as follows. The energy dissipated per cycle for a structural damped system is

$$\boldsymbol{\Delta W = \pi h X^2 = \pi \eta k X^2 = 2\pi\eta \times \frac{1}{2} k X^2 = 2\pi\eta U_m} \qquad \textbf{(2-17)}$$

where U_m is the maximum strain energy stored. Therefore, we have [47]

$$\boldsymbol{\eta = \frac{1}{2\pi}\frac{\Delta W}{U_m} = \frac{1}{2\pi}\frac{energy\ dissipated\ per\ cycle}{maximum\ strain\ energy}} \qquad \textbf{(2-18)}$$

2.5.1.3 Measuring damping

The most commonly used methods of measuring damping are:

2.5.1.3.1 Logarithmic decrement

The logarithmic decrement is used for calculating the damping ratio ξ of the cantilever beam from the recorded acceleration time histories based on the following equation:

$$\boldsymbol{\xi = \frac{1}{2\pi j} ln\left(\frac{x_i}{x_{i+j}}\right)} \qquad \textbf{(2-19)}$$

where x_i is the peak acceleration of the i^{th} peak and x_{i+j} is the peak acceleration of the peak j cycles after i^{th} peak. [2], [48]

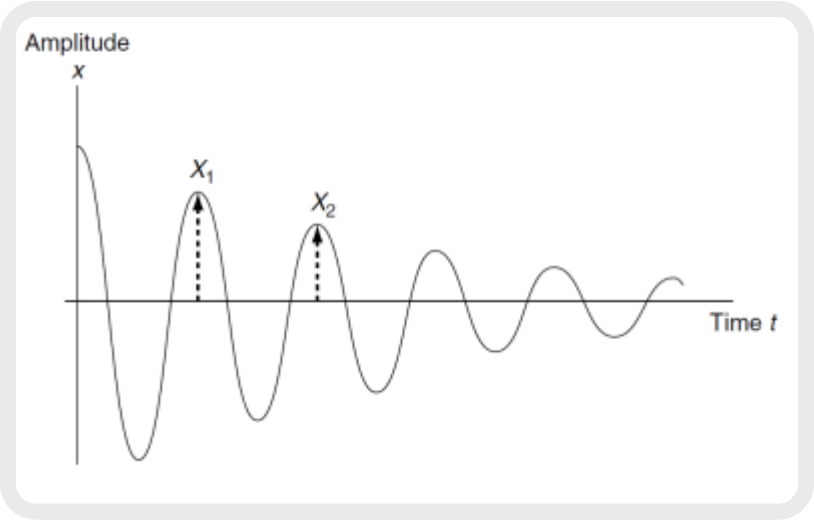

Figure 2-11: Displacement vs. time free oscillation graph [2]

2.5.1.3.2 Bandwidth technique

In the bandwidth technique

• The damped system is excited over a broad frequency range to accentuate various modes of vibration.

• The damping performance at each resonance frequency is obtained from the half-power bandwidth phenomenon at that frequency.

Mathematically this is expressed as:

$$\eta = \frac{\Delta f_n}{f_n} \tag{2-20}$$

where η is the loss factor, f is the resonance frequency and Δf_n is the bandwidth between points $3dB$ below resonance frequency.

Ψ, which is the specific damping capacity is related with η by the following equation:

$$\eta = \frac{\Psi}{2\pi} \tag{2-21}$$

2.5.2 Damping in composites

The ideal combination of material properties is low density along with high damping capacity and good mechanical properties. When it comes to metals, these properties cannot be achieved as the microscopic mechanisms involved in internal friction (namely damping capacity) depend on the parameters that control mechanical strength [7]. So, additional damping has to be introduced on the metallic structures, normally at the expense of additional weight.

On the other hand, FRC exhibit superior damping behaviour than metals, due to their various energy dissipation sources: viscoelastic nature of matrix, interphase damping mechanism, damping due to damage (matrix cracks, fibres broken etc.), viscoplastic damping and thermoplastic damping [8]. Another advantage of FRC is that they can offer far more design versatility as damping capacity, along with other specific properties, can be tailored to meet specific structural requirements [6], [9].

2.5.2.1 Damping mechanisms in composites

The damping mechanisms of composite materials are completely different than conventional materials. The sources of energy dissipation in fibre-reinforced composites are [49]:

1. Viscoelastic properties of matrix and fibre: because of their viscous properties, composite materials have a time-dependent behaviour which enable them to dissipate energy.

2. Damping due to interphase: the interphase is the region adjacent to the fibre surface along the fibre length. Energy dissipation is due to the high shear strain in the interphase region.

3. Damping due to damage: frictional damping in the unbonded regions between fibre and matrix interface or delamination. Damping occurs because of energy dissipation in the area of matrix cracks.

4. Viscoplastic damping.

5. Thermoelastic damping: it is described as the coupling between the elastic deformation in the matrix and the temperature field. In any vibrating structures, the strain field causes a change in the internal energy such that compressed regions become hotter and extended regions become colder. Energy is dissipated because of the lack of thermal equilibrium. Thermoelastic damping is preponderant for metal composites.

2.5.2.2 Damping in Natural Fibres - Flax Fibres

As it was mentioned in section **2.1.5**, CFRP's high stiffness and low weight lead to poor damping performance. This characteristic, along with its high cost, environmental concerns and low recyclability led the engineers to examine new solutions, such as NF. FF is the NF that has gained popularity during the recent years. FF is cost-effective and offers specific mechanical properties comparable to those of GF [35]. In addition to this, Assarar et al. [39] in 2011 examined the influence of water ageing on both FF and GF and observed that the effects were similar on both types of fibres. Concerning damping, FF has been compared with both CF [10] and GF [41] and it was proven that FF has the best damping performance of all.

2.5.2.3 Damping in hybrid CF/FF composites

Although FF's damping characteristics have already been reported [10], [41] the only study known to the author in the area vibration of hybrid CF/FF composites is that conducted by Vanwalleghem's [15]. In this study shaker excited methods along with acoustic wave excited ones were used to examine the damping behaviour of FF and hybrid FF/CF specimens. The conclusion was that FF have potential in acting as a damping layer in hybrid composites.

2.5.2.4 Testing methods

Damping behaviour, especially in composites, is one of the most difficult material properties to measure and quantify. As far as testing goes, a great number of papers quantifying damping used impact hammer excitation method. Tathavadekar et al. [50], Hoksbergen et al. [51] and Rath and Sahu [52] tested square composite specimens that were clamped peripherally using impact hammer (**8.1.4A.2.3)**. However, in these cases, special jigs were required and large dimensions of

specimens meant that large amount of material was used. Also, the peripheral clamping had to be further tested in order to verify results, without compromising the specimen's integrity. Using similar equipment and theory, Etaati et al. [48], Nakalswamy [53], Senthil Kumar et al. [54] and Kim et al. [55] tested small composite strips (except Nakalswamy [53] who tested metallic specimens) by mounting them as cantilever beams. However, in these studies the mounting needed to be accounted for, along with the human error involved in impact hammer excitation method. The next most widely used methodology is CIM (**5.1**) using a shaker to excite the specimen. This method was used by Dowling et al. [56], Gupta et al. [57], Vanwalleghem [15] and Pereira et al. [58] to compare the output of CIM against other testing methods. More specifically, Vanwalleghem in his MSc thesis [15] examined the damping characteristics of a CF / FF bicycle frame and shaker excited methods was compared with acoustic wave excited methods. The study concluded that the latter gives more reliable results, since in the case of the shaker excited methods accelerometers were mounted on the specimens, which compromised the results. In the same study, impact hammer was used to excite specimens of different shapes and sizes, including the complete bicycle frame in order to obtain their mode shapes. Dowling et al [56] and Gupta et al. [57] compared the results obtained from Oberst beam (**8.1.4A.2.2**) method and CIM and concluded that there isn't any significant difference between the two methods. This similarity gives advantage to the CIM, as the testing apparatus is less complicated to setup. In addition to this, Oberst beam's specimen is excited magnetically, which means in case of composite specimen a ferromagnetic strip has to be adhered to the specimen compromising the material's damping behaviour. Pereira et al. [58] compared these two methods with the Seismic Response Method and the simply supported cantilever beam method. It was concluded that most of the results were similar, with the CIM giving reliable loss factor measurements. CIM has been gaining popularity among the researchers [59], [60], [61] during the last few years and International Organization for Standardization (ISO) has produced a standard using this method [62]. One of the advantages of using CIM is the potential to use the shaker for larger testing pieces, as Chortis et al. [63], [64] did on composite wind-turbine model blade.

2.5.3 Centre Impedance Method (CIM)

2.5.3.1 Theory

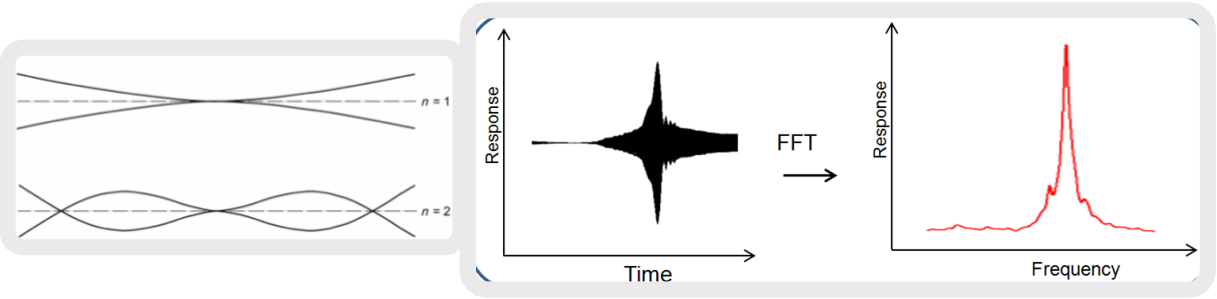

(a) (b)

Figure 2-12. (a) First two bending modes, (b) Fast Fourier Transformation on the acquired signal

CIM is based on ISO 16940 standard [62] and has been used before [56], [57], [59], [60], [61], [65], producing reliable results. In this method, the specimen is excited over a broad frequency range to accentuate the first two bending modes (**Figure 2-12(a)**). Applying Fast Fourier Transform (FFT) (**Figure 2-12(b)**) to the signal, the signal from the time space is transferred to the frequency space and the first two natural frequencies $\mathrm{f_{n_1}}$ and $\mathrm{f_{n_2}}$ are measured. In order to calculate the loss factor η half-bandwidth method was used, as shown in **Figure 2-13** [2]**,** [55], [62]. Having obtained the graph shown in **Figure 2-12 (b)** using FFT for each natural frequency, **equation (2-22)** is used:

$$2\zeta = \eta = \frac{\Delta f}{f_n} \qquad \textbf{(2-22)}$$

where Δf is the difference between the frequencies f_1 and f_2 corresponding to half power points which are the frequencies at half of the squared amplitude of the response (in our case acceleration, $\frac{\mathrm{A_{max}}}{\sqrt{2}}$) around the fundamental damped natural frequency, f_n. In the same equation, η is the loss factor and ζ is the damping ratio [55].

Duc et al. [10] used vibration beam testing (VBT) of cantilever beam specimens in order to determine the damping behaviour of the different materials. In this paper it was stated that VBT is a comparative testing, a statement which also applies to CIM test, as CIM is essentially simultaneous vibration testing of two cantilever beams.

This is due to the fact that the obtained results depend on a lot of parameters that have to be well defined and constant throughout all the different testing techniques, such as the geometry of the specimen, the exact position of the mounting and the load.

Since the vibration experiments were all performed under standard atmospheric pressure, the outcome of the response has to be examined as it may affected by aerodynamic resistance forces.

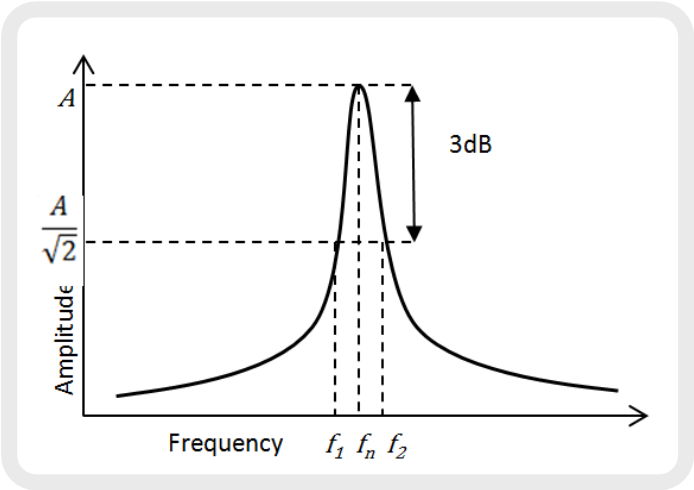

Figure 2-13. Half-bandwidth method

2.5.3.2 Air damping

According to the literature [21], [66], [67], [68], [69] air damping can be equal to the material damping for vibration amplitude to thickness ratio of two and could be up to six times higher than material damping as vibration amplitude increases. Therefore, the amplitude of the vibration was maintained low (less than 0.06mm) throughout the experiments. For relatively small amplitude:

$$\eta_{total} = \eta_{air} + \eta_{material} \quad \textbf{(2-23)}$$

Using **equation (2-24)**:

$$\eta_{air} = \frac{\rho_{air}}{\rho_{material}} \frac{w_{max}}{h} C_D \beta \quad \textbf{(2-24)}$$

where ρ_{air} and $\rho_{material}$ are the densities of the air and the composite, respectively, w_{max} is the maximum beam deflection, h is the beam thickness, C_D and

β are proportionality constants relating to the shape of the beam and the support condition, respectively [67].

2.6 Finite Elements Analysis

Finite Elements Analysis (FEA) software was used in order to model the different layups and simulate the three different test. The most important mechanical properties of the materials were acquired through testing and were used in LS-DYNA software. FEA's main aim was to be used as a tool for optimization of the mechanical performance of the layups and to develop material cards of the materials for further use in the CARBIO project. MAT_ENHANCED_COMPOSITE_DAMAGE(MAT_054) was used in modelling the material properties and mechanical behaviour [70], [71].

MAT_054 uses the Chang/Chang matrix failure criterion. It offers the ability to model arbitrary orthotropic materials, like the ones used in our simulations. Chang/Chang failure theory is used in MAT_054, which is given as follows (a=x axis, b=y axis):

- for the tensile fibre mode,

$$\sigma_{aa} > 0 \; then \; e_f^2 = \left(\frac{\sigma_{aa}}{X_t}\right)^2 + \beta\left(\frac{\sigma_{ab}}{S_c}\right) - 1 \begin{cases} \geq 0 & failed \\ < 0 & elastic \end{cases} \qquad \textbf{(2-25)}$$

$$E_a = E_b = G_{ab} = \nu_{ba} = \nu_{ab} = 0$$

- for the compressive mode,

$$\sigma_{aa} < 0 \; then \; e_c^2 = \left(\frac{\sigma_{aa}}{X_c}\right)^2 - 1 \begin{cases} \geq 0 & failed \\ < 0 & elastic \end{cases} \qquad \textbf{(2-26)}$$

$$E_a = \nu_{ba} = \nu_{ab} = 0$$

- for the tensile matrix mode,

$$\sigma_{bb} > 0 \; then \; e_m^2 = \left(\frac{\sigma_{bb}}{Y_t}\right)^2 + \left(\frac{\sigma_{ab}}{S_c}\right) - 1 \begin{cases} \geq 0 & failed \\ < 0 & elastic \end{cases} \qquad \textbf{(2-27)}$$

$$E_a = \nu_{ba} = 0. \quad \rightarrow G_{ab} = 0$$

- and for the compressive matrix mode,

$$\sigma_{bb} < 0 \; then \; e_b^2 = \left(\frac{\sigma_{bb}}{2S_c}\right)^2 + \left[\left(\frac{Y_c}{2S_c}\right)^2 - 1\right]\frac{\sigma_{bb}}{Y_c} + \left(\frac{\sigma_{ab}}{S_c}\right)^2 - 1 \begin{cases} \geq 0 & failed \\ < 0 & elastic \end{cases} \quad \textbf{(2-28)}$$

$$E_b = \nu_{ba} = \nu_{ab} = 0. \quad \rightarrow G_{ab} = 0$$

$$X_c = 2Y_c \quad for \; 50\% \; fibre \; volume$$

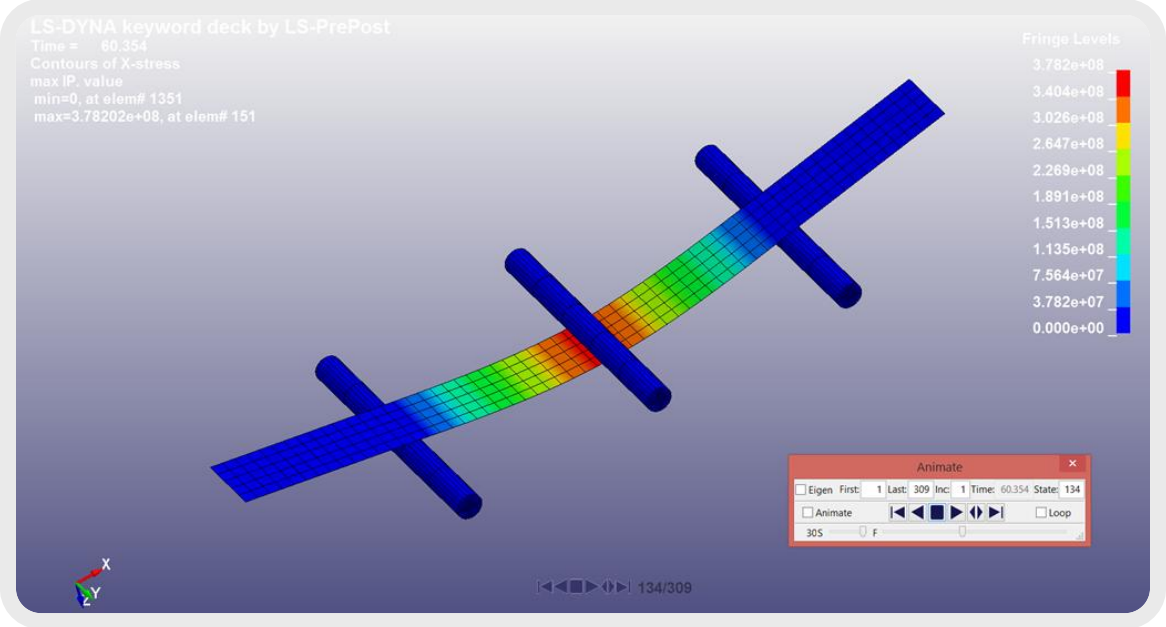

Figure 2-14. LS-DYNA 3 point bending simulation

2.7 Gap in Literature

After the study of existing work on NF it was understood that FF is the material mostly preferred due to its relatively easy and low-cost production and appealing mechanical properties [35]. Despite this fact, though, FF is relatively new in research in composites and most of the research has been focused on the special surface treatments of the fibres. This, also, explains the fact that hybrid CF/FF composites have not been extensively examined. The most important researches on hybrids are Vanwalleghem's [15], Dhakal et al. [42], Bagheri's [44], [45], [46] and Fiore's [43], of whom only the first one tested the damping properties of the materials.

Vanwalleghem [15] tested hybrid specimens only in vibrations examining the relation of the results of shaker excited methods with acoustic wave excited methods. Only one type of FF and hybrid composite was tested, of which limited information is given. It was concluded that acoustic wave method produced more reliable results than specific shaker methods used in the study, but since the setup was completed one week before the writing of the report no final conclusion was reported. Dhakal et al. [42] tested hybrid FF/CF specimens on water absorption, thermal and mechanical properties and concluded that hybrids were plausible and quite stable, offering an alternative to pure CF without dramatic effects on performance. Bagheri et al. [44], [45], [46] focused on the biocompatibility of the material, since the hybrid sandwich layup was tested for orthopaedic bone implant. In these papers a set of mechanical tests (tensile, flexural, fatigue) was performed along with biocompatibility tests, without examining the damping performance of the layup, concluding that the tested layup consisted of a promising solution for bone implant. Both Vanwalleghem [15] and Bagheri et al. [44], [45], [46] used FF unidirectional fabric. Fiore et al. [43] tested asymmetric hybrid layups replacing one layer of FF with one layer of CF in a six-layers layup and compared it with pure FF layup. In this study flexural and tensile tests results led to the conclusion that hybrid layup was stronger than pure FF layup.

All of the researchers mentioned above tested only one hybrid FF/CF layup and compared it with pure CF and FF layups. Fiore et al [43] and Dhakal et al. [42], however, tested two different types of FF. In these studies, though, the hybrid layups were asymmetric, which limited their applicability due to unbalanced mechanical performance [5]. Also, only Vanwalleghem [15] conducted damping tests without managing to complete the experimental setup in time, thus producing no final results. Finally, no FEA of hybrid layups was conducted in any of the studies.

2.8 Aim and Objectives

The aim of this study was to produce and examine hybrid CF/FF layups which would offer cost efficient solutions of enhancing the damping performance of a structure with low compromise in mechanical performance.

The objectives that were set in order to reach this aim were to:

- Understand the mechanics involved in vibrations and damping of composite parts by studying the existing literature.
- Set up an experiment to test composite parts in vibrations, in order to characterize different layups' properties.
- Produce a comprehensive database of mechanical and damping characteristics of CF, FF and optimise their performance by conducting a wide range of test procedures (tensile, 3-point bending, damping test).
- Model all the experimental procedures using FE, in order to compare different layup solutions and to optimize them.
- Produce material cards for FF and CF for further use in FEA for accurate simulations.

3 METHODOLOGY

3.1 Flow Chart

As it is shown in **Figure 3-1**, three different sets of specimens were tested. After each set of tests was completed, optimization through processing and FEA was completed. In **Figure 6-1, Figure 6-6** and **Figure 6-11** the three sets of specimens are listed. The aim of the first set was to derive the basic properties of CF and FF for the FEA material cards (viz. density, elastic modulus and tensile strength) and to compare two different layup solutions for the hybrid composite. After the best solution was chosen, the second set of experiments was conducted, which aimed at defining the best type of FF, along with examination of the bio-resin. Afterwards, having chosen the best type of FF to use and having acquired the basic properties for FEA, the optimized hybrid composite solution was tested during the third set of experiments. Along with that, a hybrid composite with bio-resin was tested and further tests for some additional properties (shear modulus, shear strength) were performed.

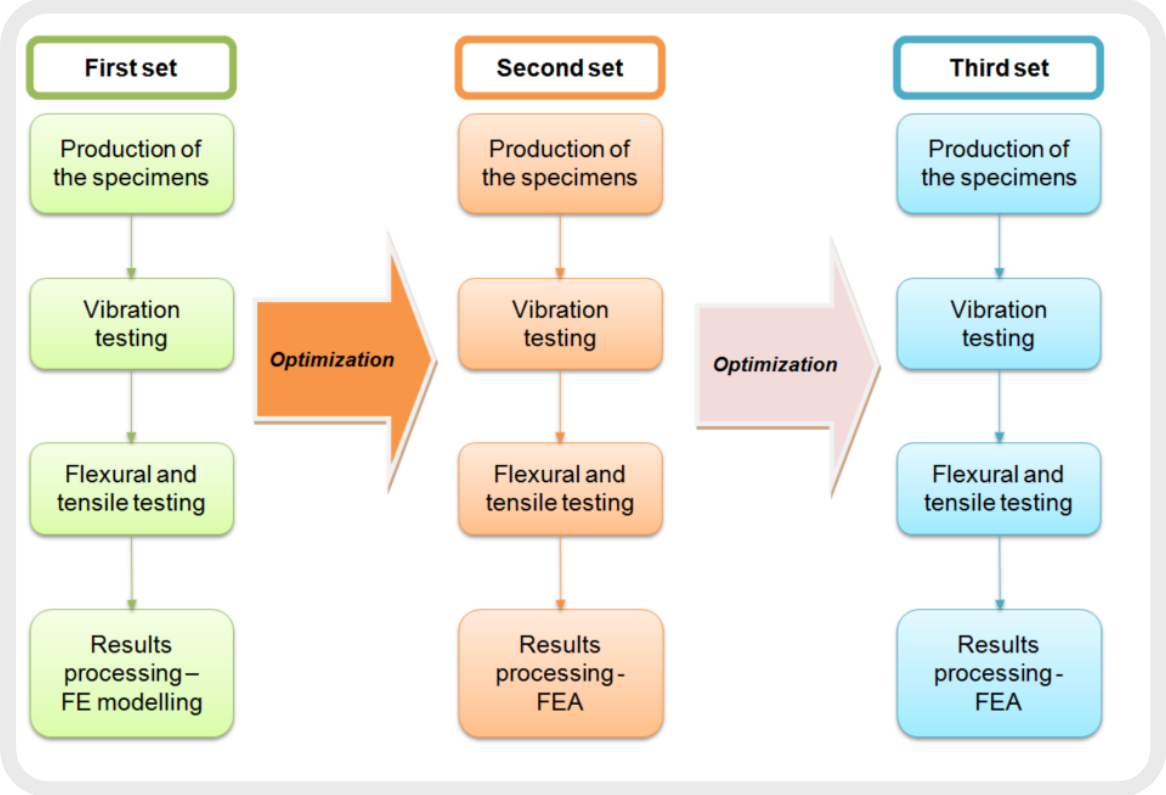

Figure 3-1. Flow chart (FE: Finite Elements, FEA: Finite Elements Analysis)

Figure 3-2 depicts the procedure that was followed for each test set. Since the damping experiment setup is non-destructive (see **5.1.1** for more info), to begin with, all the specimens were tested for damping characteristics. This is why their dimensions were based on damping test standard ISO 16940:2008 [62]. After that, five of them were tested on the tensile test machine (after tabbing the specimens) and the rest five on the flexural 3-point test jig (see **5.2** and **5.3** for more info).

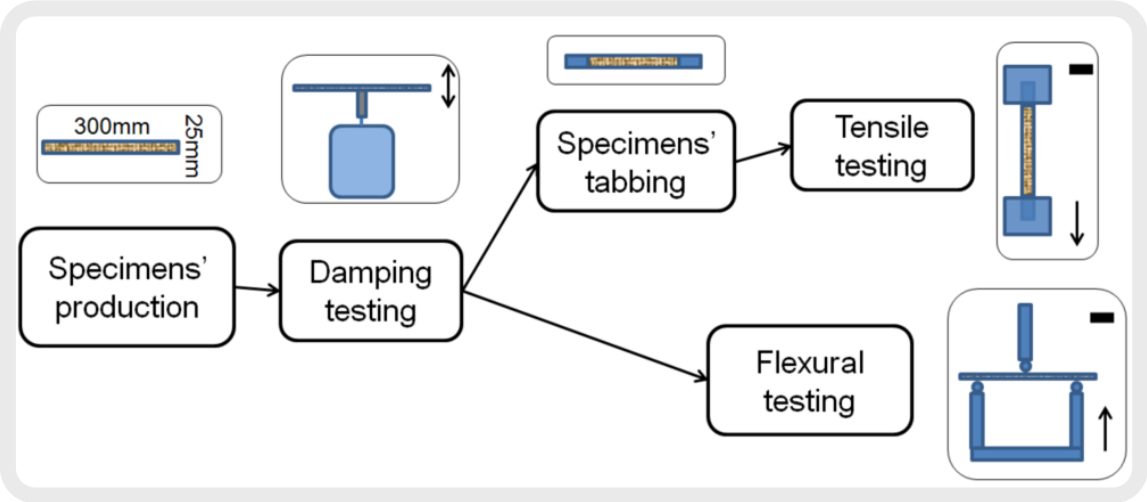

Figure 3-2. Test methodology

4 Materials

4.1 Fibre and Polymer Matrix for the experiments

4.1.1.1 Carbon Fibres

2/2 twill weave (TW) prepregs CF 3k T300 fabrics were used for the production of the specimens. The fabric average weight (FAW) of the fabric was 200 g/m^2 and the resin content was 42% by weight.

4.1.1.2 Flax Fibres

2/2 TW prepregs Biotex FF fabrics were used for the production of the specimens. The FF fabric was dried at 85^o C for 15 hours. The FAW of the fabric was 200 g/m^2 and 400 g/m^2 and the resin content was 50% by weight.

In the second set of experiments (**6.2**) FF 600gsm biaxial - Biotex Flax ±45 biaxial stitched non-crimp fabric was used, whose FAW was 600 g/m^2. Also, FF 275gsm unidirectional - Biotex Flax unidirectional fabric was used, whose FAW was 275g/m^2.

4.1.1.3 Epoxy Matrix

The epoxy resin used as a matrix was the MTC510 produced by SHD composites. The bio-resin DF250 was the same formulation with MTC510 but with the addition of 25% CNSL. It was produced by SHD composites. Both fabrics were prepregs, with resin percentage 42% by weight in CF and 50% in FF.

4.2 Composites Processing

All materials were stored at -18°C and were thawed for 24 hours prior to processing. Aluminium plates polished with Freekote 700 have been used as tools for the layup. The fabrics were cut in shapes, placed on an aluminium tooling plate and were closed with a second plate. The cure cycle was 85°C for half an hour and then 138°C for one and a half hours, both cycles at one and a half bars pressure.

4.3 Test sample set up

All tests were performed at room temperature (21°C) and under standard atmospheric pressure. The specimens were 300±2 mm long and 25±1mm wide. The tensile tests' specimens were tabbed with 0.8mm thick, 25 wide and 50mm long

aluminium tabs on both edges. Tabs were glued on the specimens using two-part epoxy glue which was cured at 60°C for four hours.

5 Experimental setup

5.1 Centre Impedance Method (CIM)

As discussed in **2.5.3** CIM is a viable option to quantify damping for composite specimens and to compare different solutions. CIM reliability has been proven in numerous occasions in research where it was used. In the following section the CIM setup that was used in this study is described.

5.1.1 Setup

Schematics of the test setup used in this study are shown in **Figure 5-2**, and the actual setup is shown in **Figure 5-3**. The impedance head (C) was glued at the middle of the specimen (D) (25 mm x 300mm), using cyanoacrylate glue and then mounted on the shaker's moving head. The shaker (B) was excited using a sine wave signal generator (A). The signal generated from the impedance head are collected from the sensor signal conditioner, which then transmits them to the signal acquisition system. DASYLab software was responsible for handling the data.

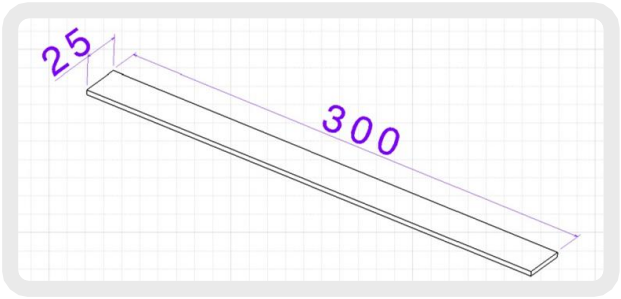

Figure 5-1. Specimen's dimensions in mm

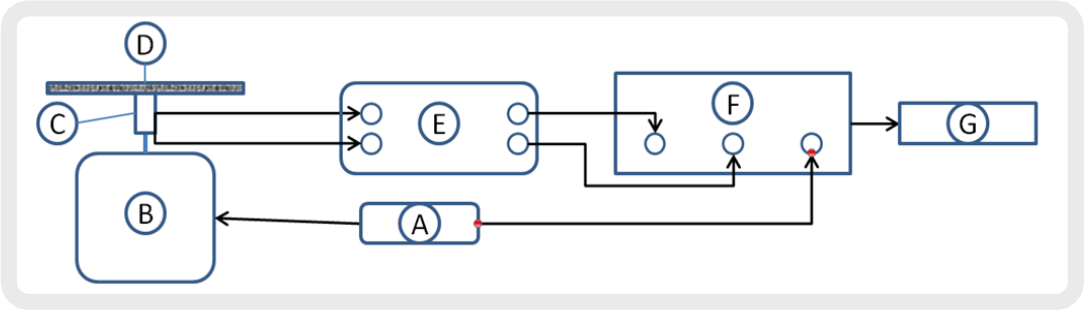

Figure 5-2. Damping test setup schematic: A) Signal Generator BlackStar Jupiter 2010, B) TMS Mini SmastShaker K2007E01, C) Impedance head PCB 288D01, D) Specimen, E) Sensor Signal Conditioner PCB 482C15, F) WaveBook/516 data logger, G) Personal Computer, DasyLab V8

(a) (b)

Figure 5-3. (a) CIM actual setup, (b) Data acquisition system

5.2 Tensile test

5.2.1 On-axis loading

100kN Mayes Instron testing machine was used for tensile test. The tests were performed according to ASTM D3039 [72]. Head displacement velocity was $1mm/min$ for all the specimens and 100kN load cell was used for the tensile tests. Laser extensometer *Electronic Instruments Research LE-05* was used to measure the strain of the specimen.

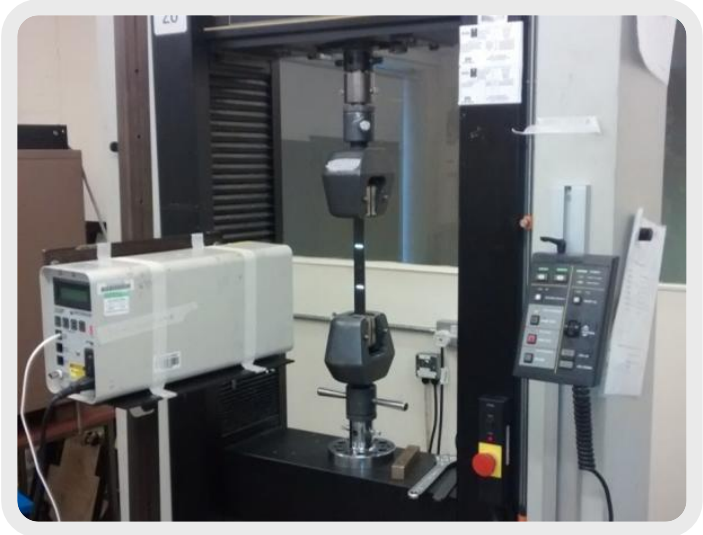

Figure 5-4. On-axis loading tensile test using Laser Electronic Instruments Research LE-05

After processing the results of the tensile tests obtained by following the procedure from ASTM D3039 [72] the tensile strength, F_{max}, the maximum tensile strain, ε_{max}, and the tensile modulus of elasticity,E was obtained.

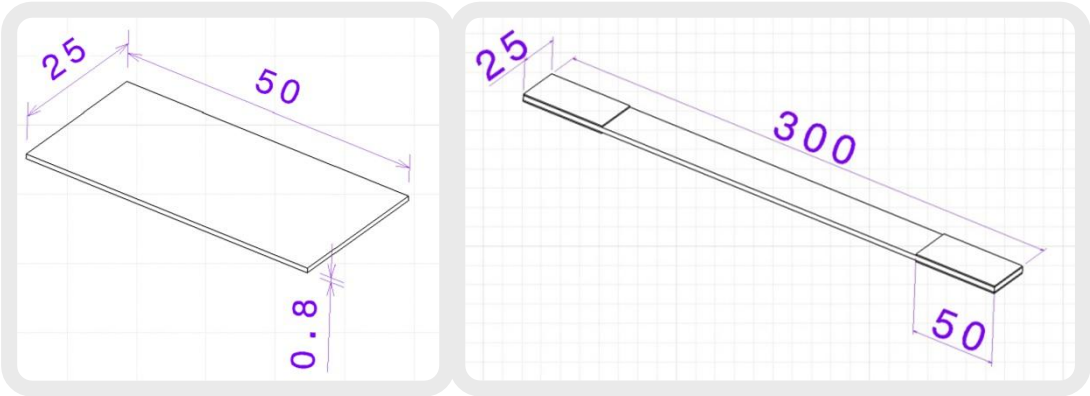

(a) (b)

Figure 5-5. (a) Tab's dimensions in mm, (b) Tabbed specimen's dimensions in mm

5.2.2 . Off-axis loading (45º)

The same testing machine was used for ±45º laminates tests in order to examine their in-plane shear response according to ASTM D3518 [73]. *Dantec Dynamics Digital Image Correlation (DIC) Q400* system was used to measure the x-axis and y-axis strain in order to calculate the shear strain. 100kN load cell was used during the tests.

Figure 5-6. Off-axis loading tensile tests using Dantec Dynamics DIC Q400 setup

After processing the results of the tensile tests obtained by following the procedure from ASTM D3518 [73] the flexural strength, $\sigma_{f(max)}$, the maximum flexural strain, $\varepsilon_{f(max)}$, and the flexural modulus of elasticity,E_f were calculated.

5.3 Flexural test

Flexural tests (3 point bending) were performed according to ASTM D790 [74] and BS ISO 14125 [75] on the same testing machine. As it is shown in **Figure 5-7,** the 3-point test jig consists of a reversed **Π** base on which the specimen is placed. The two supports are $10mm$ radius cylinders. The jig was moving upwards with its displacement rate being $15mm/min$, and the loading was applied on the specimen in the middle by a $10mm$ radius head. The span length was $160mm$. 30 kN load cell was used.

Figure 5-7. Flexural 3-point bending test

After processing the results of the tensile tests obtained by following the procedure from ASTM D790 and BS EN ISO 14125:1998 [74], [75] shear strength, $\tau_{12(max)}$, the maximum shear strain, $\gamma_{12(max)}$, and the shear modulus of elasticity, G_{12} were obtained.

5.4 Finite Elements Analysis

LS-DYNA software was used for FEA of the experimental procedures. LS-PrePost 4.2 was used during the modelling. FEA was used mainly for the comparison of the different solutions and optimization of the hybrid layups. At the same time, material cards were developed to be used for accurate simulations.

5.4.1 Layup modelling

LS-DYNA's ELEMENT_SHELL_OFFSET_COMPOSITE offers the ability to model the different layup of each specimen using the same model (surface). The only information it needs for each specimen is the number of the plies and each ply's thickness, material and orientation. In **Figure 5-8** (a) and (b) a 45º FE model orientation and layer's stack, respectively.

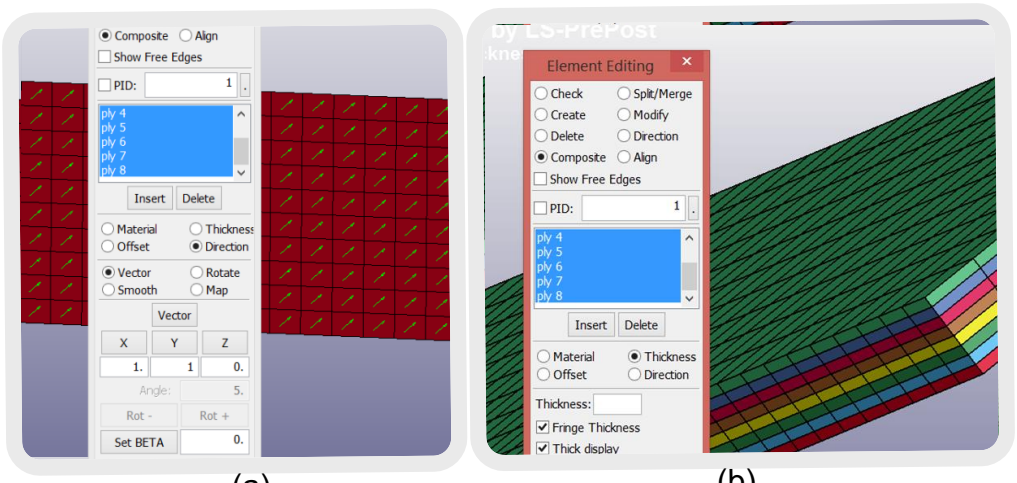

(a) (b)

Figure 5-8. (a) LS_DYNA FE model's 45º ply orientation and (b) stack of plies

5.4.2 FE models

5.4.2.1 Modal analysis model

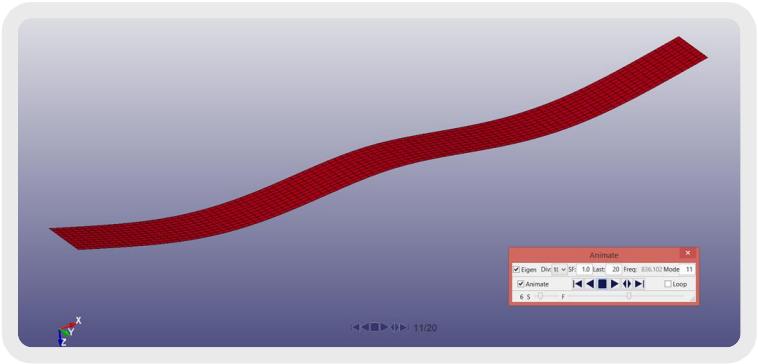

Figure 5-9. Modal analysis FE model (second bending mode)

In **Figure 5-9** the second bending mode of the modal analysis model is shown. Modal analysis model was used to simulate the damping tests, in which the first two bending modes were examined (**Figure 2-12 (a)**). In order to simulate the test setup as accurately as possible, a concentrated mass had to be modelled using mass nodes on the centre of the specimen, as shown in **Figure 5-10 (b)**. This mass is the sum of the impedance head and the shaker's moving element (see **8.1.4A.3** for more info).

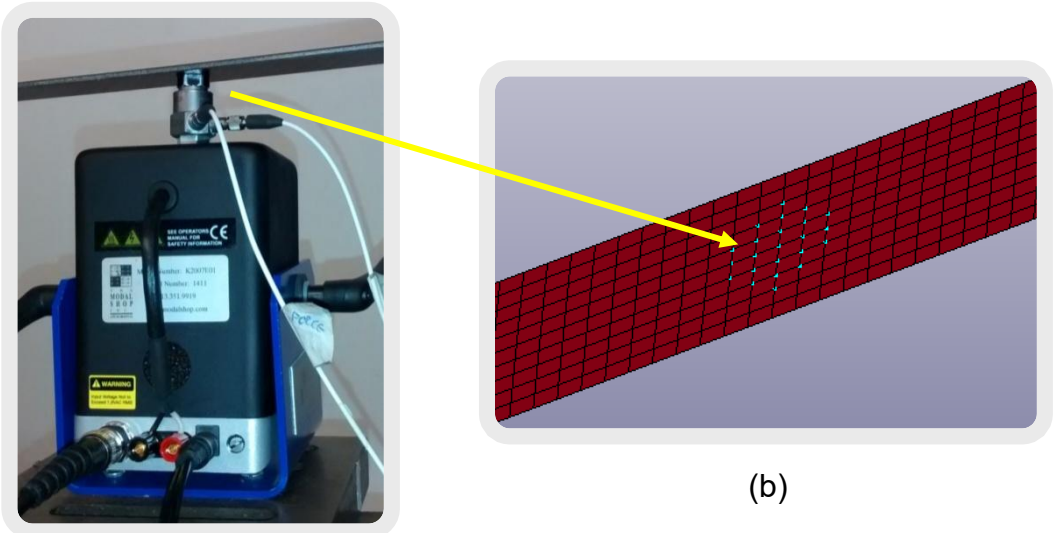

(a) (b)

Figure 5-10. (a) Actual damping test setup, (b) Mass nodes in modal analysis FE model

5.4.2.2 Tensile test FE model

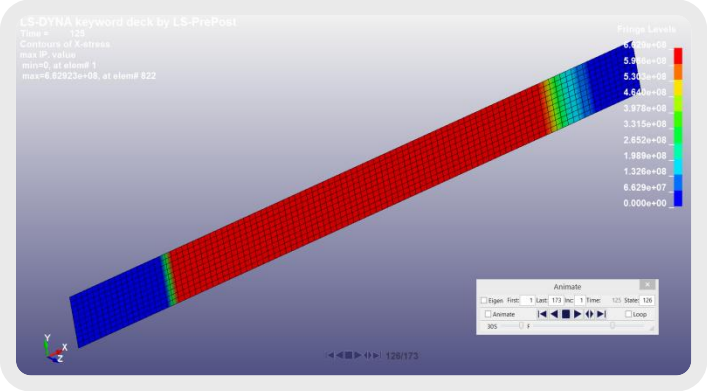

Figure 5-11. Tensile test FE model

In **Figure 5-11** the tensile test FE model is depicted. The model simulated the exact test parameters. Load was applied at the same rate (*1mm/min*). One end was clamped (left end in **Figure 5-11**) and on the other end the displacement was applied (right end in **Figure 5-11***).*

5.4.2.3 Flexural test FE model

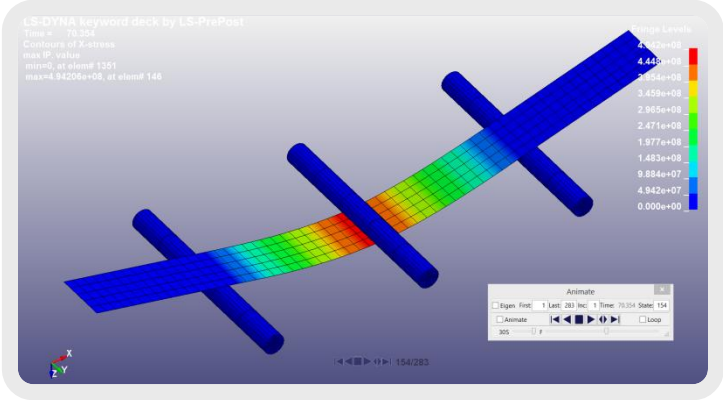

Figure 5-12. Flexural 3-point bending FE model.

In **Figure 5-12** the flexural test FE model is depicted. In order to simulate the loading of a 3-point bending test, three solid cylinders were used in the model. Two of them acted as supports of the specimen, with a span length of *160mm*, and the third one (the middle one in **Figure 5-12**) loaded the specimen with a displacement rate of *15mm/min*, as in the actual experiment.

6 RESULTS AND DISCUSSION

6.1 First set of experiments

- *FF: Flax Fibre 200gsm twill weave*
- *CF: Carbon Fibre 200gsm twill weave*

Resin used: Epoxy MTC 510

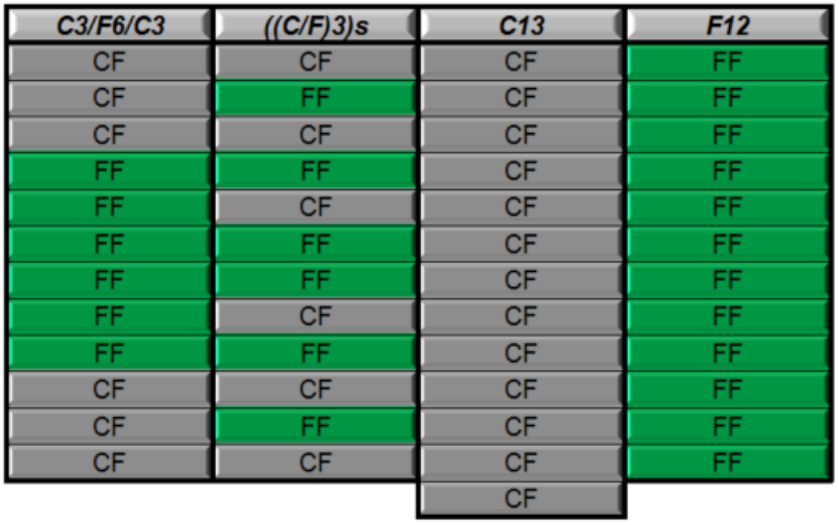

C3/F6/C3	((C/F)3)s	C13	F12
CF	CF	CF	FF
CF	FF	CF	FF
CF	CF	CF	FF
FF	FF	CF	FF
FF	CF	CF	FF
FF	FF	CF	FF
FF	FF	CF	FF
FF	CF	CF	FF
FF	FF	CF	FF
CF	CF	CF	FF
CF	FF	CF	FF
CF	CF	CF	FF
		CF	

Figure 6-1. Layups' abbreviations and materials of the first set of specimens

The four different layups tested during the first set of experiments are listed in **Figure 6-1,** and detailed information is shown in **Table 6-1.** In this set, pure CF and FF specimens were tested in order to establish the mechanical characteristics of the materials. In addition to this, knowing that CF specimens should have the lowest loss factor and FF the highest [10], the upper and lower limits of achievable damping performance were set. As it has been explained in section **5.1**, it should be noted that the thickness of the specimens was kept at similar levels (2.66mm -2.86mm, except F12 (3.24mm)), see **Table 6-1)**

Table 6-1. Information on first set of specimens (average values)

Abbreviations	*Thickness (mm)*	*Specimen's weight (gr)*	*Density (kg/m^3)*
C13	*2.86*	*31.9*	*1482*
F12	*3.24*	*32.8*	*1307*
C3F6C3	*2.66*	*28.7*	*1365*
((C/F)3)s	*2.69*	*28.7*	*1393*

6.1.1 Tensile tests

The results of the tensile tests are depicted in **Table 6-2** and **Figure 6-2**. The average stress-strain curves can be seen in **Figure 6-4 (b)**. As shown in **Table 6-2**, C3F6C3 has 52.1% higher tensile modulus than ((C/F)3)s, 6.5% higher tensile strength but 42.7% lower maximum strain. FF's hydrophilic nature [34] could be the explanation for the higher tensile modulus of C3F6C3, since $((C/F)_3)s$ has larger CF and FF interface surface than C3F6C3, which seems to make it weaker and unstable. F12 exhibits expected tensile behaviour, with greater maximum strain than all the other three. **Figure 6-2** shows the specific tensile modulus $E_{(sp)}$. C3F6C3's specific tensile modulus, $E_{(s)}$, is 26.9% lower than C13, but since C3F6C3 has 7.9% lower density than C13 the difference between them is smaller, but still significant.

Table 6-2. Tensile tests results of first set of specimens

Layup	*Elastic modulus E (GPa)*	*Max Stress F_{max} (MPa)*	*Max Strain ε_{max} (%)*
C13	*61.8 ± 3.6*	*664.3 ± 28.9*	*1.00 ± 0.06*
F12	*8.4 ± 1.8*	*117.6 ± 2.7*	*1.79 ± 0.15*
C3F6C3	*40.3 ± 4.0*	*335.3 ± 19.4*	*0.89 ± 0.07*
((C/F)3)s	*26.5 ± 6.4*	*314.7 ± 32.2*	*1.27 ± 0.38*

6.1.2 Flexural tests

The results of the flexural (3 point bending) tests are depicted in **Table 6-3** and **Figure 6-3**. In **Figure 6-4 (a)** the average load-displacement curves can be seen. As it was expected, C3F6C3 performs significantly better in flexural loading than the ((C/F)3)s having 32% higher flexural modulus E_f and 33.5% higher flexural strength. This can be explained by the fact that during the bending of the specimen the outer layers are the one that handle most of the stress of the loading, especially the layers at the bottom that are subjected to tensile loads [5]. In C3F6C3 specimens, three layers of carbon fibre are responsible for handling the loading, while in ((C/F)3)s there are two layers of CF and one of FF in the same place, which makes it weaker. Also, the larger CF and FF interface surface of $((C/F)3)_s$ seems to make it weaker in bending, as mentioned in the previous paragraph for tensile tests. In **Figure 6-3** specific flexural modulus $E_{f(s)}$ is examined. Due to its lower density, C3F6C3 shows larger $E_{f(s)}$ than C13 (2.5% higher).

Table 6-3. Flexural tests results of first set of specimens

Layup	*Flexural Modulus E_f (GPa)*	*Flexural Strength $\sigma_{f(max)}$ (MPa)*	*Max Displacement (mm)*
C13	*55.0 ± 3.6*	*786.3 ± 7.2*	*23.3 ± 0.4*
F12	*10.2 ± 1.4*	*119.8 ± 1.6*	*30.6 ± 0.3*
C3F6C3	*50.3 ± 5.2*	*504.9 ± 58.6*	*17.1 ± 2.7*
((C/F)3)s	*38.1 ± 3.7*	*378.1 ± 34.5*	*18.3 ± 0.6*

6.1.3 Damping tests

6.1.3.1 Air damping

As it was stated in **2.5.3.2,** the air effect on the damping of the specimen has to be calculated. In this study, the specimen was considered to behave as two cantilever beams of half-length of the actual specimen. Hence, the constants as quoted in the literature were used in calculations. The larger tip displacement was measured to be $0.2mm$ during the C13 experiments using a miniature piezoelectric accelerometer (PCB 352A24). So, assuming $\rho_{air} = 1.225\frac{kg}{m^3}$, $\rho_{material} = 1500\frac{kg}{m^3}$, specimen's thickness $h = 2.8\,mm$, $\beta = 1.98$ and $C_D = 2$ [67], [68], we have $\eta_{air} = 0.00023$ for each tip, which is two orders of magnitude lower compared to the lowest value of loss factor monitored. As a result, air damping wasn't taken into account in any of the experiments, including the other two sets.

6.1.3.2 Results

In **Figure 6-5 ((a), (b), (c) and (d))** the first two resonant frequencies and the corresponding loss factors are shown. For all the layups, second mode's loss factor is significantly lower than the 1st mode [55], [60]. Nevertheless, the same pattern was observed, with both C3F6C3 and ((C/F)3)s having loss factor that lie between C13 and F12 ones, with F12 having the highest amongst them. The fact that F12 has higher loss factor than C13 can be confirmed in literature, too [10]. Also, C3F6C3 shows slightly greater damping performance than ((C/F)3)s in both modes (14.3% higher in 1st mode and 13% higher in 2nd mode). As far as the resonant frequencies go, it is known that the bending mode resonant frequency depends mainly on the bending stiffness [2]. Hence, C13 has the highest value followed closely by C3F6C3.

((C/F)3)s follows them with noticeable gap between itself and C3F6C3, and F12 shows the lowest value. Also, is should be noted that the behaviour in bending vibrations performance (**Figure 6-5** (c) and (d)) and flexural performance (**Figure 6-3** and **Table 6-3**) follow the same pattern, which means that both test validate each other outputs

6.1.4 Brief discussion

After processing of the results of the first set of specimens, it was observed that the "sandwich" layup (layers of FF sandwiched between layers of CF placed on either side of them, such as C3F6C3) had better mechanical and damping performance than the "alternate" (alternate layers of CF and FF used, with two of FF in the middle). So, it was decided that only the "sandwich" layup would be examined further. This is why the second set of experiments was focused on testing different types of FF.

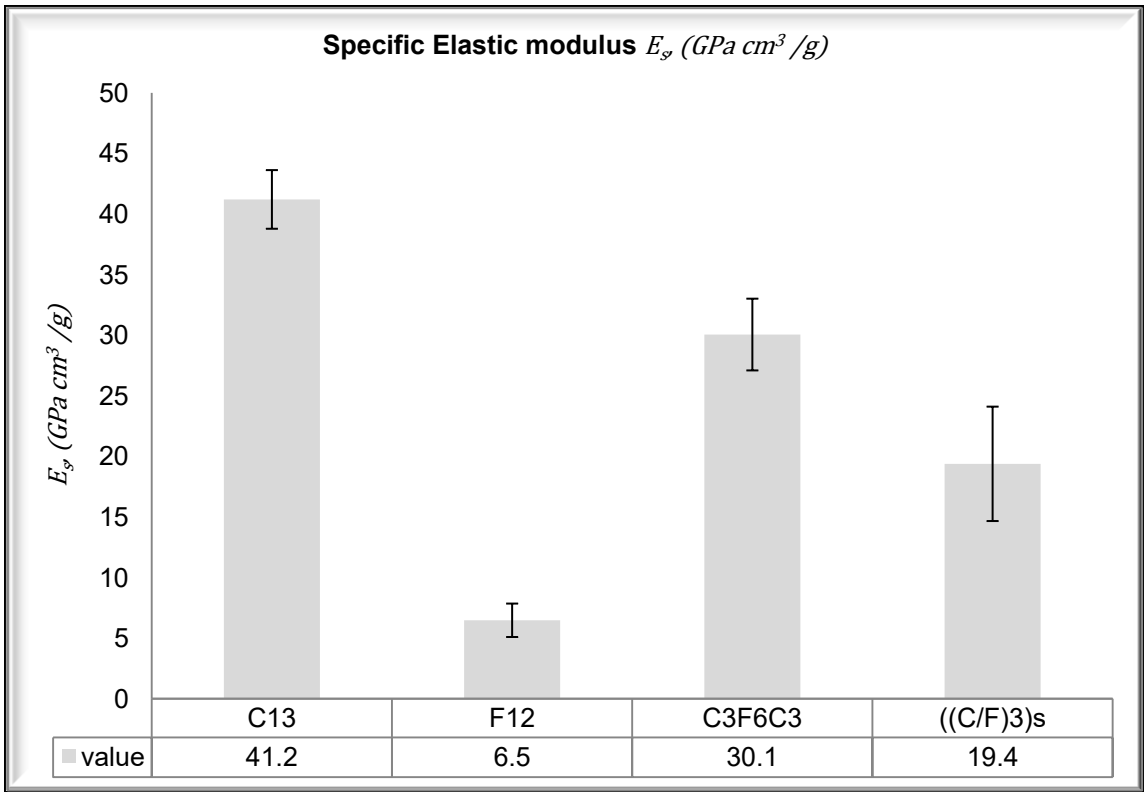

Figure 6-2. First set: Specific Elastic Modulus, E_s

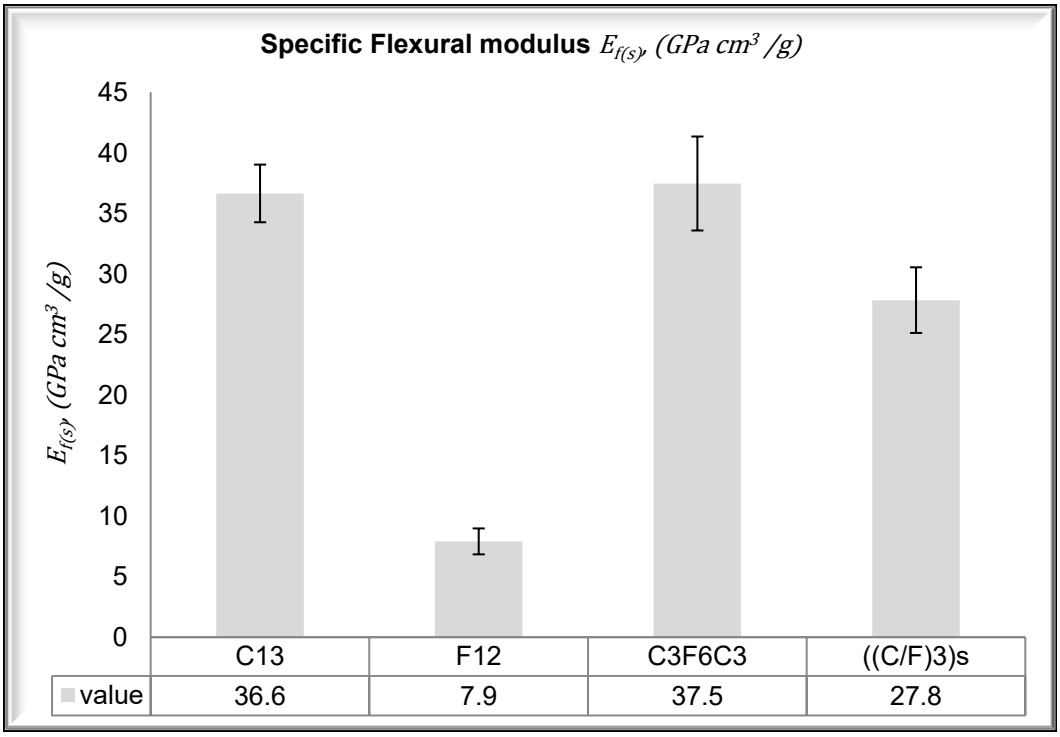

Figure 6-3. First set: Specific Flexural Modulus, $E_{f(s)}$

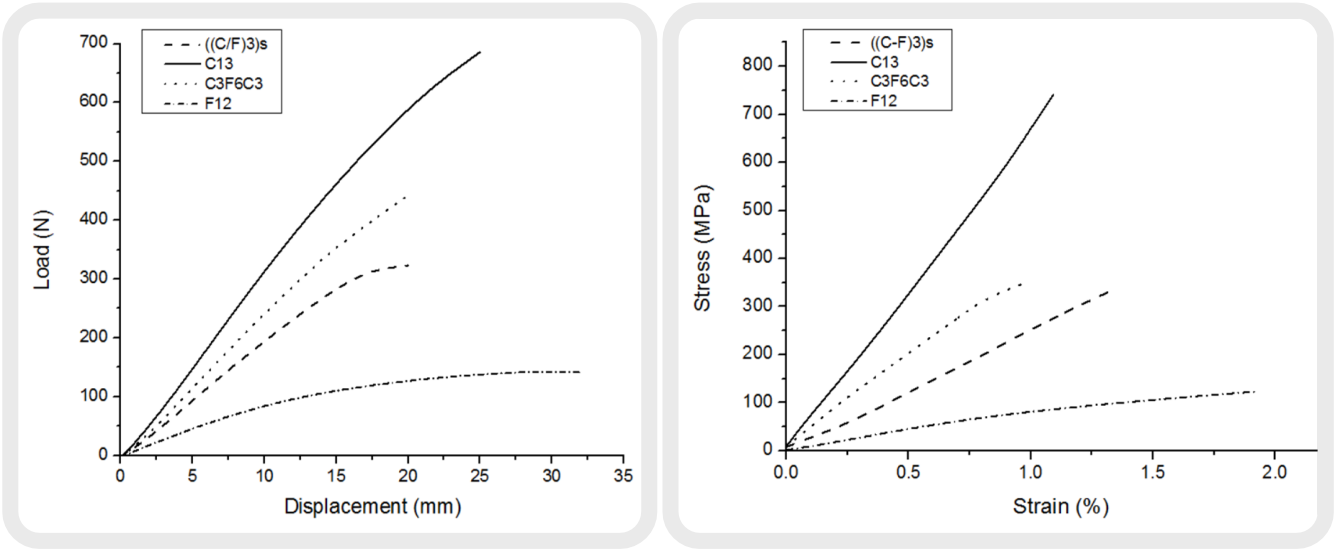

(a) (b)

Figure 6-4. First set: (a) Load vs. Displacement flexural testing curves, (b) Stress vs. Strain tensile testing curves

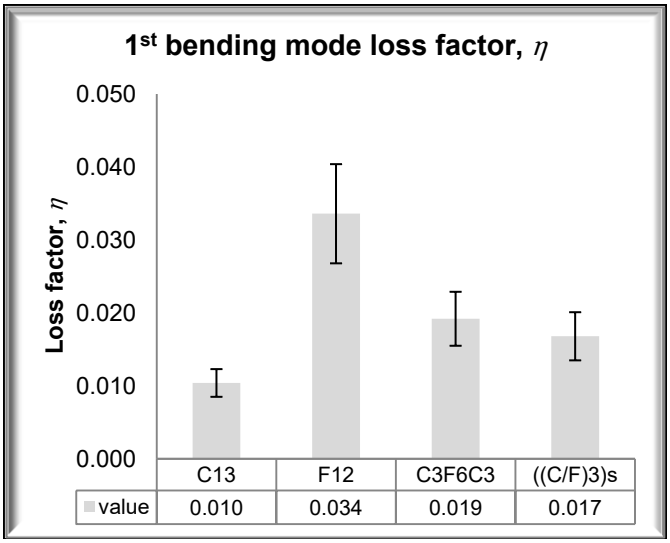

(a)

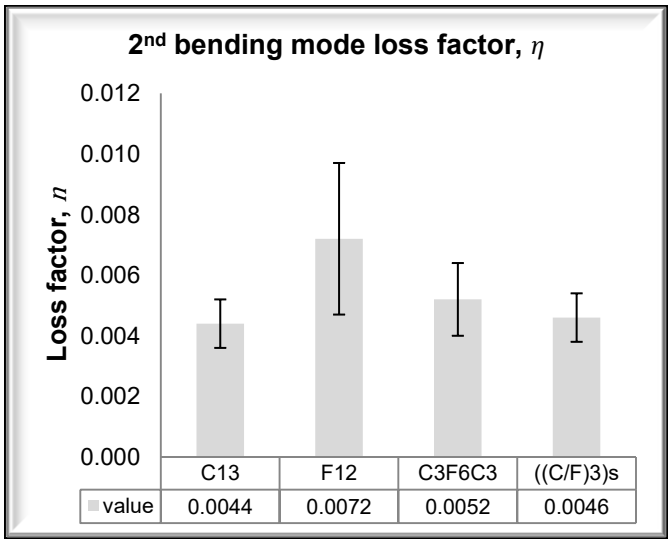

(b)

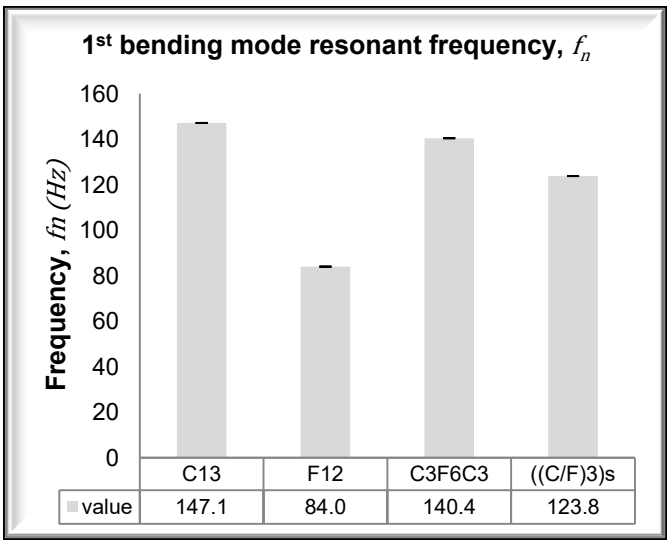

(c)

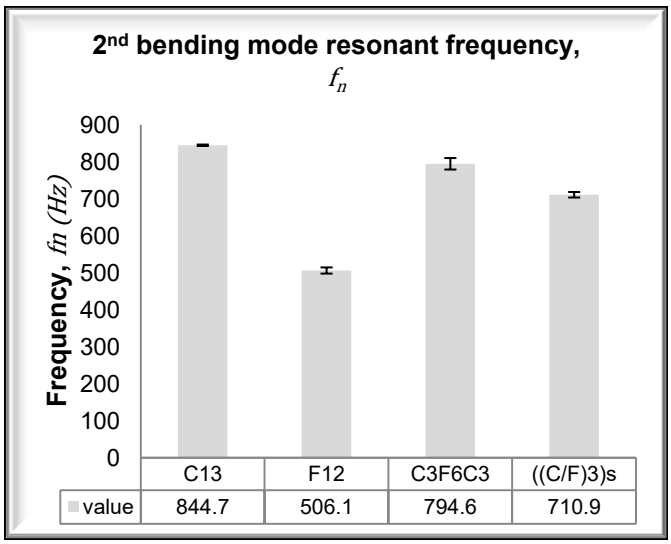

(d)

Figure 6-5. First set of experiments: (a) 1st bending mode's loss factor, (b) 2nd bending mode's loss factor, (c) 1st bending mode's resonant frequency, (d) 2nd bending mode resonant frequency.

6.2 Second set of experiments

- *FF_200: Flax Fibre 200gsm twill weave*
- *FF_400: Flax Fibre 400gsm twill weave*
- *FF_600_BIAX: Flax Fibre 600gsm biaxial*
- *FF_275_UD: Flax Fibre 275gsm unidirectional (ud)*

If DF exists in the abbreviation, bio-resin DF250 was used. If not, standard epoxy resin MTC510 was used

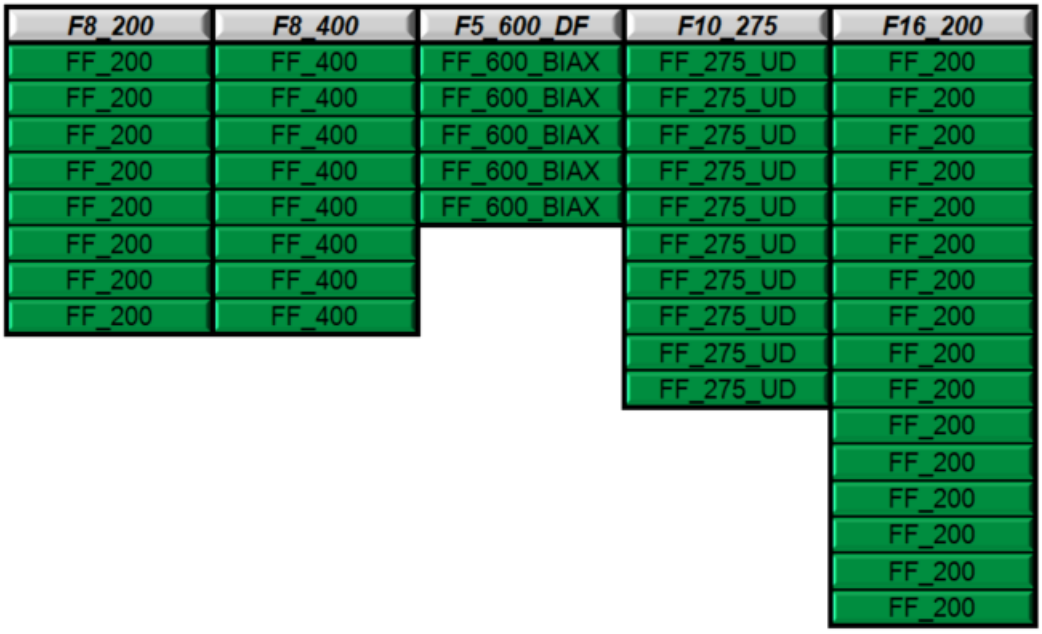

Figure 6-6. Layups' abbreviations and materials of the second set of specimens

In the second set of experiments different types of FF were tested. Also, the type of FF (200gsm twill weave) used in the 3mm thick samples was examined in two more layups in order to examine how thickness affects the damping performance of the specimen (**Figure 6-6** and **Table 6-4**). In F5_600_DF case bio-epoxy resin DF250 was used in order to have a first look on its performance.

Table 6-4. Information on second set of specimens (average values)

Abbreviations	*Thickness (mm)*	*Specimen's weight (gr)*	*Density (kg/m^3)*
F8_200	*2.30*	*21.4*	*1196*
F8_400	*3.86*	*39.0*	*1266*
F5_600_DF	*3.30*	*34.9*	*1376*
F10_275	*3.06*	*31.4*	*1342*
F16_200	*4.40*	*36.5*	*1058*

6.2.1 Tensile tests

The results of the tensile tests are depicted in **Table 6-5** and **Figure 6-7.** In **Figure 6-4 (b)** the average stress-strain curves can be seen. As it was expected, F10_275 (unidirectional 275gsm fabric) had the highest tensile modulus, almost double (99% higher) than the second best, which was F5_600_DF (biaxial 600gsm fabric). Also, F10_275 exhibits the highest max stress, 54.4% higher than F8_200. This high performance of F8_200 can be explained by the small number of layers (8 layers) compared to the F16_200 (16 layers), which means less imperfections which cause failure. Also, F8_400 was the first batch of FF 400gsm and the fabric was still under development, which explains its low performance. Concerning specific elastic modulus, the most noticeable performance was F16_200, since it comes third thanks to its low density. As far as max strain goes, F8_200 has the highest max strain, and F8_400 comes second best. The remaining three have much lower max strain (more than 25% lower).

Table 6-5. Tensile tests results of second set of specimens

Layup	*Elastic modulus E (GPa)*	*Max Stress F_{max} (MPa)*	*Max Strain ε_{max} (%)*
F8_200	*10.8 ± 0.9*	*138.7 ± 5.2*	*1.96 ± 0.33*
F8_400	*9.5 ± 0.8*	*70.8 ± 7.7*	*1.78 ± 0.42*
F5_600_DF	*11.6 ± 1.0*	*95.5 ± 5.8*	*1.07 ± 0.05*
F10_275	*23.1 ± 2.0*	*214.2 ± 15.6*	*1.16 ± 0.11*
F16_200	*9.3 ± 0.9*	*97.1 ± 2.9*	*1.32 ± 0.15*

6.2.2 Flexural tests

The results of the flexural (3 point bending) tests are depicted in **Table 6-6** and **Figure 6-8.** In **Figure 6-9 (a)** the average load-displacement curves can be seen. F10_275 exhibited the best flexural performance, with its flexural modulus being 39.6% higher than F5_600_DF. This performance can be explained by the superior mechanical characteristics of unidirectional fabrics than biaxial and twill weave fabrics [5]. The remaining three show similar performance, but quite lower than F10_275 (more than 51.3% lower), with F16-200 having the lowest flexural modulus. Similar pattern was noticed in specific flexural modulus, with F10_275's and F5_600's being the two highest, and the rest were even more balanced due to their slight differences

in densities. The most noticeable results in max displacement was F10_275's, which is quite high (third highest, 6.1% lower than F8_200), considering that it performed the lowest max strain in the tensile tests (see **Table 6-5)**.

Table 6-6. Flexural tests results of second set of specimens

Layup	*Flexural Modulus* E_f *(GPa)*	*Flexural Strength* $\sigma_{f(max)}$ *(MPa)*	*Max Displacement* (mm)
F8_200	*11.3 ± 0.4*	*83.8 ± 4.9*	*31.2 ± 3.3*
F8_400	*11.5 ± 0.4*	*137.2 ± 10.9*	*29.4 ± 2.8*
F5_600_DF	*16.9 ± 1.3*	*180.6 ± 14.5*	*24.4 ± 0.9*
F10_275	*23.6 ± 1.9*	*226.9 ± 12.6*	*29.3 ± 0.5*
F16_200	*10.3 ± 1.1*	*116.5 ± 2.0*	*23.7 ± 0.9*

6.2.3 Damping tests

In **Figure 6-10 ((a), (b), (c) and (d))** the first two resonant frequencies and the corresponding loss factors are shown. F8_200 showed the highest damping performance, with its loss factor being 0.028. The rest four had similar performance, with the highest loss factor among them being the F5_600_DF's. The most interesting outcome of the damping test was the comparison of the damping properties of FF 400gsm with those of FF 200gsm. As it was mentioned before (see **5.1**) thickness affects the loss factor. So, in order to make a fair comparison of the loss factor of different materials, specimens of the same thickness must be tested. Since this was not completely achievable in composites, and especially in NF, in this case three different layups of FF 200gsm were tested (F8_200, F12_200 and F16_200) with their thicknesses being 2.3mm, 3.24mm and 4.4mm, respectively (these experiments, also, provided results concerning the thickness and how it affects the loss factor). So, a fair assumption was to compare the average loss factor of F12_200 and F16_200 with the one of F8_400 (3.86mm thick), which was thicker than the first and thinner than the second. In this case, F8 400's loss factor was 0.018, 27.4% lower than the average of F12_200 and F16_200. This can be explained by the higher number of layers of 200gsm layups and the thicker weave of the 400gsm fabric. These two characteristics meant that during the vibrations less energy was dissipated due to less imperfections, leading to lower loss factor (**eq. (2-17)**). Similar behaviour was

noticed in 2nd bending mode loss factor among all the specimens except F10_275 which have the lowest loss factor of all. Concerning the resonant frequencies, F16_200 was the highest, due to its highest thickness. F10_275, F5_600_DF and F8_400 follow with very small difference among them (9.8% the highest difference) and F8_200 had the lowest frequency due to its lowest thickness. The same pattern was followed in both modes.

6.2.4 Brief discussion

Considering the results of the first and the second set of experiments, the decision to prefer FF 400gsm rather than FF 200gsm was made. This decision was based on the fact that since the "sandwich" layup was chosen, the thickness of the flax layers was the most important factor during its design. Bearing in mind that, FF 400gsm offers the advantage of achieving the same thickness with smaller number of layers, which means less labour costs. In addition to that, despite the fact that FF 400gsm had lower flexural specific modulus (10.5% lower) and tensile specific modulus (22.3% lower), the effect on the final "sandwich" layups was insignificant, since it was used along with CF whose mechanical properties were dominant. Finally, the aforementioned arguments made the fact that FF 400gsm had lower loss factor than FF 200gsm obsolete, since it is still higher than CF's (80% higher).

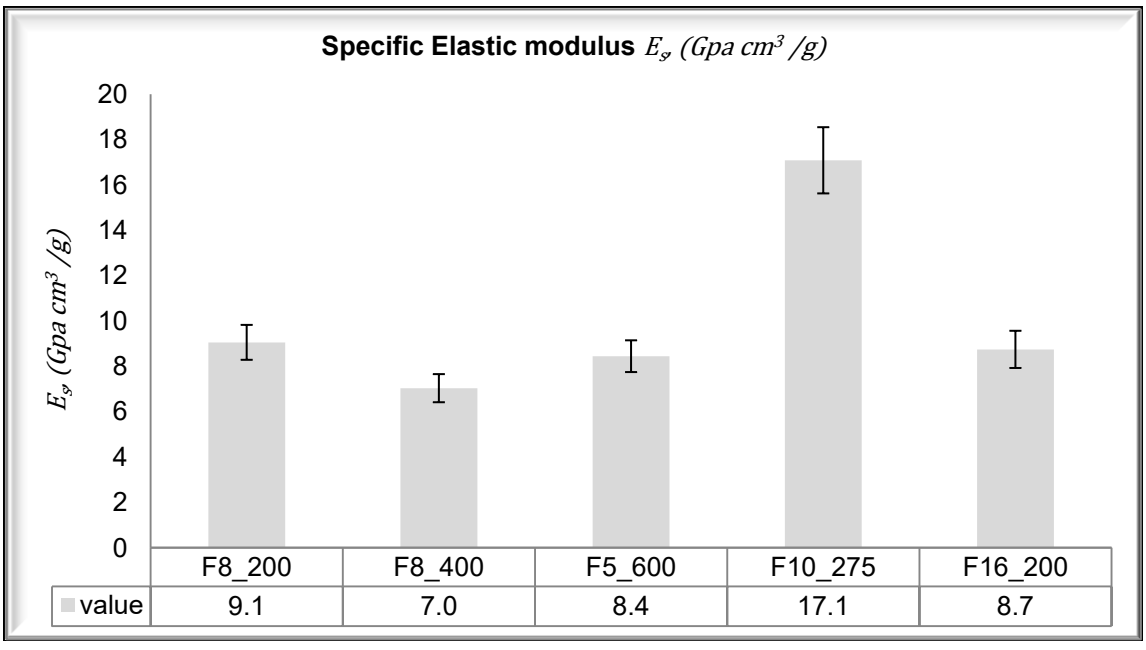

Figure 6-7. Second set: Specific Elastic Modulus, E_s

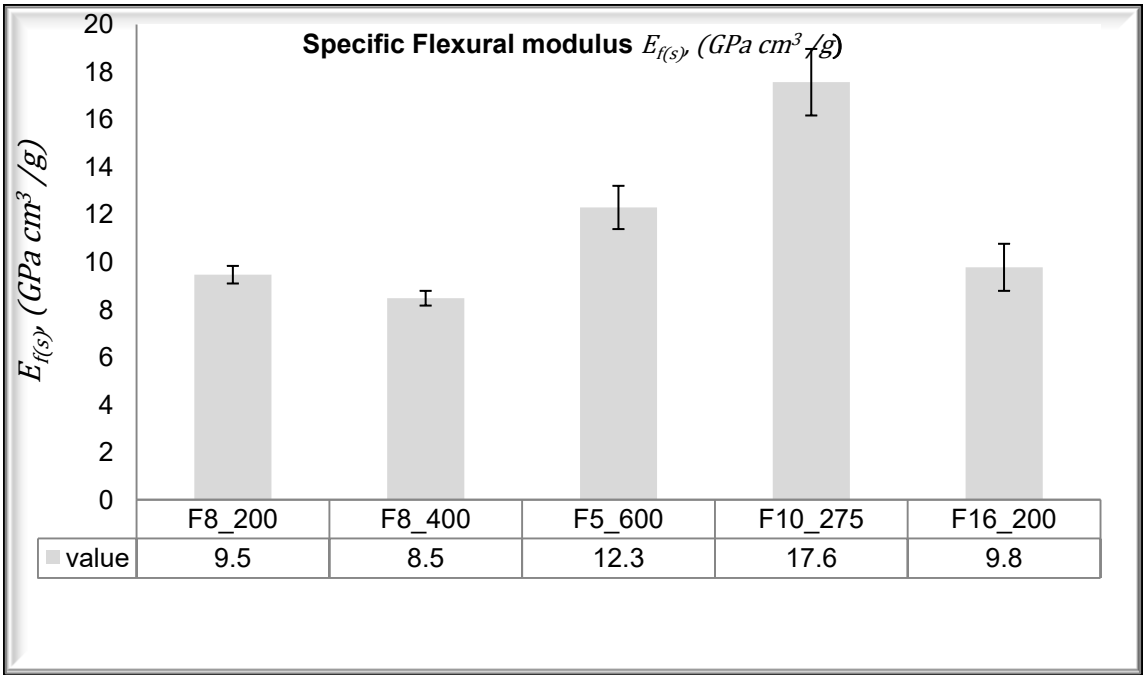

Figure 6-8. Second set: Specific Flexural Modulus, $E_{f(s)}$

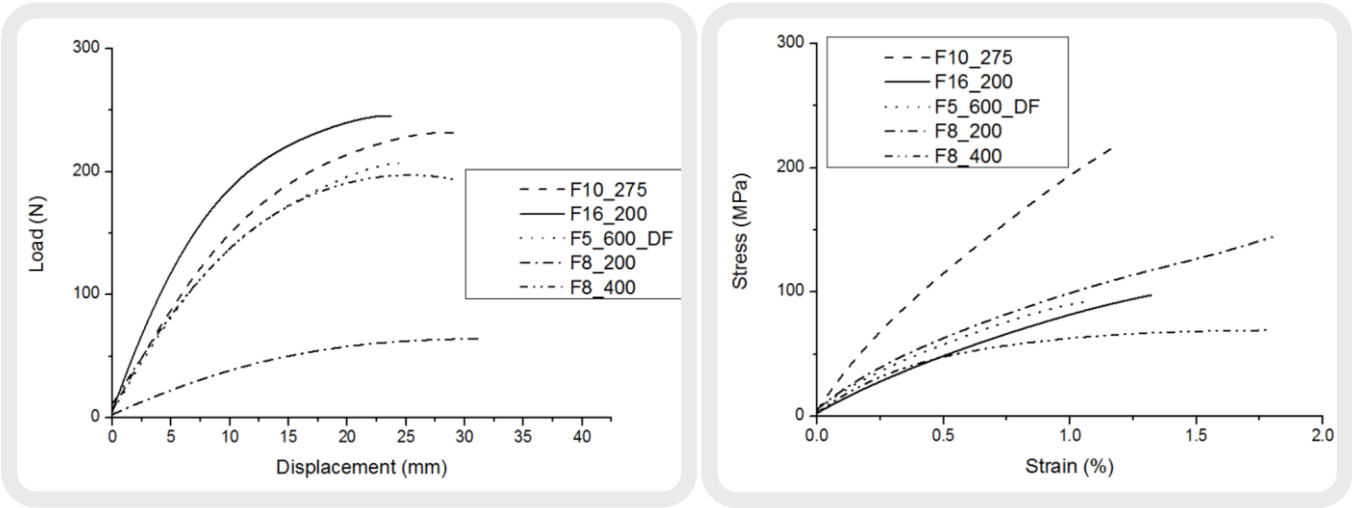

(a) (b)

Figure 6-9. Second set: (a) Load vs. Displacement flexural testing curves, (b) Stress vs. Strain tensile testing curves

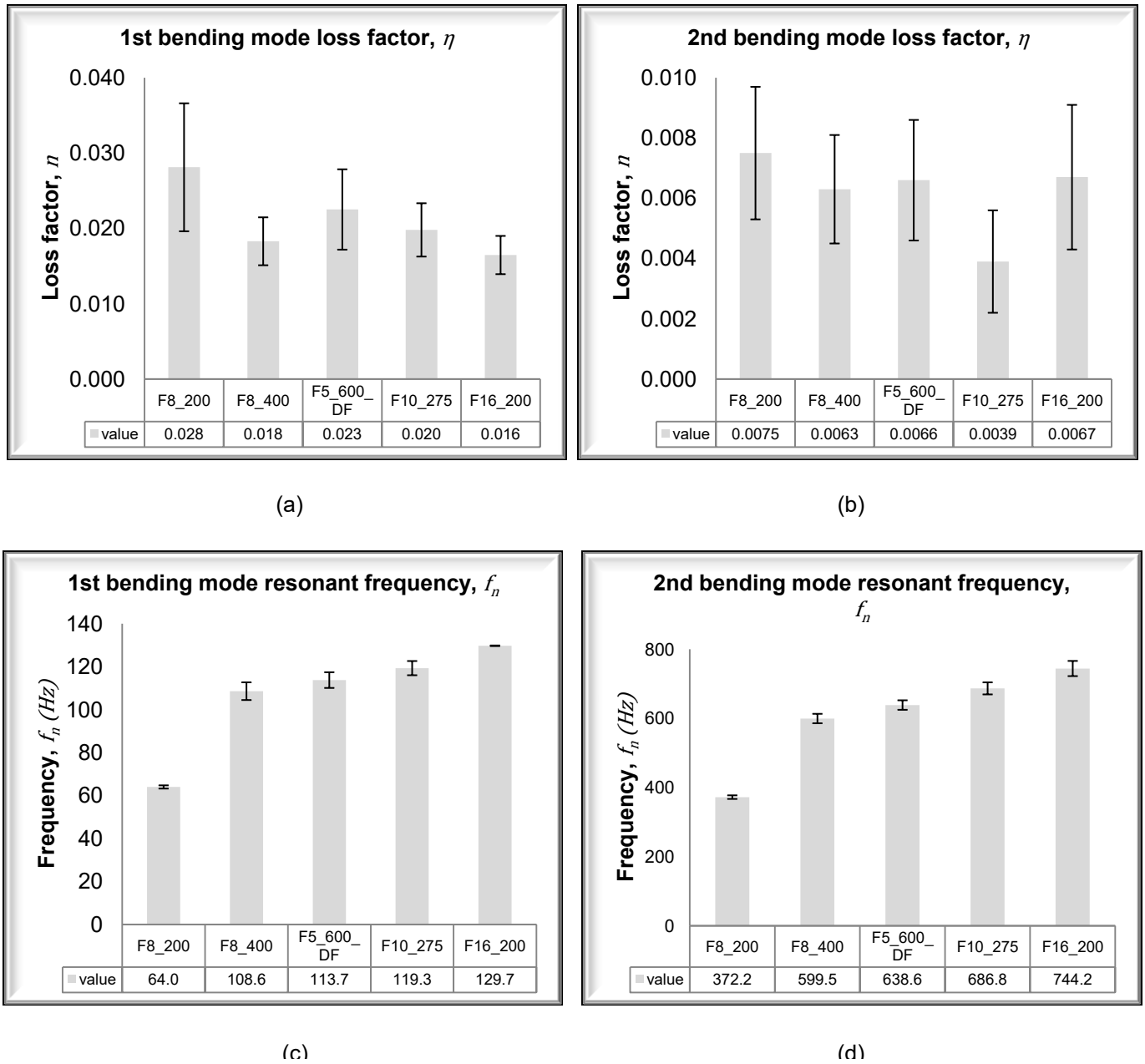

Figure 6-10. Second set of experiments: (a) 1st bending mode's loss factor, (b) 2nd bending mode's loss factor, (c) 1st bending mode's resonant frequency, (d) 2nd bending mode resonant frequency.

6.3 Third set of experiments

- *FF_400: Flax Fibre 400gsm twill weave*
- *CF_400: Carbon Fibre 200gsm twill weave*
- *FF_400_45º: Flax Fibre 400gsm 45º orientation*
- *CF_400_45º: Carbon Fibre 400gsm 45º orientation*

If DF exists in the abbreviation, Bio-resin DF250 was used, if not, standard epoxy resin MTC510 was used. Also, if there is not any info on orientation, 0 degrees is used.

F8_400_45	F8_400_DF	C15_200_DF	C4F4C4_DF	C4F3C4	C15_45
FF_400_45º	FF_400	CF_200	CF_200	CF_200	CF_400_45º
FF_400_45º	FF_400	CF_200	CF_200	CF_200	CF_400_45º
FF_400_45º	FF_400	CF_200	CF_200	CF_200	CF_400_45º
FF_400_45º	FF_400	CF_200	CF_200	CF_200	CF_400_45º
FF_400_45º	FF_400	CF_200	FF_400	FF_400	CF_400_45º
FF_400_45º	FF_400	CF_200	FF_400	FF_400	CF_400_45º
FF_400_45º	FF_400	CF_200	FF_400	FF_400	CF_400_45º
FF_400_45º	FF_400	CF_200	FF_400	CF_200	CF_400_45º
		CF_200	CF_200	CF_200	CF_400_45º
		CF_200	CF_200	CF_200	CF_400_45º
		CF_200	CF_200	CF_200	CF_400_45º
		CF_200	CF_200		CF_400_45º
		CF_200			CF_400_45º
		CF_200			CF_400_45º
		CF_200			CF_400_45º

Figure 6-11. Layups' abbreviations and materials of the third set of specimens

In the third set of experiments, two different "sandwich" solutions were tested, along with shear specimens (off-axis 45º tensile test) of CF 200gsm and FF 400gsm. Also, pure CF and FF layups manufactured with DF250 bio-resin were tested in order to compare its performance with the epoxy resin MTC510. It should be noted that one of the sandwich layups was made with DF250 so that its performance in sandwich layups is tested. (**Figure 6-11** and **Table 6-7**)

Table 6-7. Information on third set of specimens (average values)

Abbreviations	*Thickness (mm)*	*Specimen's weight (gr)*	*Density (kg/m^3)*
C4F3C4	*2.81*	*30.4*	*1431*
C4F4C4_DF	*3.25*	*34.3*	*1370*
C15_DF	*2.72*	*30.9*	*1515*
F8_400_DF	*3.48*	*35.2*	*1303*

6.3.1 Tensile tests

The results of the tensile test are depicted in **Figure 6-13** and **Table 6-8**. In **Figure 6-15 (b)** the average stress-strain curves can be seen. In results it can be seen that C4F3C4 was better in most of the characteristics than C4F4C4_DF. More specifically, it had 13.9% higher elastic modulus, 11.3% higher specific elastic modulus and 4.5% higher tensile strength, and only 11.5% lower max strain. These differences can be explained by the higher CF percentage of C4F3C4 (72.7%) than of C4F4C4_DF (66.7%) and by the severe delamination of C4F4C4_DF (see **Figure 6-12 (b)**). C15_DF and F8_400_DF are compared with the relevant MTC510 in **6.4.3**.

Table 6-8. Tensile tests results of third set of specimens

Layup	*Elastic modulus E (GPa)*	*Max Stress F_{max} (MPa)*	*Max Strain ε_{max} (%)*
C4F3C4	*42.3 ± 3.9*	*328.5 ± 20.5*	*0.77 ± 0.07*
C4F4C4_DF	*36.4 ± 4.5*	*314.5 ± 23.1*	*0.87 ± 0.06*
C15_DF	*59.6 ± 10.7*	*691.6 ± 70.1*	*1.06 ± 0.12*
F8_400_DF	*11.7 ± 0.6*	*82.0 ± 4.3*	*1.28 ± 0.26*

6.3.2 Flexural tests

The results of the flexural (3 point bending) tests are depicted in **Table 6-9** and **Figure 6-14**. In **Figure 6-15 (a)** the average load-displacement curves can be seen. The same pattern was noticed in flexural results, with C4F3C4 having 13.5% higher Flexural Modulus, 8.5% higher specific flexural modulus, 12.8% higher flexural strength and 15.9% higher displacement. The latter can be explained by severe delamination that was noticed during the experiment. It should be noted that

delamination is expected to happen in hybrid layups due to different elastic modulus and strain behaviour of the materials (in our case quite high difference of elastic modulus between CF and FF), but in C4F4C4_DF was quite severe (see **Figure 6-12 (a)**) (a)). C15_DF and F8_400_DF are compared with the relevant MTC510 ones in **6.4.3**.

Table 6-9. Flexural tests results of third set of specimens

Layup	*Flexural Modulus* E_f *(GPa)*	*Flexural Strength* $\sigma_{f(max)}$ *(MPa)*	*Max Displacement (mm)*
C4F3C4	*64.1 ± 2.7*	*724.2 ± 34.2*	*18.2 ± 0.8*
C4F4C4_DF	*56.5 ± 4.7*	*641.8 ± 63.0*	*15.7 ± 1.3*
C15_DF	*66.2 ± 4.0*	*832.5 ± 43.1*	*21.8 ± 1.3*
F8_400_DF	*10.9 ± 1.2*	*130.8 ± 10.1*	*29.3 ± 2.8*

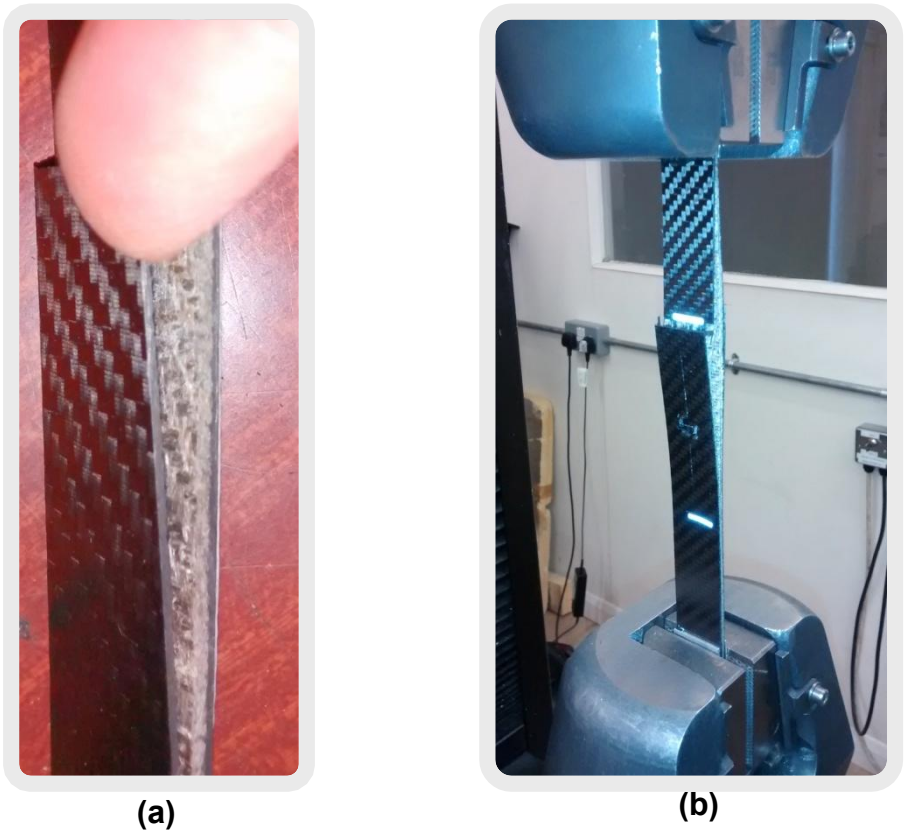

(a) **(b)**

Figure 6-12. (a) C4F4C4_DF 3 point bending specimen and (b) tensile specimen

6.3.3 Damping tests

In **Figure 6-17 ((a), (b), (c) and (d))** the first two resonant frequencies and the corresponding loss factors are shown. C4F4C4_DF has 58.3% higher loss factor than C4F3C4 in the first bending mode and 13.9% higher in second bending mode. As far as resonant frequencies go, C4F4C4_DF has higher resonant frequencies in both modes, due to its larger thickness. The rest are compared with their relevant layups in **6.4**.

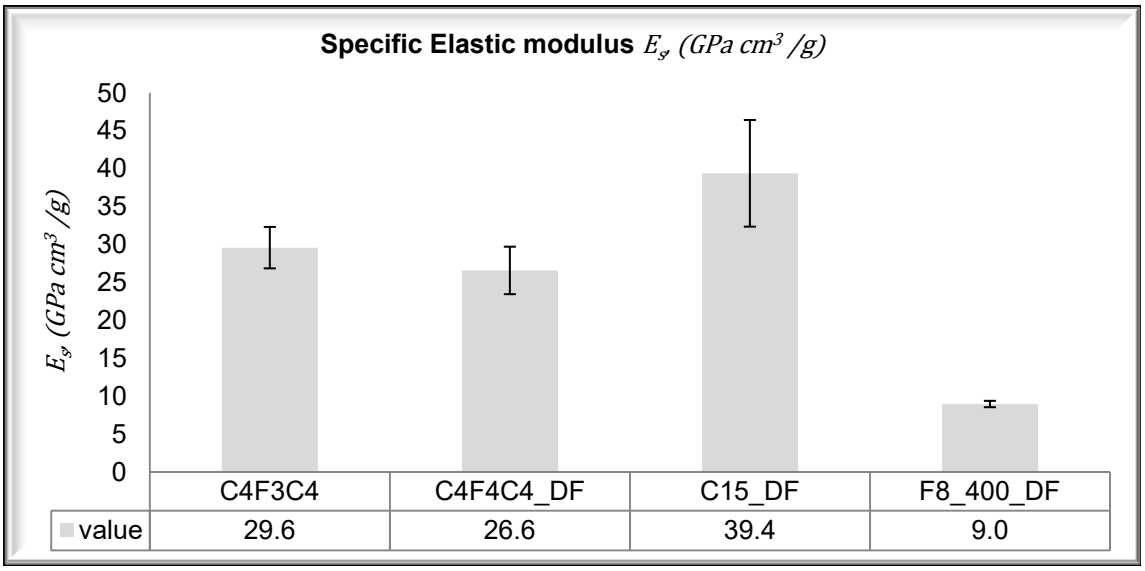

Figure 6-13. Third set: Specific Elastic Modulus, E_s

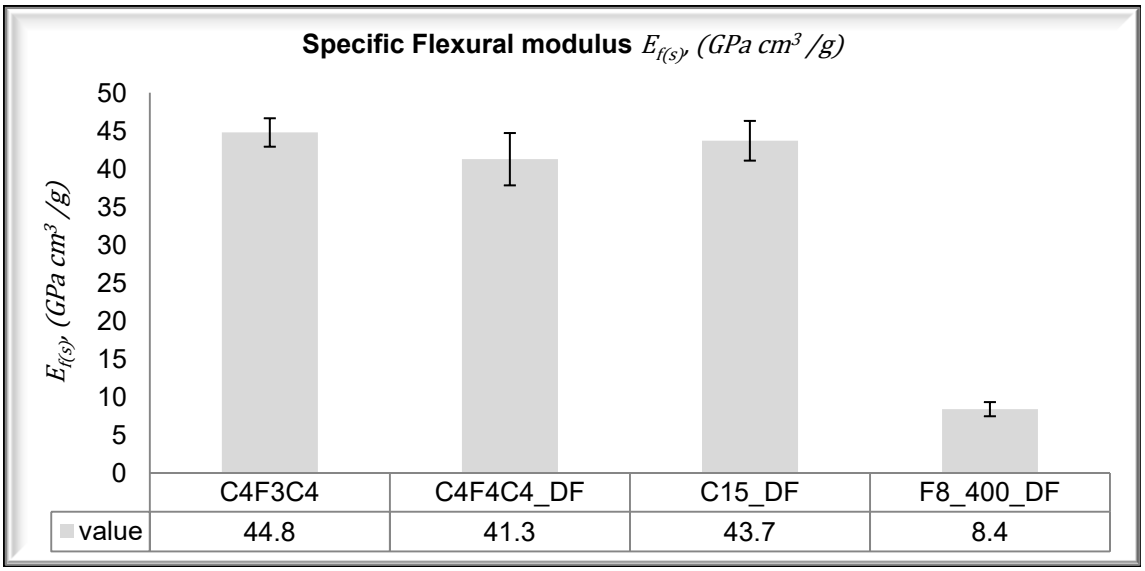

Figure 6-14. Third set: Specific Flexural Modulus, $E_{f(s)}$

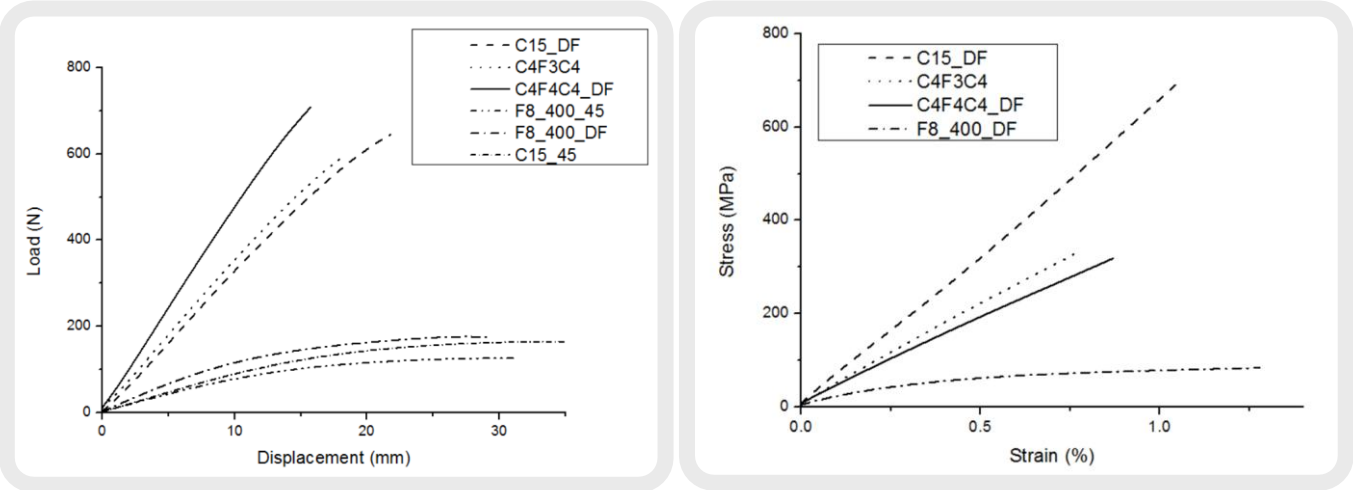

(a) (b)

Figure 6-15 . Third set: (a) Load vs. Displacement flexural testing curves, (b) Stress vs. Strain tensile testing curves

6.3.4 Off-axis 45º loading tensile tests

Table 6-10 contains information on the specimens that were tested in off-axis tensile tests. Results of the tests are shown in

Table 6-11 and in **Figure 6-16** the average shear stress - shear strain are depicted. The results were used in FEA models.

6.3.5 Brief discussion

C4F4C4_DF seems to be the best solution tested in this project. Further discussion is in **6.4.2**

Table 6-10. Information on shear test set of specimens (average values)

Abbreviations	*Thickness (mm)*	*Specimen's weight (gr)*	*Density (kg/m³)*
C15_45	*2.89*	*32.5*	*1491*
F8_400_45	*3.69*	*37.0*	*1310*

Table 6-11. Shear tests results of third set of specimens

Layup	*Shear Modulus G_{12} (GPa)*	*Shear Strength $\tau_{12(max)}$ (MPa)*	*Max Shear Strain $\gamma_{12(max)}$*
C15_45	*3.4 ± 0.7*	*118.8 ± 1.6*	*4.36 ± 1.24*
F8_400_45	*2.1 ± 0.4*	*24.4 ± 2.5*	*1.60 ± 0.28*

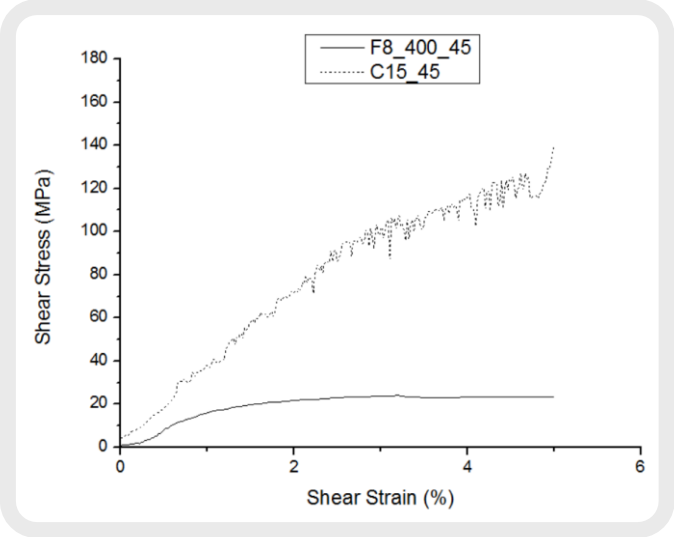

Figure 6-16. Third set of specimens: shear stress vs shear strain curve.

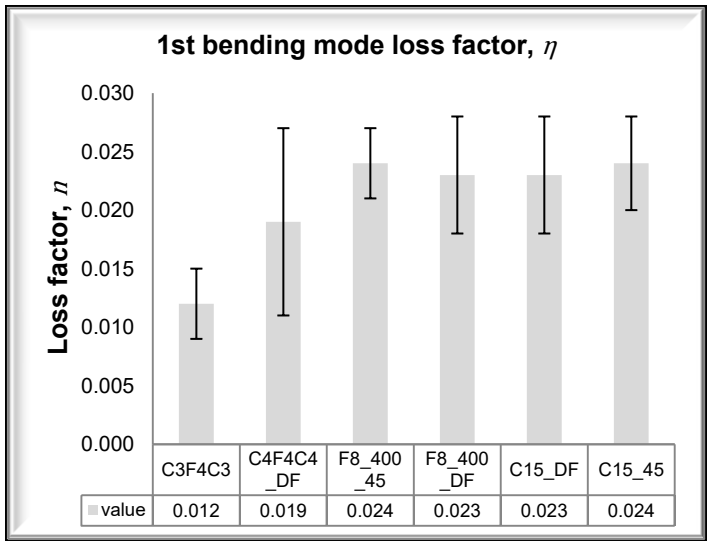

(a)

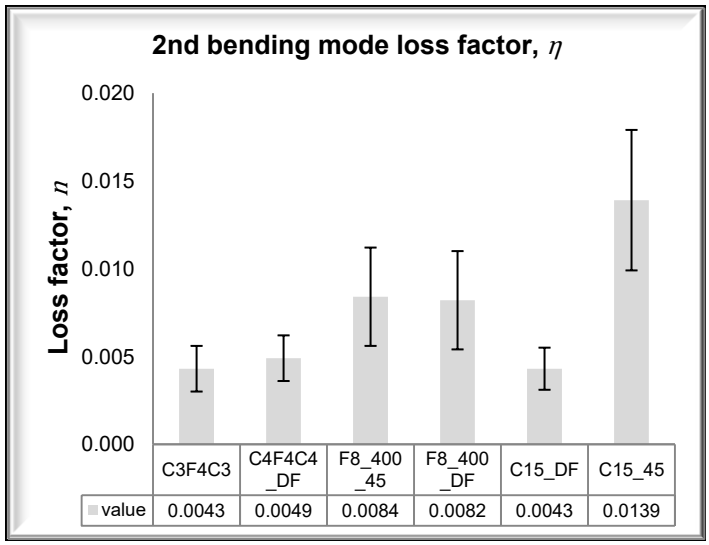

(b)

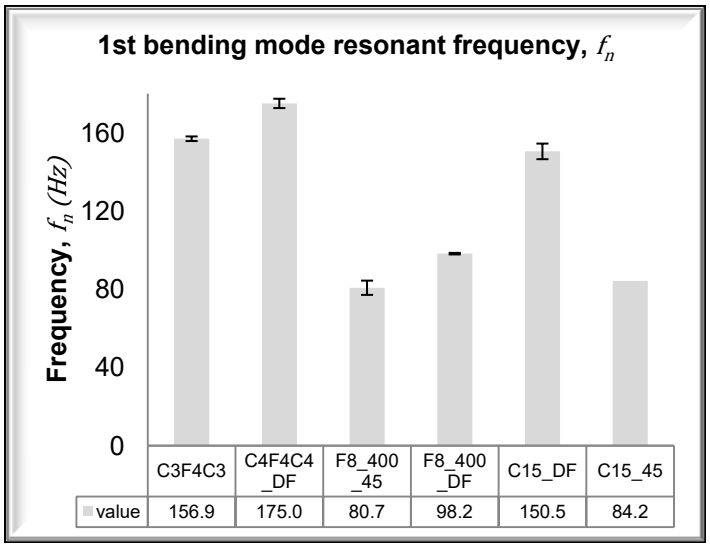

(c)

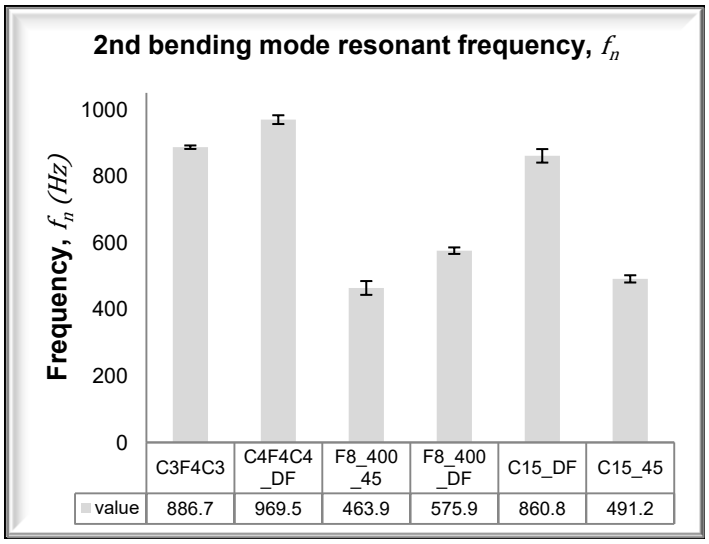

(d)

Figure 6-17. Third set of experiments: (a) 1st bending mode's loss factor, (b) 2nd bending mode's loss factor, (c) 1st bending mode's resonant frequency, (d) 2nd bending mode resonant frequency

6.4 Comparisons

In this chapter the different hybrid layups are compared and lead to conclusions on their suitability for project CARBIO. It should be noted that comparisons of layups that were in the same set of experiments is omitted, such as the "alternate" and "sandwich" layup. These conclusions can be found in each "Basic discussion" paragraph of chapter **6 (6.1.4 and 6.2.4**)

*The loss factor is the one of the 1st bending mode

** The average of F12 and F16_400

6.4.1 FF_400gsm vs. FF 200gsm

In **Table 6-12** it is shown that FF_400gsm fabric has similar mechanical properties with FF_200gsm fabric (4.5% lower specific flexural modulus and 7.9% lower specific elastic modulus), 28% lower loss factor and 7% higher density. Although these characteristics should make FF_200gsm the best solution, F8_400 was preferred. This is explained by the fact that in "sandwich" layups (which had already been chosen over the "alternate" ((refer to section **6.1.4**)) the thickness of the FF layers was more important than its mechanical characteristics. This was because CF had much higher mechanical characteristics than FF, so it dominated it. Since FF_400gsm can achieve the same thickness with FF_200gsm with lower number of layers, it means that the labour cost will be lower. Also, FF_400gsm's loss factor is significantly higher than CF, despite the fact that is lower than FF_200gsm.

Table 6-12. FF_400gsm vs. FF 200gsm

Abbreviations	*Thickness (mm)*	*Density (kg/m³)*	*Specific Elastic Modulus, E_s (GPa)*	*Specific Flexural Modulus, $E_{f(s)}$ (GPa)*	*Loss factor*, n*
F8_400	*3.86*	*1266*	*7.0 ± 0.6*	*8.5 ± 0.3*	*0.018 ± 0.003*
*FF_200gsm***	*3.82*	*1183*	*7.6 ± 1.1*	*8.9 ± 1.1*	*0.025 ± 0.005*

6.4.2 C4F3C4 vs. C13 vs. C3F6C3 vs. C4F4C4_DF

In **Table 6-13** all the "sandwich" layups and the pure CF C13 are listed. It should be noted that all "sandwich" layups have higher $E_{f(s)}$ than C13. Other than that,

C4F3C4 has the highest $E_{f(s)}$ (8.5% higher than C4F4C4_DF and 19.5% than C3F6C3), the second highest E_s (11.3% higher than C4F4C4_DF and 1.7% lower than C3F6C3) and the lowest loss factor, 36.8% lower than both C4F4C4_DF and C3F6C3. The choice of a hybrid layup to be used, would depend on the parameters that are outlined in the requirements. For example, if the main concern is the loss factor, C4F4C4_DF seems to be quite promising solution, but if the main concern is its mechanical properties then probably C4F3C4 is the most ideal solution. So, the best compromise between the characteristics should be selected.

Table 6-13. C4F3C4 vs. C13 vs. C3F6C3 vs. C4F4C4_DF

Abbreviations	*Thickness* (mm)	*Density* (kg/m^3)	*Specific Elastic Modulus,* E_s (GPa)	*Specific Flexural Modulus,* $E_{f(s)}$ (GPa)	*Loss factor*,* n
C4F3C4	*2.81*	*1431*	*29.6 ± 2.7*	*44.8 ± 1.9*	*0.012 ± 0.003*
C4F4C4_DF	*3.25*	*1370*	*26.6 ± 3.3*	*41.3 ± 3.4*	*0.019 ± 0.008*
C3F6C3	*2.66*	*1365*	*30.1 ± 3*	*37.5 ± 3.9*	*0.019 ± 0.004*
C13	*2.86*	*1482*	*41.2 ± 2.4*	*36.6 ± 2.4*	*0.010 ± 0.002*

6.4.3 C15_DF vs. C13 vs. C15_45 and F8_400_DF vs. F8_400 vs. F8_400_45

In **Table 6-14** the effect of bio-resin DF250 and of the 45º orientation on the properties of CF and FF and more significantly on the loss factor is examined. It can be seen that the bio-resin layups had quite high loss factor (130% in CF, 27.8% in FF) than the standard MTC510 epoxy resin. 45º oriented fibres had the same effect on the loss factor, too (140% in CF, 33.3% in FF). As far as the mechanical properties go, C13 has 4.6% higher E_s and 16.2% lower $E_{f(s)}$ than C15_DF, and F8_400 has 22.2% lower E_s and 1.1% higher $E_{f(s)}$ than F8_400_DF.

Table 6-14. C15_DF vs. C13 vs. C15_45 and F8_400_DF vs. F8_400 vs. F8_400_45

Abbreviations	*Thickness (mm)*	*Density (kg/m³)*	*Specific Elastic Modulus, E_s (GPa)*	*Specific Flexural Modulus, $E_{f(s)}$ (GPa)*	*Loss factor*, n*
C13	*2.86*	*1482*	*41.2 ± 2.4*	*36.6 ± 2.4*	*0.010 ± 0.002*
C15_DF	*2.72*	*1515*	*39.4 ± 7.0*	*43.7 ± 2.6*	*0.023 ± 0.005*
C15_45	*2.89*	*1491*	-	-	*0.024 ± 0.004*
F8_400	*3.86*	*1266*	*7.0 ± 0.6*	*8.5 ± 0.3*	*0.018 ± 0.003*
F8_400_DF	*3.48*	*1303*	*9.0 ± 0.4*	*8.4 ± 0.9*	*0.023 ± 0.005*
F8_400_45	*3.69*	*1310*	-	-	*0.024 ± 0.003*

6.4.4 F8_200 vs F12 vs F16_200

In **Table 6-15** the effect of thickness on the properties of FF is examined. It is interesting that F12 has the highest loss factor ($\eta=0.034$), with F8_200 following (n=0.028) and F16_200 has the lowest one ($\eta=0.016$). Further work must be done to investigate the relation between the thickness and the loss factor.

Table 6-15. F8_200 vs F12 vs F16_200

Abbreviations	*Thickness (mm)*	*Density (kg/m³)*	*Specific Elastic Modulus, E_s (GPa)*	*Specific Flexural Modulus, $E_{f(s)}$ (GPa)*	*Loss factor*, n*
F8_200	*2.3*	*1196*	*9.1 ± 0.8*	*9.5 ± 0.4*	*0.028 ± 0.008*
F12	*3.24*	*1307*	*6.5 ± 1.4*	*7.9 ± 1.1*	*0.034 ± 0.007*
F16_200	*4.4*	*1058*	*8.7 ± 0.8*	*9.8 ± 1.0*	*0.016 ± 0.003*

6.5 FEA

The most important mechanical characteristics of the materials were derived from processing the results acquired from tensile and 3-point bending tests. Five different material cards were produced:

- CF 200gsm 2/2 twill weave with standard epoxy resin MTC510 (**CF_200gsm_MTC510**) and the same fabric with bio-resin DF250 (**CF_200gsm_DF250**),
- FF 200gsm 2/2 twill weave with standard epoxy resin MTC510 (**FF_200gsm_MTC510**)
- FF 400gsm 2/2 twill weave with standard epoxy resin MTC510 (**FF_400gsm_MTC510**) and the same fabric with bio-resin DF250 (**FF_400gsm_DF250**)

In **Table 6-16** and

Table 6-17 the data used in FEA are shown. It must be noted that the data in **bold** characters are from the experiments. All the others were obtained from literature [76] (using exactly the same value or similar), or were derived from the analysis themselves matching the results with the experiments. It should be noted that MAT_054 needs some inputs that are used in crash analysis and need crash tests to get their experimental values. In our case the models were not used to simulate crash experiments, so they were ignored.

6.5.1 Results and discussion

6.5.1.1 Flexural (3-point bending tests)

As it is shown in **Figure 6-18** and **Figure 6-19**, the models of the hybrid layups simulated quite accurately the experiments outcomes, with only some of them having some divergence at the point of failure. C15_DF and C13 models, also, were quite realistic, with the former having slightly larger divergence. On the other hand, FF models had quite significant divergence from the experiments, except F12. This can be attributed to the large displacements, which means local failure mechanisms and the non-linear behaviour of FF. These two different factors were not simulated using the FEA software module and material model that was used. Similar divergence can be noticed in both C15_45 and F8_400_45, which again can be explained by the large displacements.

6.5.1.2 Tensile tests

The same results can be seen in tensile test models (**Figure 6-20** and **Figure 6-21**). More specifically, the outputs from hybrid specimens' models and CF (in this case both C15_DF and C13) replicate the experimental outputs quite well. The same thing can be said for the off-axis 45º tensile test, although the FEA model cannot follow the non-linearity of the experimental . As for the FF, despite the non-linear of the experiments, FEA models seem to be close enough.

6.5.1.3 Resonant frequencies

In order to get the first two bending resonant frequencies, modal analysis models of the layups were developed (**Table 6-18**). In **Table 6-18** it can be seen that hybrid layups' models give 4.2% -7.7% divergence from the actual results, while C13 and

C15_DF give 0.2% and 6.7% divergence, respectively. On the other hand, F12 and F8_400_45 give 13.6% and 13% divergence, respectively. This can be attributed to the non-linearity of FF. Even larger divergence was observed in F8_400_45 (20.8%) and C15_45 (19.5%). Considering the fact that C13 model had only 0.2% divergence, 45º specimens' models have poor performance. The 45º and FF models' poor performance can be attributed to the large displacements, which lead to large strains and cause local failure mechanisms. This assumption is supported by the fact that all these models give much lower resonant frequency, meaning that the models' behaviour is stiffer.

Table 6-16. CF material cards

Variable	Description	CF_200gsm_MTC510	CF_200gsm_DF510
RO	Density (kg/m^3)	**1482**	**1515**
EA	Axial Young's modulus (Pa)	**62e+09**	**64e+09**
EB	Transverse Young's modulus (GPa)	**62e+09**	**64e+09**
GAB	Shear modulus (GPa)	**3.43e+09**	3.3e+09
PRBA	Minor Poisson's ratio	0.043	0.043
XT	Axial tensile strength (MPa)	**664.3e+06**	**691.6e+06**
XC	Axial compressive strength (MPa)	520e+06	540e+06
YT	Transverse tensile strength (MPa)	**664.3e+06**	**691.6e+06**
YC	Transverse compressive strength (MPa)	520e+06	540e+06
SC	Shear strength (MPa)	**118.8e+06**	130e+06
DFAILT	Axial tensile failure strain (mm/mm)	0.025	0.0223
DFAILC	Axial compressive failure strain (mm/mm)	-0.3	-0.0127
DFAILM	Transverse failure strain (mm/mm)	0.1	0.014
DFAILS	Shear failure strain (mm/mm)	0.0436	0.05

Table 6-17. FF material cards

Variable	Units	FF_200gsm_MTC510	FF_400gsm_MTC510	FF_400gsm_DF250
RO	kg/m^3	**1187**	**1266**	**1303**
EA	GPa	**9.5e+09**	**9.5e+09**	**12.3e+09**
EB	GPa	**9.5e+09**	**9.5e+09**	**12.3e+09**
GAB	GPa	2e+09	**2.1e09**	2e+09
PRBA	-	0.03	0.03	0.03
XT	MPa	**117.8e+06**	**70.8e+06**	**82e+06**
XC	MPa	90e+06	50e+06	63e+06
YT	MPa	**117.8+06**	**70.8e+06**	**82e+06**
YC	MPa	90+06	50e+06	63e+06
SC	MPa	20e+06	**24.41e+06**	25e+06
DFAILT	mm/mm	0.0378	0.0408	0.05
DFAILC	mm/mm	-0.1	-0.05	-0.5
DFAILM	mm/mm	0.01	0.1	0.5
DFAILS	mm/mm	0.03	0.03	0.5

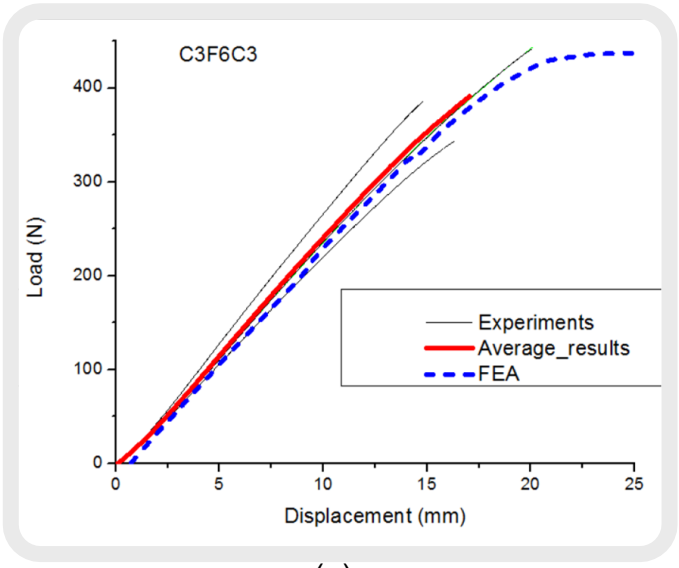

(a)

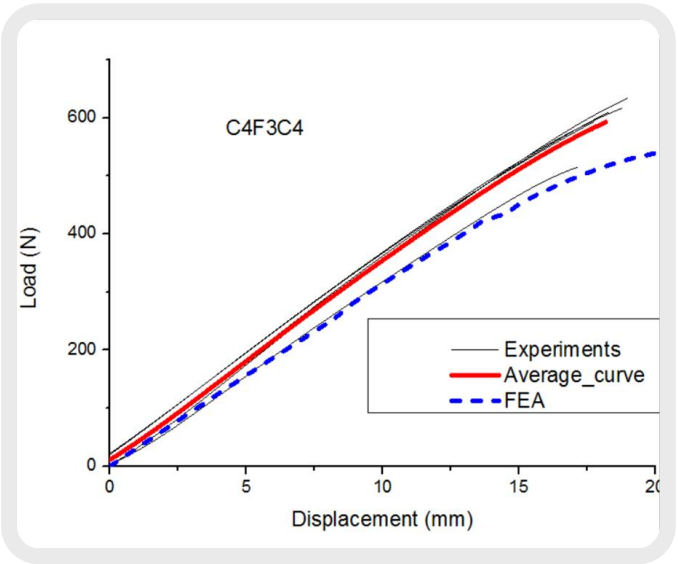

(b)

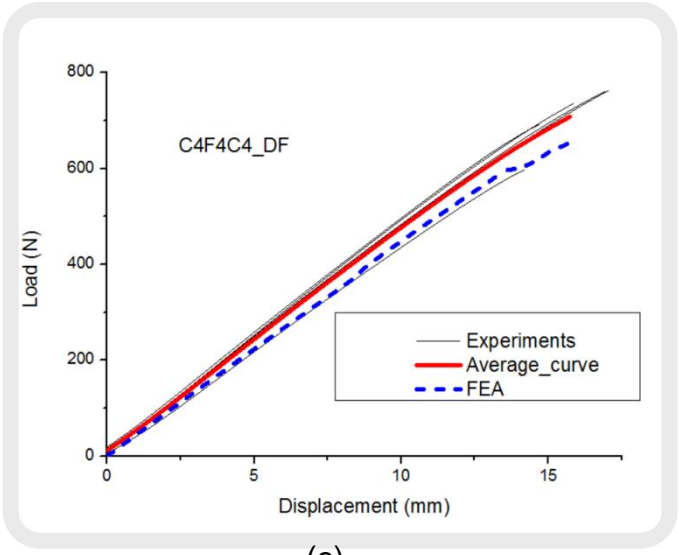

(c)

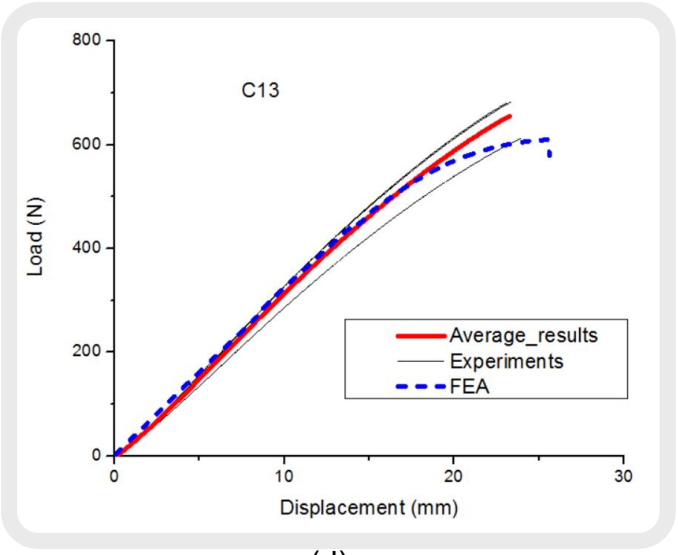

(d)

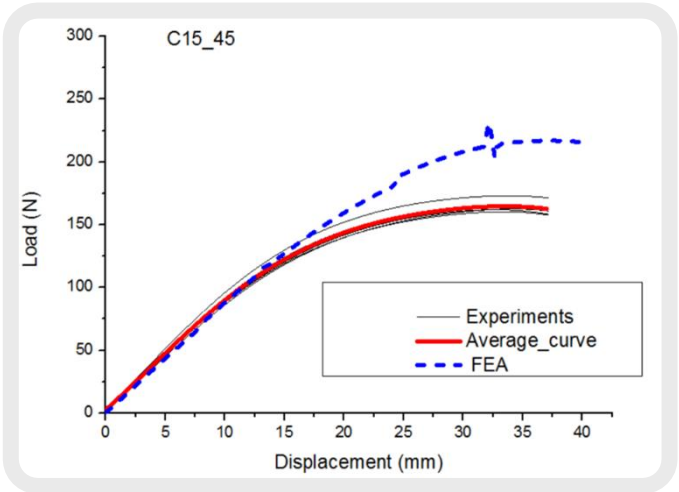

(e)

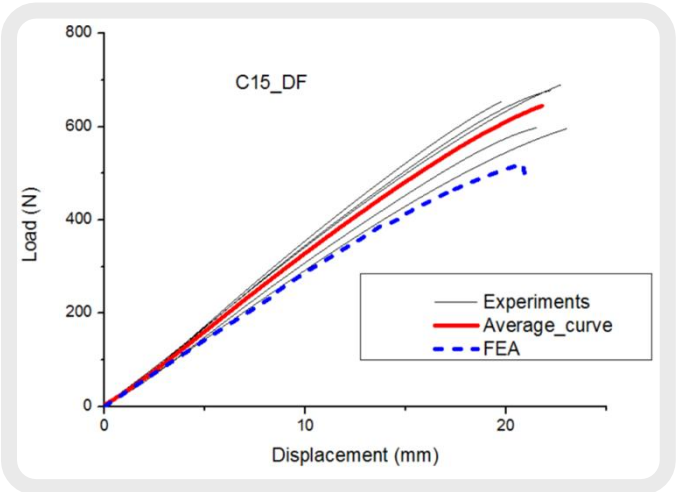

(f)

Figure 6-18. Experimental and FEA load-displacement 3-point bending curves

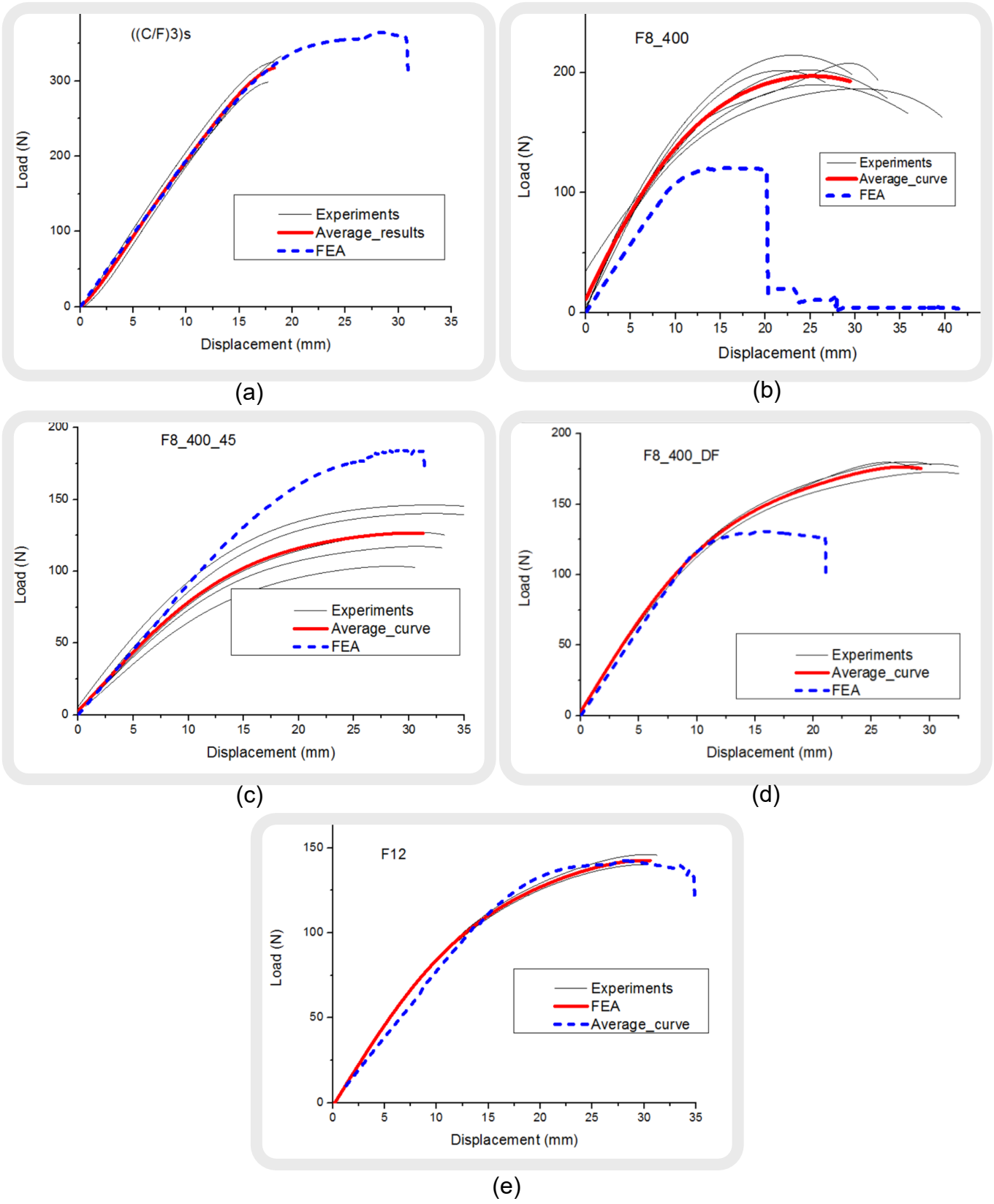

Figure 6-19. Experimental and FEA load-displacement 3-point bending curves

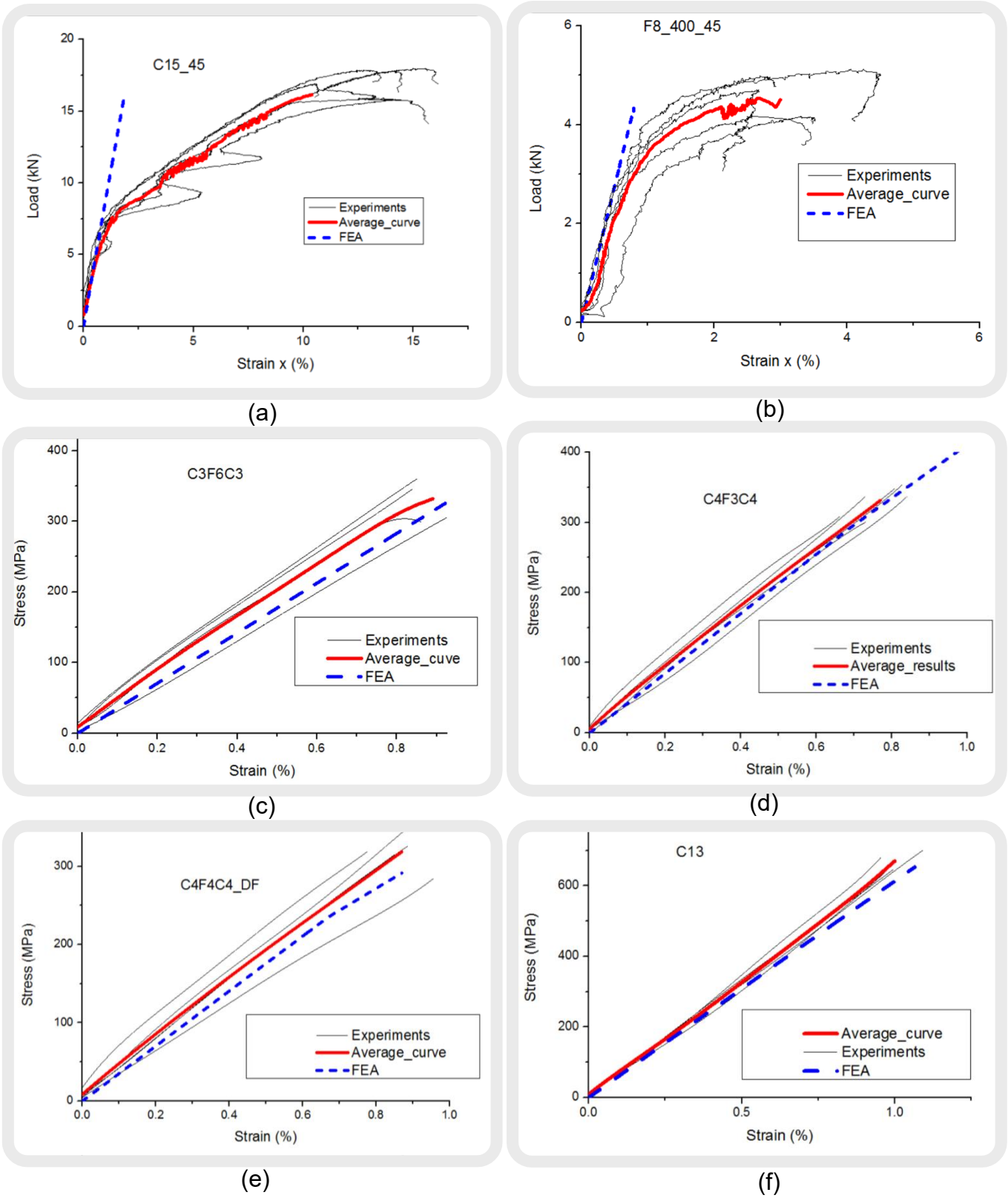

Figure 6-20. Experimental and FEA stress-strain tensile curves

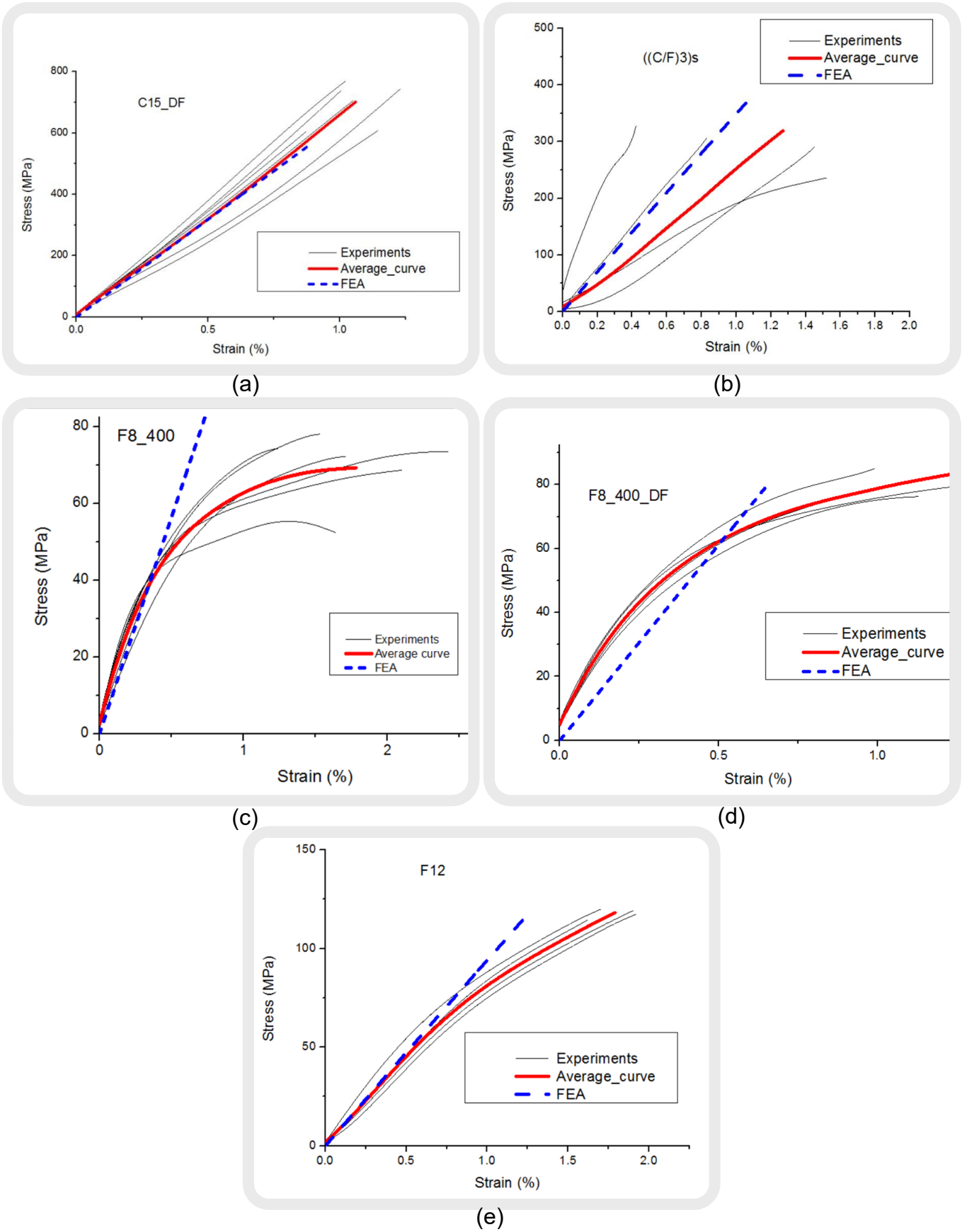

Figure 6-21. Experimental and FEA stress-strain tensile curves

Table 6-18. FEA modal analysis and experimental results

Layup	1st bending frequency (Hz)			2nd bending frequency (Hz)		
	Experimental	FEA	Divergence (%)	Experimental	FEA	Divergence (%)
C13	147.1	147.4	0.2	844.7	846.4	0.2
C15_DF	150.5	140.4	6.7	860.8	808.4	6.1
C4F3C4	156.9	144.9	7.7	886.7	836.1	5.7
C4F4C4_DF	175.0	163.7	6.5	969.5	927.6	4.3
C3F6C3	140.4	134.3	4.3	794.6	777.5	2.2
((C/F)3)s	123.8	118.6	4.2	710.9	689.8	3.0
F12	84.0	72.6	13.6	506.1	424.2	16.2
F8_400	108.6	85.2	21.6	599.5	492.1	17.9
F8_400_DF	98.2	85.4	13.0	575.9	494.2	14.2
C15_45	84.2	67.8	19.5	491.2	414.4	15.6
F8_400_45	80.7	63.9	20.8	463.9	373.7	19.4

7 CONCLUSIONS

This study was part of CARBIO project. Vibrations consist of one of the most important problems that designers and researchers face in automotive sector. CARBIO acknowledged that hybrid CF/FF composites could consist of a solution that will combine the advantages of FRC with the optimum damping characteristics of FF. FF was the preferred material due to its relatively easy and low-cost production and appealing mechanical properties.

So, the aim of this study was to produce and examine hybrid CF/FF layups which would offer cost efficient solutions of enhancing the damping performance of a structure with low compromise in mechanical performance. In order to achieve that a damping experiment was set up and was used to examine the damping behaviour of different hybrid layups solutions, along with their mechanical characteristics. Different solutions were tested and compared with pure FF and CF. Also, FEA models were developed for the most important layups.

More specifically, extensive research was conducted on damping test methods of composites and the use of CIM was preferred. After further research, the equipment to be used was chosen and the experiment was set up. Along with damping tests, standard tensile and flexural tests were conducted. Firstly, alternate FF and CF layers and "sandwich" hybrid solutions were tested, with the "sandwich" having 14.3% higher loss factor than the alternate one. In addition to this, "sandwich" layup had better flexural and tensile performance than the alternate one, with 55.2% higher E_s and 34.9% higher $E_{f(s)}$, which was 2.5% higher than pure CF, too. After that, further testing was completed in order to compare different types of FF fabrics, with FF_400gsm fabric being chosen. Having chosen FF type, two more sandwich hybrid layups were tested. The two additional sandwich hybrid layups that were tested proved to be more appealing solutions than the first one, with each one performing better in different sector. Hence, C4F3C4 has 8.5% higher $E_{f(s)}$ than C4F4C4_DF and 19.5% higher than C3F6C3, 11.3% higher E_s than C4F4C4_DF and 1.7% lower than C3F6C3 but 36.8% lower η than both C4F4C4_DF and C3F6C3. Having in mind these results, it was obvious that the choice of a hybrid layup to be used, should depend on the parameters that are outlined in the requirements of its application. In

this way the extensive library of damping and mechanical characteristics of different hybrid layups and pure CF and FF layups properties that was generated can be used to choose the solution which matches each application's needs.

In addition to the layup testing, the effect of the bio-resin DF250 on the η was tested on both CF and FF. It was proven that DF250 had 130% higher η in CF specimens and 27.8% higher η in FF specimens.

FEA models of the three test techniques (damping test, tensile and 3-point bending test) were, also, developed for the most important layups. In order for this to be achieved, five different material cards were developed covering each variation of FF and CF that were considered the most important ones. Having developed these material cards any layup can be modelled and they can, also, be used in any part's model.

In summary, this study proved that hybrid CF/FF solution is viable as a substitute for pure CF in order to enhance part's damping properties with small compromise on mechanical properties.

8 FURTHER WORK

8.1.1 Damping test

As described in **5.1.1** a manual Signal Generator BlackStar Jupiter 2010 is responsible for generating the sine wave signal to accentuate the shaker. It was noticed that the signal was not quite plain with its amplitude not being stable. Also, since the signal generation was controlled manually, the human factor usually leads to errors and possible inconsistency, which makes the multiple repetition of each experiment necessary. This issue could be solved with an automatic signal generator, so that the experiment would not be that time consuming and more accurate.

8.1.2 FF and FF/CF hybrids

FF and FF/CF specimens' results showed greater deviation than pure CF ones. This is mostly due to the hydrophilic nature of FF which absorbs moisture leading to structural inconsistencies. These inconsistencies lead to local failure which makes the FF specimens' behaviour difficult to predict. Also, severe delamination was noticed in most of the hybrid specimens between FF and CF. Although this is expected, the severity of the delamination was not constant among the different specimens. Further research on this issue could lead to prediction of this failure mechanism.

8.1.3 Damping parameters

As it was discussed in **6.4**, thickness and plies' orientation affected the damping performance of the specimen. Further work could focus on the relationship between these parameters and the damping performance.

8.1.4 FEA

In **6.5** it was noticed that FF and 45^{o} models had quite significant divergence from the experimental results, which can be explained by the large strains. These strains lead to local failure mechanisms and non-linearity. Further research on modelling this behaviour could solve this problem.

REFERENCES

[1] B. S. Ben, B. A. Ben, K. Adarsh, K. A. Vikram, and C. Ratnam, “Damping measurement in composite materials using combined finite element and frequency response method,” presented at the National Conferenc on “Advances in Modelling and Analysis of Aerodynamic Systems” (AMAAS-2013), National Institute of Technology Rourkela (ODISHA), 2013, pp. 89–97.

[2] D. Thorby, “Damping,” in *Structural Dynamics and Vibration in Practice: An Engineering Handbook*, Butterworth-Heinemann, 2008, pp. 99–118.

[3] J.-M. Berthelot, M. Assarar, Y. Sefrani, and A. E. Mahi, “Damping analysis of composite materials and structures,” *Compos. Struct.*, vol. 85, no. 3, pp. 189–204, Oct. 2008.

[4] S. S. Rao, “Free Vibration of Single-Degree-of-Freedom Systems,” in *Mechanical Vibrations*, N.J.: Prentice Hall: 5th ed. Upper Saddle River, 2011, pp. 124–258.

[5] ASM International Handbook, *Composites*., ASM International, 2001.

[6] M. R. Maheri and R. D. Adams, “Vibration Properties of Structural FRP Composites,” *JSME Int. J. Ser. A*, vol. 42, no. 3, pp. 307–320, 1999.

[7] H. Lu, X. Wang, T. Zhang, Z. Cheng, and Q. Fang, “Design, Fabrication, and Properties of High Damping Metal Matrix Composites—A Review,” *Materials*, vol. 2, no. 3, pp. 958–977, Aug. 2009.

[8] R. Chandra, S. P. Singh, and K. Gupta, “Damping studies in fiber-reinforced composites – a review,” *Compos. Struct.*, vol. 46, no. 1, pp. 41–51, 1999.

[9] D. A. Saravanos and C. C. Chamis, “Tailoring of composite links for optimal damped elasto-dynamic performance,” presented at the 1989 Design Automotive Conference, Montreal, Canada, 1989.

[10] F. Duc, P. E. Bourban, and J.-A. E. Månson, “The role of twist and crimp on the vibration behaviour of flax fibre composites,” *Compos. Sci. Technol.*, vol. 102, pp. 94–99, 2014.

[11] J. Zhu, H. Zhu, J. Njuguna, and H. Abhyankar, “Recent Development of Flax Fibres and Their Reinforced Composites Based on Different Polymeric Matrices,” *Materials*, vol. 6, no. 11, pp. 5171–5198, Nov. 2013.

[12] S. V. Joshi, L. T. Drzal, A. K. Mohanty, and S. Arora, “Are natural fiber composites environmentally superior to glass fiber reinforced composites?,” *Compos. Part Appl. Sci. Manuf.*, vol. 35, no. 3, pp. 371–376, Mar. 2004.

[13] K. Oksman, M. Skrifvars, and J.-F. Selin, “Natural fibres as reinforcement in polylactic acid (PLA) composites,” *Compos. Sci. Technol.*, vol. 63, no. 9, pp. 1317–1324, 2003.

[14] D. B. Dittenber and H. V. S. GangaRao, “Critical review of recent publications on use of natural composites in infrastructure,” *Compos. Part Appl. Sci. Manuf.*, vol. 43, no. 8, pp. 1419–1429, Aug. 2012.

[15] J. Vanwalleghem, “Study of the damping and vibration behaviour of flax-carbon composite bicycle racing frames,” Master Thesis, Ghent University, Gent, 2009.

[16] A. P. Vassilopoulos and T. Keller, “Introduction to the Fatigue of Fiber-Reinforced Polymer Composites,” in *Fatigue of Fiber-reinforced Composites*, Springer-Verlag London, 2011, pp. 1–23.

[17] N. Tucker and K. Lindsey, “What are Composites?,” in *An Introduction to Automotive Composites*, iSmithers Rapra Publishing, 2002, pp. 9–22.

[18] V. V. Vasiliev and E. Morozov, “Introduction,” in *Mechanics and Analysis of Composite Materials*, Elsevier, 2001, pp. 1–28.

[19] D. Gay, S. V. Hoa, and S. W. Tsai, “Ply Properties,” in *Composite Materials: Design and applications*, CRC Press, 2003, pp. 38–61.

[20] D. Gay, S. V. Hoa, and S. W. Tsai, “Composites, materials, interest and properties,” in *Composite Materials: Design and applications*, CRC Press, 2003, pp. 14–26.

[21] R. M. Crane and J. W. Gillespie Jr., “Characterization of the vibration damping loss factor of glass and graphite fiber composites,” *Compos. Sci. Technol.*, vol. 40, no. 4, pp. 355–375, 1991.

[22] D. Gay, S. V. Hoa, and S. W. Tsai, “Composite Materials for other applications,” in *Composite Materials: Design and applications*, CRC Press, 2003, pp. 187–209.

[23] A. K. Bledzki, O. Faruk, and V. E. Sperber, “Cars from Bio-Fibres,” *Macromol. Mater. Eng.*, vol. 291, no. 5, pp. 449–457, May 2006.

[24] B. Dahlke, H. Larbig, H. D. Scherzer, and R. Poltrock, “Natural Fiber Reinforced Foams Based on Renewable Resources for Automotive Interior Applications,” *J. Cell. Plast.*, vol. 34, no. 4, pp. 361–379, Jul. 1998.

[25] A. L. Leao, R. Rowell, and N. Tavares, “Applications of Natural Fibers in Automotive Industry in Brazil — Thermoforming Process,” in *Science and Technology of Polymers and Advanced Materials*, P. P. N. Prasad, P. J. E. Mark, P. S. H. Kandil, and D. Z. H. Kafafi, Eds. Springer US, 1998, pp. 755–761.

[26] J. Zhu, H. Abhyankar, E. Nassiopoulos, and J. Njuguna, “Tannin-based flax fibre reinforced composites for structural applications in vehicles,” presented at the IOP Conference Series: Materials Science and

Engineering, Cranfield Univrsity, Bedfrodshire, UK, 2012, vol. 40, p. 012030.

[27] J. Zhu, H. Zhu, K. Immonen, J. Brighton, and H. Abhyankar, “Improving mechanical properties of novel flax/tannin composites through different chemical treatments,” *Ind. Crops Prod.*, vol. 67, pp. 346–354, May 2015.

[28] E. Nassiopoulos and J. Njuguna, “Thermo-mechanical performance of poly(lactic acid)/flax fibre-reinforced biocomposites,” *Mater. Des.*, vol. 66, Part B, pp. 473–485, Feb. 2015.

[29] O. Faruk, A. K. Bledzki, H.-P. Fink, and M. Sain, “Biocomposites reinforced with natural fibers: 2000–2010,” *Prog. Polym. Sci.*, vol. 37, no. 11, pp. 1552–1596, 2012.

[30] P. Wambua, J. Ivens, and I. Verpoest, “Natural fibres: can they replace glass in fibre reinforced plastics?,” *Compos. Sci. Technol.*, vol. 63, no. 9, pp. 1259–1264, Jul. 2003.

[31] R. Ikeda, H. Tanaka, H. Uyama, and S. Kobayashi, “Synthesis and curing behaviors of a crosslinkable polymer from cashew nut shell liquid,” *Polymer*, vol. 43, no. 12, pp. 3475–3481, Jun. 2002.

[32] L. Y. Mwaikambo and M. P. Ansell, “Hemp fibre reinforced cashew nut shell liquid composites,” *Compos. Sci. Technol.*, vol. 63, no. 9, pp. 1297–1305, Jul. 2003.

[33] A. Awal, M. Rana, and M. Sain, “Thermorheological and mechanical properties of cellulose reinforced PLA bio-composites,” *Mech. Mater.*, vol. 80, Part A, pp. 87–95, Jan. 2015.

[34] H. L. Bos, *The potential of flax fibres as reinforcement for composite materials*. Eindhoven: Technische Universiteit Eindhoven, 2004.

[35] L. Yan, N. Chouw, and K. Jayaraman, “Flax fibre and its composites – A review,” *Compos. Part B Eng.*, vol. 56, pp. 296–317, Jan. 2014.

[36] K. Charlet, J. P. Jernot, S. Eve, M. Gomina, and J. Bréard, “Multi-scale morphological characterisation of flax: From the stem to the fibrils,” *Carbohydr. Polym.*, vol. 82, no. 1, pp. 54–61, Aug. 2010.

[37] C. Baley, “Analysis of the flax fibres tensile behaviour and analysis of the tensile stiffness increase,” *Compos. Part Appl. Sci. Manuf.*, vol. 33, no. 7, pp. 939–948, Jul. 2002.

[38] K. Charlet, S. Eve, J. P. Jernot, M. Gomina, and J. Breard, “Tensile deformation of a flax fiber,” *Procedia Eng.*, vol. 1, no. 1, pp. 233–236, Jul. 2009.

[39] M. Assarar, D. Scida, A. El Mahi, C. Poilâne, and R. Ayad, “Influence of water ageing on mechanical properties and damage events of two reinforced composite materials: Flax–fibres and glass–fibres,” *Mater. Des.*, vol. 32, no. 2, pp. 788–795, Feb. 2011.

[40] F. Duc, P. E. Bourban, C. J. G. Plummer, and J.-A. E. Månson, “Damping of thermoset and thermoplastic flax fibre composites,” *Compos. Part Appl. Sci. Manuf.*, vol. 64, pp. 115–123, Sep. 2014.

[41] S. Prabhakaran, V. Krishnaraj, M. S. kumar, and R. Zitoune, “Sound and Vibration Damping Properties of Flax Fiber Reinforced Composites,” *Procedia Eng.*, vol. 97, pp. 573–581, 2014.

[42] H. N. Dhakal, Z. Y. Zhang, R. Guthrie, J. MacMullen, and N. Bennett, “Development of flax/carbon fibre hybrid composites for enhanced properties,” *Carbohydr. Polym.*, vol. 96, no. 1, pp. 1–8, 2013.

[43] V. Fiore, A. Valenza, and G. D. Bella, “Mechanical behavior of carbon/flax hybrid composites for structural applications,” *J. Compos. Mater.*, vol. 46, no. 17, pp. 2089–2096, Aug. 2012.

[44] Z. S. Bagheri, I. El Sawi, E. H. Schemitsch, R. Zdero, and H. Bougherara, “Biomechanical properties of an advanced new carbon/flax/epoxy composite material for bone plate applications,” *J. Mech. Behav. Biomed. Mater.*, vol. 20, pp. 398–406, 2013.

[45] Z. S. Bagheri, I. El Sawi, H. Bougherara, and R. Zdero, “Biomechanical fatigue analysis of an advanced new carbon fiber/flax/epoxy plate for bone fracture repair using conventional fatigue tests and thermography,” *J. Mech. Behav. Biomed. Mater.*, vol. 35, pp. 27–38, Jul. 2014.

[46] Z. S. Bagheri, E. Giles, I. El Sawi, A. Amleh, E. H. Schemitsch, R. Zdero, and H. Bougherara, “Osteogenesis and cytotoxicity of a new Carbon Fiber/Flax/Epoxy composite material for bone fracture plate applications,” *Mater. Sci. Eng. C*, vol. 46, pp. 435–442, Jan. 2015.

[47] C. Cai, H. Zheng, M. S. Khan, and K. C. Hung, “Modeling of material damping properties in ANSYS,” in *CADFEM Users’ Meeting & ANSYS Conference*, 2002, pp. 9–11.

[48] A. Etaati, S. A. Mehdizadeh, H. Wang, and S. Pather, “Vibration damping characteristics of short hemp fibre thermoplastic composites,” *J. Reinf. Plast. Compos.*, vol. 33, no. 4, pp. 330–341, Feb. 2014.

[49] G. Lepoittevin, “Composite laminates with integrated vibration damping treatments,” Diss., Eidgenössische Technische Hochschule ETH Zürich, Nr. 19945, 2012, 2012.

[50] P. Tathavadekar, T. Onsay, and W. Liu, “Damping Performance Measurement of Non-uniform Damping Treatments,” SAE International, Warrendale, PA, SAE Technical Paper 2007-01-2199, May 2007.

[51] J. S. Hoksbergen, M. Ramulu, P. Reinhall, and T. M. Briggs, “A Comparison of the Vibration Characteristics of Carbon Fiber Reinforced Plastic Plates with those of Magnesium Plates,” *Appl. Compos. Mater.*, vol. 16, no. 5, pp. 263–283, Oct. 2009.

[52] M. K. Rath and S. K. Sahu, “Experimental Investigation for Free Vibration of Woven Fiber Composite Plates Subjected to Hygrothermal Loading,” *Therm. Energy Power Eng.*, 2013.

[53] K. Nakalswamy, “Experimental and numerical analysis of structures with bolted joints subjected to impact load,” *UNLV ThesesDissertationsProfessional Pap.*, May 2010.

[54] K. Senthil Kumar, I. Siva, P. Jeyaraj, J. T. Winowlin Jappes, S. C. Amico, and N. Rajini, “Synergy of fiber length and content on free vibration and damping behavior of natural fiber reinforced polyester composite beams,” *Mater. Des.*, vol. 56, pp. 379–386, 2014.

[55] H. C. Kim, E. H. Kim, I. Lee, J. H. Byun, B. S. Kim, and S. M. Ahn, “Fabrication of carbon nanotubes dispersed woven carbon fiber/epoxy composites and their damping characteristics,” *J. Compos. Mater.*, vol. 47, no. 8, pp. 1045–1054, Apr. 2013.

[56] J. M. Dowling and P. Saha, “A Correlation between Oberst Bar and Center Point Damping Results,” SAE Technical Paper, Warrendale, PA, 2009-01-2134, May 2009.

[57] A. Gupta, S. Gadi, G. R. Kathawate, F. Fey, and D. Larson, “Effectiveness of a sprayable damper studied using multiple test methods,” in *Proceedings of the 23rd International Modal Analysis Conference*, Orlando, Florida, USA, 2005, pp. 1–6.

[58] R. Pereira, J. P. Arenas, and E. Zumelzu, “Comparison of four test methods to measure damping properties of materials by using piezoelectric transducers,” *Mater. Des.*, vol. 32, no. 4, pp. 2423–2428, Apr. 2011.

[59] Z. Li and M. J. Crocker, “Effects of thickness and delamination on the damping in honeycomb–foam sandwich beams,” *J. Sound Vib.*, vol. 294, no. 3, pp. 473–485, 2006.

[60] D. Malogi, A. Gupta, and G. R. Kathawate, “Center Impedance Method for Damping Measurement,” *Adv. Acoust. Vib.*, vol. 2009, Article ID 319538, Feb. 2010.

[61] S. Kurano, “Experimental study on effects of elastomer coating on the vibration-damping property of steel and CFRP plates for ship’s hull,” *Nippon Kikai Gakkai Ronbunshu HenTransactions Jpn. Soc. Mech. Eng. Part AJapan*, vol. 17, no. 6, p. 982, 2005.

[62] Quality and Standards Authority of Ethiopia (QSAE), *ET ISO 16940: Glass in building -- Glazing and airborne sound insulation -- Measurement of the mechanical impedance of laminated glass*. 2008.

[63] D. I. Chortis, D. S. Varelis, and D. A. Saravanos, “Prediction of material coupling effect on structural damping of composite beams and blades,” *Compos. Struct.*, vol. 94, no. 5, pp. 1646–1655, 2012.

[64] D. I. Chortis, *Structural Analysis of Composite Wind Turbine Blades*, vol. 1. Heidelberg: Springer International Publishing, 2013.

[65] P. Saha, S. Deshpande, J. Fisk, and D. Owen, “Damping Performance Using a Panel Structure,” SAE Technical Paper 2013-01-1938, 1938 2013.

[66] J.-S. Jang, J. Varischetti, and J. Suhr, “Strain dependent energy dissipation in multi-scale carbon fiber composites containing carbon nanofibers,” *Carbon*, vol. 50, no. 11, pp. 4277–4283, Sep. 2012.

[67] V. Kostopoulos and D. T. Korontzis, “A new method for the determination of viscoelastic properties of composite laminates: a mixed analytical–experimental approach,” *Compos. Sci. Technol.*, vol. 63, no. 10, pp. 1441–1452, Aug. 2003.

[68] P. A. Zinoviev and Y. N. Ermakov, “Energy Dissipation in Vibrating Composite Bars,” in *Energy Dissipation in Composite Materials*, CRC Press, 1994, pp. 179–198.

[69] W. E. Baker, W. E. Woolam, and D. Young, “Air and internal damping of thin cantilever beams,” *Int. J. Mech. Sci.*, vol. 9, no. 11, pp. 743–766, Nov. 1967.

[70] “LS-DYNA - Theory Manual.” Livermore Software Technology Corporation (LSTC), Mar-2015.

[71] “LS-DYNA Keywords user’s manual - Volume II Materials.” Livermore Software Technology Corporation (LSTC), Mar-2015.

[72] ASTM D3039 / D3039M - 14, “Standard Test Method for Tensile Properties of Polymer Matrix Composite Materials,” 2008.

[73] ASTM D3518, “Test Method for In-Plane Shear Response of Polymer Matrix Composite Materials by Tensile Test of a 45 Laminate,” ASTM International, 2013.

[74] ASTM D790 - 10, “Standard Test Methods for Flexural Properties of Unreinforced and Reinforced Plastics and Electrical Insulating Materials,” 2000.

[75] BS ISO 14125:1998, “Fibre-reinforced plastic composites. Determination of flexural properties,” 1998.

[76] B. Wade, P. Feraboli, and M. Osborne, “Simulating laminated composites using LS-DYNA material model MAT54 part I: [0] and [90] ply single-element investigation,” Baltimore, MD, Technical Report, 2012.

[77] Agilent Technologies, “The fundamentals of modal testing.” [Online]. Available: http://cp.literature.agilent.com/litweb/pdf/5954-7957E.pdf. [Accessed: 21-Jul-2014].

APPENDICES

Appendix A LS-DYNA

A.1 *MAT _ENHANCED_COMPOSITE_DAMAGE_054

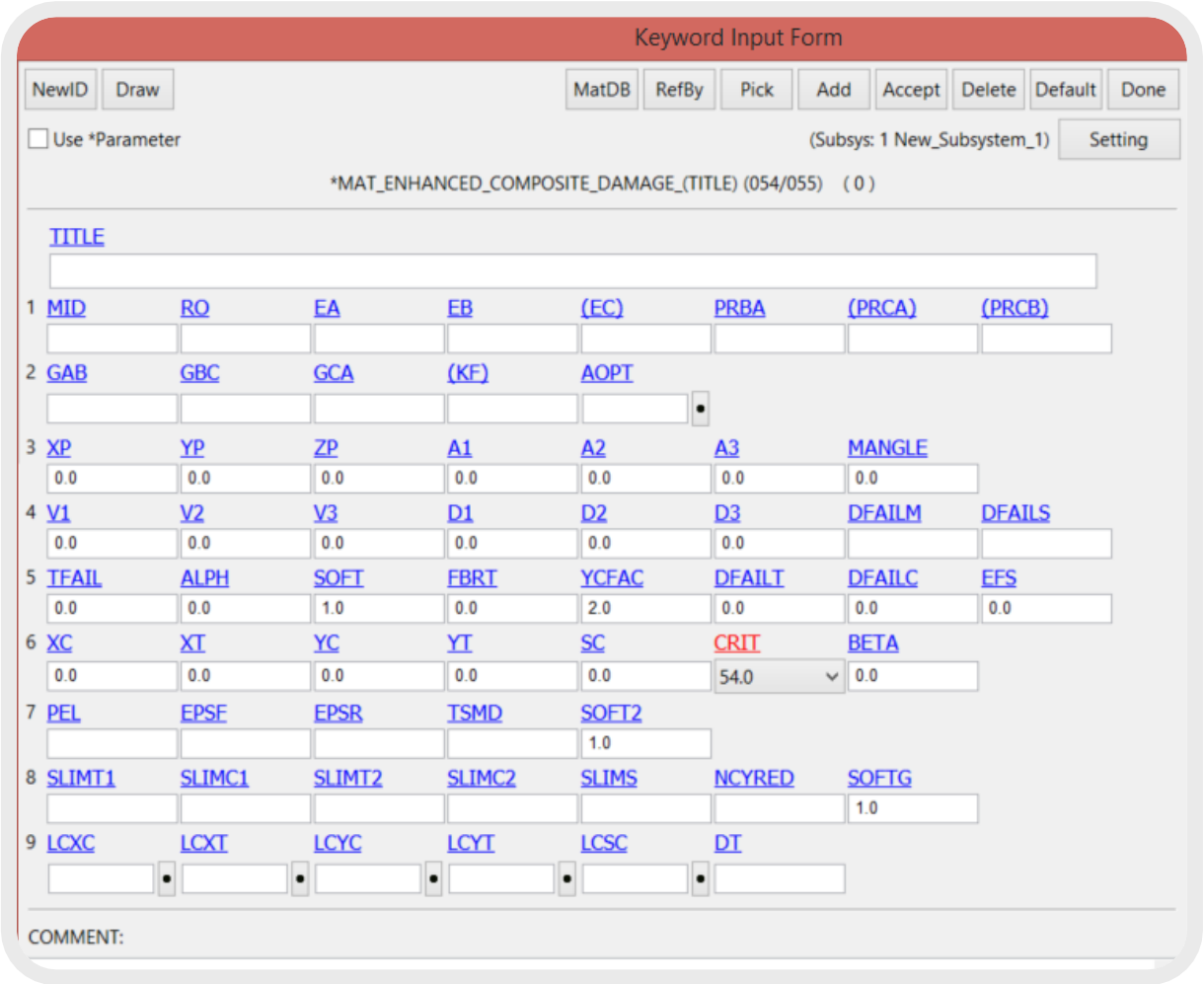

Figure A-1. MAT_ENHANCED_COMPOSITE_DAMAGE_054

RO	Mass density
EA	E_a, Young's modulus - longitudinal direction
EB	E_b, Young's modulus - transverse direction
EC	E_c, Young's modulus - normal direction
PRBA	v_{ba}, Poisson's ratio ba
PRCA	v_{ca}, Poisson's ratio ca
PRCB	v_{cb}, Poisson's ratio cb
GAB	Gab, shear modulus ab

GBC	Gbc, shear modulus bc
GCA	Gca, shear modulus ca
DFAILM	Maximum strain for matrix straining in tension or compression (active only for MAT_054 and only if DFAILT > 0). The layer in the element is completely removed after the maximum strain in the matrix direction is reached. The input value is always positive.
DFAILS	Maximum tensorial shear strain (active only for MAT_054 and only if DFAILT > 0). The layer in the element is completely removed after the maximum shear strain is reached. The input value is always positive.
TFAIL	Time step size criteria for element deletion: tfail ≤ 0: no element deletion by time step size. The crashfront algorithm only works if tfail is set to a value above zero. 0 < tfail ≤ 0.1: element is deleted when its time step is smaller than the given value, tfail > 0.1: element is deleted when the quotient of the actual time step and the original time step drops below the given value.
ALPH	Shear stress parameter for the nonlinear term, see Material 22
SOFT	Softening reduction factor for material strength in crashfront elements (default = 1.0). TFAIL must be greater than zero to activate this option.
FBRT	Softening for fiber tensile strength:
EQ.0.0:	tensile strength = XT
GT.0.0:	tensile strength = XT, reduced to XT × FBRT after failure has occurred in compressive matrix mode.
YCFAC	Reduction factor for compressive fiber strength after matrix compressive failure (MAT_054 only). The compressive strength in the fibRE direction after

	compressive matrix failure is reduced to: = YCFAC × Yc, (default: YCFAC = 2.0)
DFAILT	Maximum strain for fiber tension (MAT_054 only). (Maximum 1 = 100% strain). The layer in the element is completely removed after the maximum tensile strain in the fibre direction is reached. If a nonzero value is given for DFAILT, a nonzero, negative value must also be provided for DFAILC.
DFAILC	Maximum strain for fibre compression (MAT_054 only). (Maximum -1 = 100% compression). The layer in the element is completely removed after the maximum compressive strain in the fibre direction is reached. The input value should be negative and is required if DFAILT > 0.
EFS	Effective failure strain (MAT_054 only).
XC	Longitudinal compressive strength (absolute value is used).
GE.0.0:	Poisson effect (PRBA) after failure is active.
LT.0.0:	Poisson effect after failure is not active, i.e. PRBA = 0.
XT	Longitudinal tensile strength, see below.
YC	Transverse compressive strength, b-axis (positive value), see below.
YT	Transverse tensile strength, b-axis, see below.
SC	Shear strength, ab plane, see below.
CRIT	Failure criterion (material number):
EQ.54.0:	Chang matrix failure criterion (as Material 22) (default),
EQ.55.0:	Tsai-Wu criterion for matrix failure.
BETA	Weighting factor for shear term in tensile fiber mode (MAT_054 only). (0.0 ≤ BETA ≤ 1.0)
PFL	Percentage of layers which must fail until crashfront is initiated. E.g. |PFL| = 80.0, then 80 % of layers must fail until strengths are reduced in neighbouring elements.

	Default: all layers must fail. A single layer fails if 1 in-plane IP fails (PFL > 0) or if 4 in-plane IPs fail (PFL < 0). (MAT_054 only, thin shells only).
EPSF	Damage initiation transverse shear strain. (MAT_054 only, thin shells only).
EPSR	Final rupture transverse shear strain. (MAT_054 only, thin shells only).
TSMD	Transverse shear maximum

A.2 Damping test methods

A.2.1 Geiger Plate - SAE J671

In the Geiger plate test method the damping material is bonded to a 500mm × 500mm × 6mm thick steel plate supported on four pins along the nodal line of the panel. Results are obtained around 160 Hz and the damping performance is expressed in terms of decay rate. Although there are quite a few advantages of this method there are, also, a few significant disadvantages also. Some of these are:

• The plate thickness (6mm) is much greater than the typical automotive body panels (~1mm) where damping materials are used.

• Results are obtained only at 160 Hz and there are no accepted ways to extrapolate the data at other frequencies where the actual problem may be.

A.2.2 Oberst Bar - SAE J1637/ASTM E-756

The oberst bar test method is presented in the following lines, also known as complex modulus test method. In this method the damping material is bonded on a thin steel bar and the bar is excited magnetically by a non-contacting transducer under a clamped-free boundary condition. Measurements are made at various modes of vibration to obtain the loss factor of the system.

When this method was developed several years ago most of the damping materials were extruded and were sheet based materials of uniform thickness. However with the advancement of the polymer science technology and the manufacturing process, now there are sprayable damping materials which have inherent challenges in testing using Oberst bar test method [65]. Also, the same challenges are confronted when this method is used for testing composite parts, since the gluing of a thin metallic strip on the composite specimen is necessary due to the magnetic excitation.

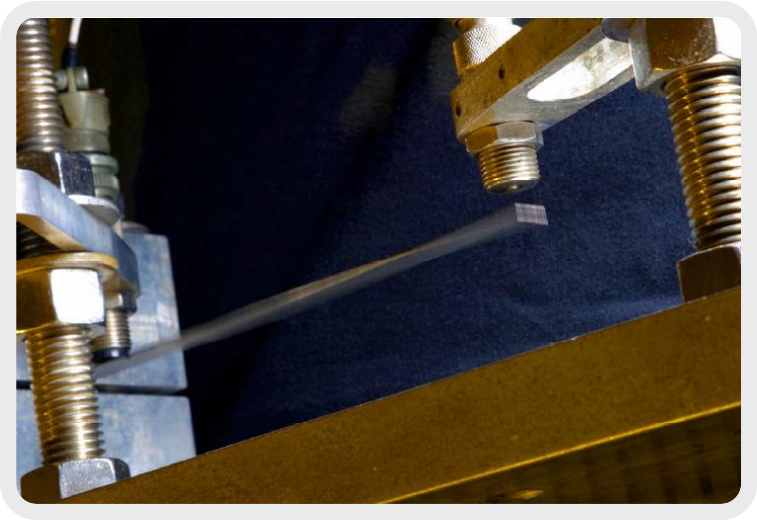

Figure A-2. Oberst bar setup [56]

A.2.3 Impact Hammer Excitation

Another common excitation mechanism in modal test is an impact hammer. Although it is a relatively simple technique to implement, it's difficult to obtain consistent results. The convenience of this technique is attractive because it requires very little hardware and provides shorter measurement times.

Since the force is an impulse, the amplitude level of the energy applied to the structure is a function of the mass and the velocity of the hammer. It is difficult though to control the velocity of the hammer, so the force level is usually controlled by varying the mass. The frequency content of the energy applied to the structure is a function of the stiffness of the contacting surfaces and, to a lesser extent, the mass of the hammer. The stiffness of the contacting surfaces affects the shape of the force pulse, which in turn determines the frequency content. Impact test has two potential signal processing problems associated with it. The first – noise – can be present in either the force or response signal as a result of a long time record. The second – leakage – can be present in the response signal as a result of a short time record. [77]

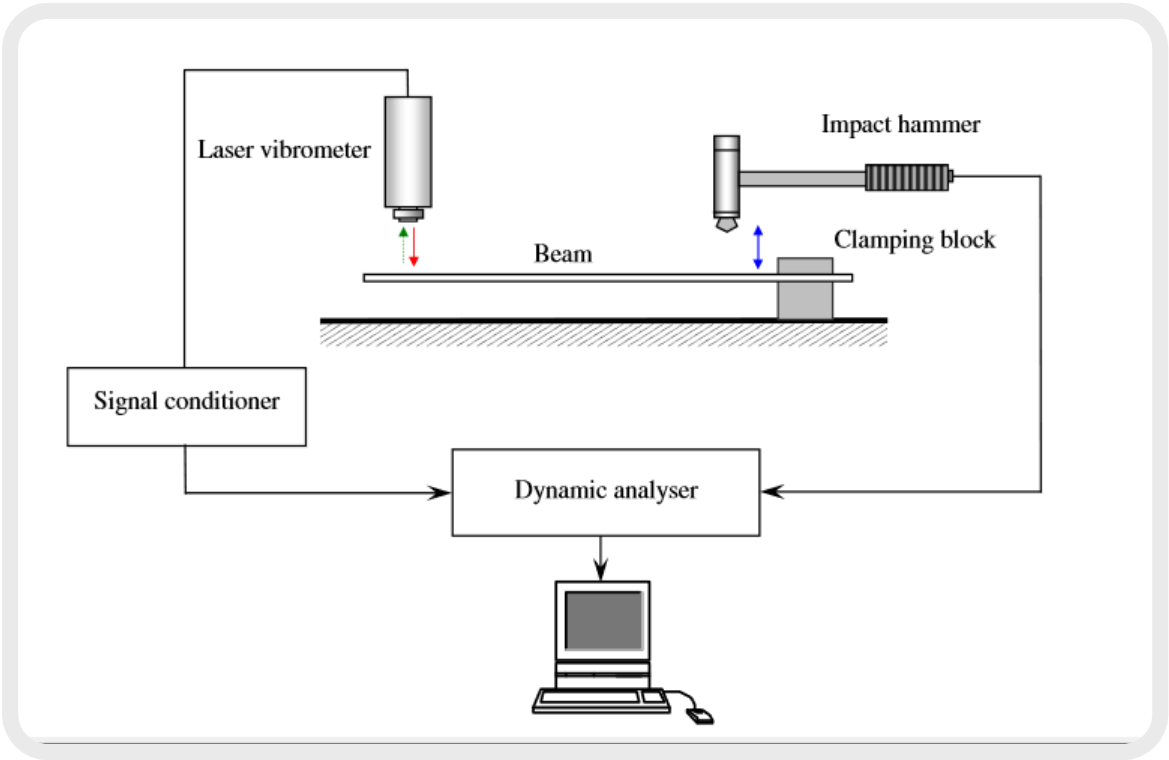

Figure A-3. Impact hammer setup [3]

A.3 Centre Impedance Method (CIM)

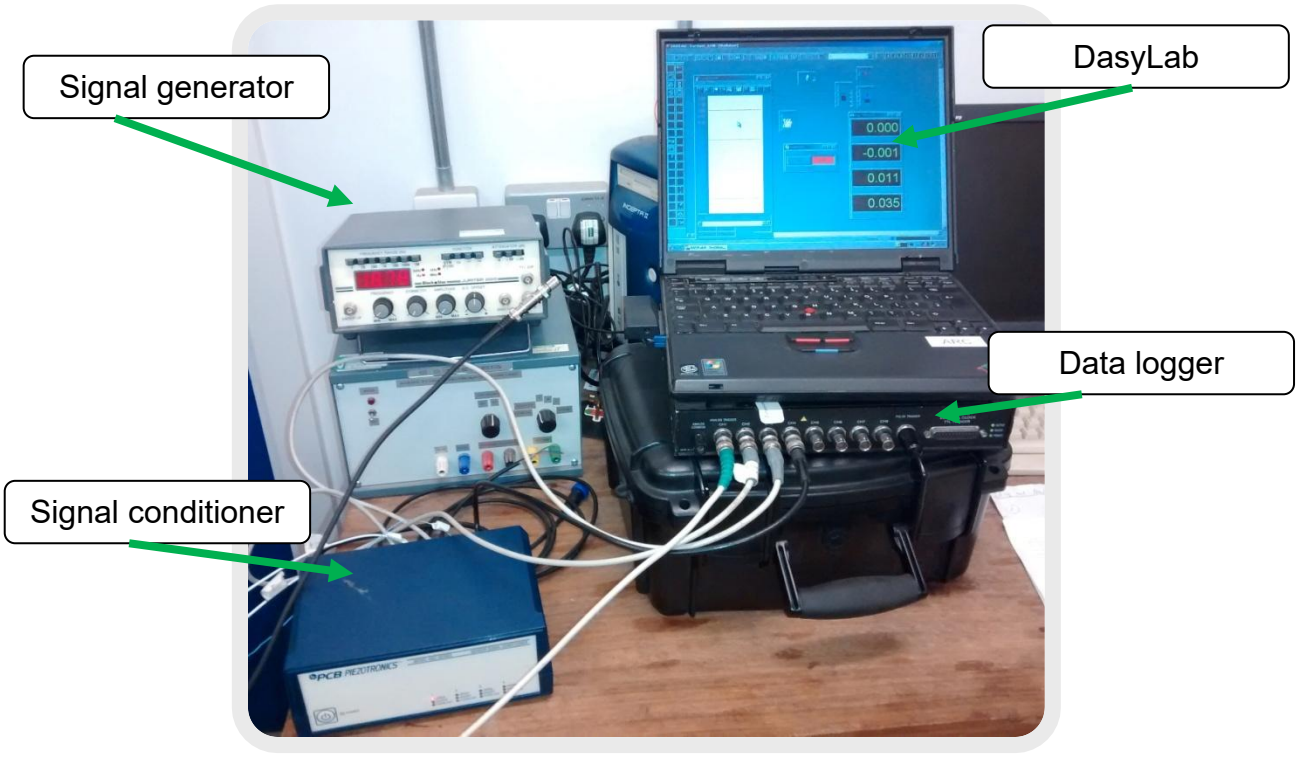

Figure A-4. CIM data acquisition system

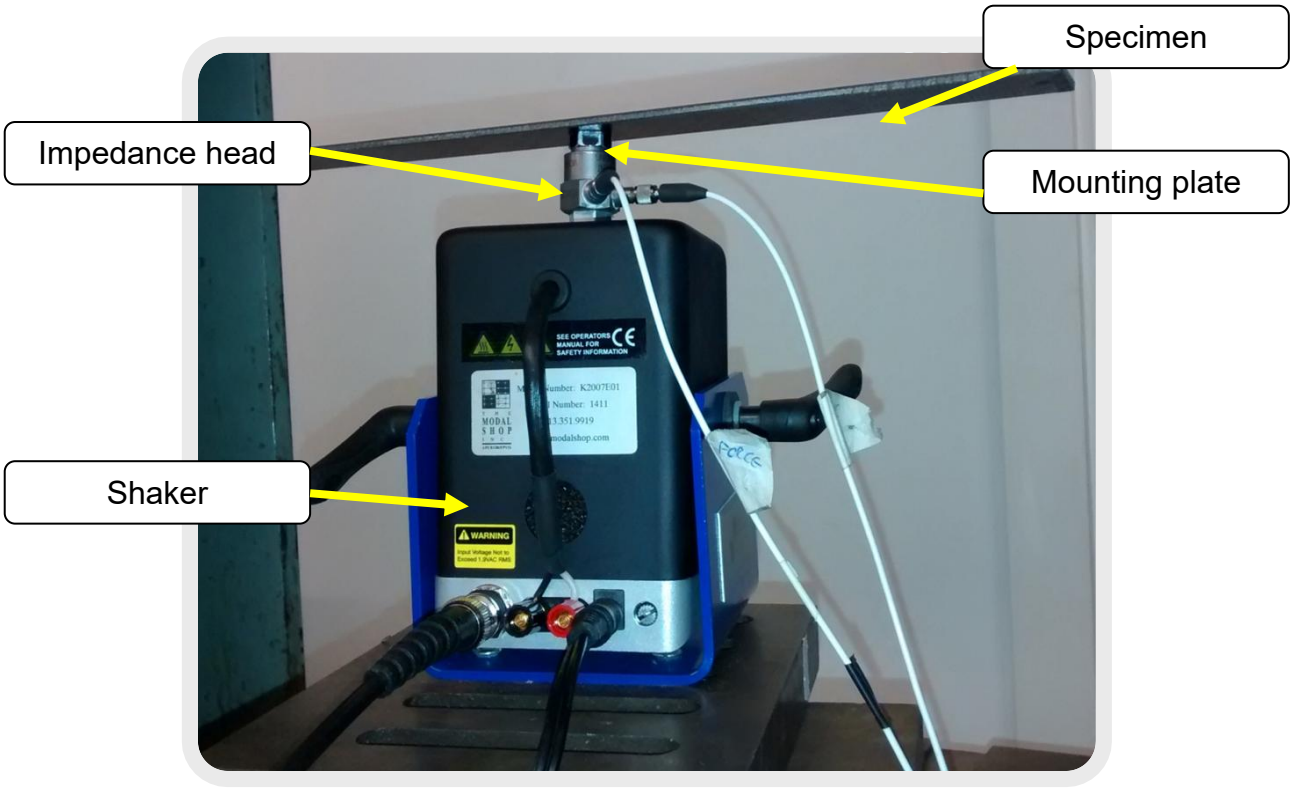

Figure A-5. CIM setup

A.3.1 Data acquisition setup

First the signal generator is connected to both data logger and shaker (**Figure A-4**). Then the data logger is connected to the personal computer and DasyLab software is commenced. After that, the signal conditioner is connected to the data logger.

A.3.2 Specimen's mounting

First, the impedance head is mounted on the shaker's moving head by mounting stud and is connected to the signal conditioner (**Figure A-5** and **Figure A-7 (a)**). The mounting plate is glued in the middle of the specimen using acrylic glue (**Figure A-8** and **Figure A-7 (b)**). After that, the specimen is mounted on the impedance head using a mounting stud. Then, the levelness of the specimen is checked (**Figure A-6**). After this check, the experiment advances as described in **5.1.1**.

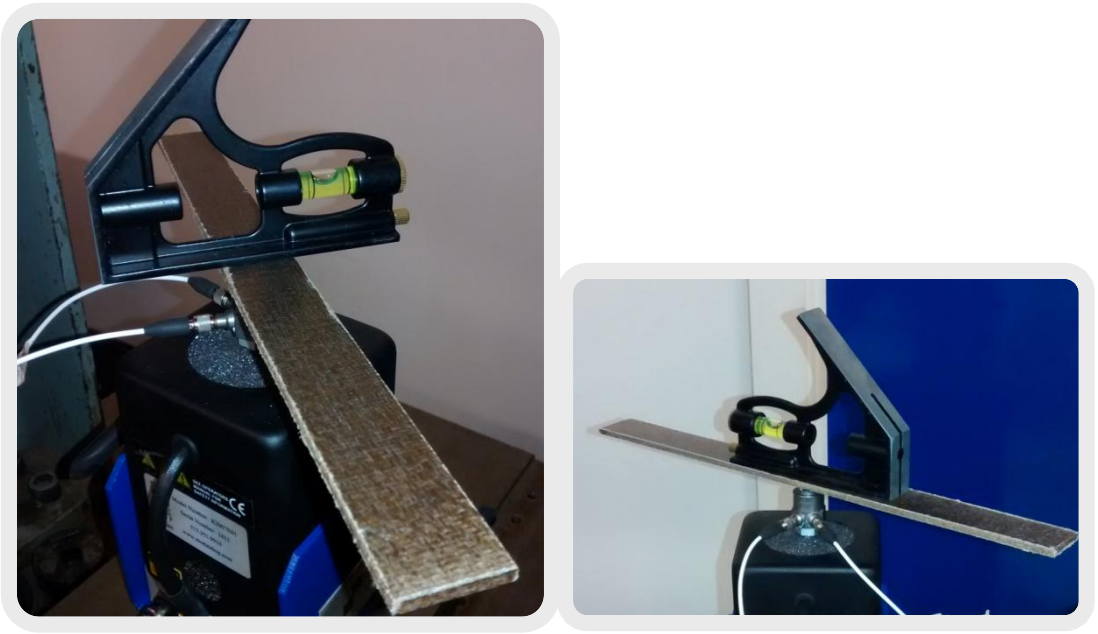

Figure A-6 (a), (b). Levelness check

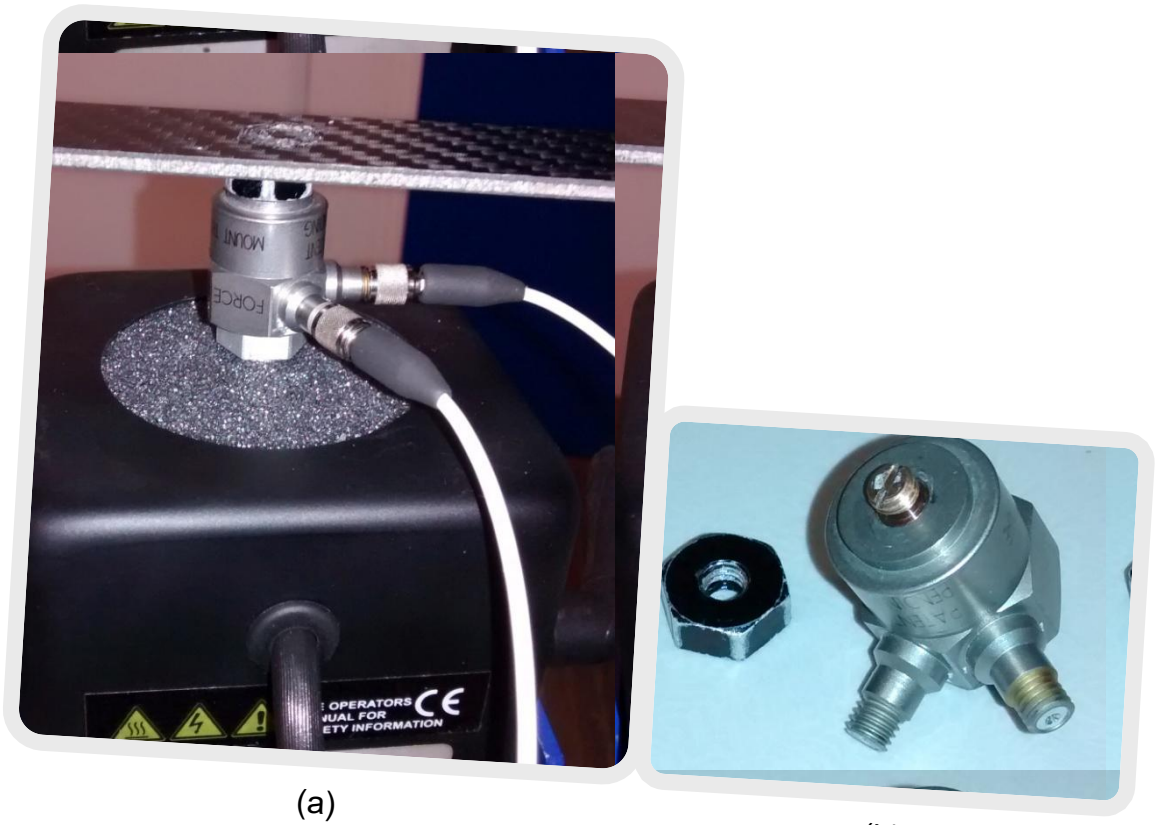

(a) (b)

Figure A-7. (a) Close shot, (b) PCB 288D01 impedance head and mounting plate

Figure A-8. Specimen, vernier caliper and glue